UNIVERSITÀ DEGLI STUDI DI MILANO

Facoltà di Scienze Matematiche Fisiche e Naturali

Doctorate School in Chemical Sciences and Technologies

Dipartimento di Chimica Inorganica, Metallorganica e Analitica "Lamberto Malatesta"

Ph.D. Studies in Industrial Chemistry, XXIV Course

On the Relationships Between Catalytic Activity and Morphology of the Metallic Phase in Catalysts Prepared by Chemisorption-Hydrolysis

CHIM/03

Ph.D. Student
Nicola Scotti

Tutor
Prof. Luigi Garlaschelli

Co-Tutor
Dr. Nicoletta Ravasio

Ph.D. Coordinator
Prof. Dominique Roberto

Academic Year 2010-2011

Table of Contents

Chapter 1

General Considerations

1.1 General Introduction

Role of heterogeneous catalysts

Catalysts and in particular heterogeneous catalysts, play a fundamental role in industrial chemical transformations. Approximately 85–90% of the chemical products of the industry are prepared with a catalytic processes. A catalyst offers a more energetically favorable mechanism with respect to the non-catalytic reaction, thus enabling processes that can be carried out under (industrially) milder conditions of pressure and temperature [1, 2]. Catalysis rapresents a delicate balance between

Reaction	Catalyst
Catalytic cracking of crude oil	Zeolites
Hydrotreating of crude oil	Co–Mo, Ni–Mo, Ni–W (sulfidic form)
Reforming of naphtha (to gasoline)	Pt, Pt–Re, Pt–Ir
Alkylation	H_2SO_4, HF, solid acids
Polymerization of ethylene, propylene, a.o.	Cr, $TiCl_x$/$MgCl_2$
Ethylene epoxidation to ethylene oxide	Ag
Vinyl chloride (ethylene + Cl_2)	Cu (as chloride)
Steam reforming of methane to CO + H_2	Ni
Water-gas shift reaction	Fe (oxide), Cu–ZnO
Methanation	Ni
Ammonia synthesis	Fe
Ammonia oxidation to NO and HNO_3	Pt–Rh
Acrylonitrile from propylene and ammonia	Bi–Mo, Fe–Sb (oxides)
Hydrogenation of vegetable oils	Ni
Sulfuric acid	V (oxide)
Oxidation of CO & hydrocarbons (car exhaust)	Pt, Pd
Reduction of NOx (in exhaust)	Rh, vanadium oxide

Table 1.1. Largest processes based on heterogeneous catalysis [1].

several factors (typically energetic, electronic and steric ones): a certain material can be a good catalyst only if the bond strength between the adsorbed surface species and the active sites is neither too weak nor too strong. If the bond strength is too weak the reactants cannot be readily activated, if too strong either the reactants can completely decomposed on the surface or the products cannot desorbs [3].

Catalyst performances can be evaluated by means of three key parameters: activity, selectivity, and stability. To Achieve a good and sustainable activity and selectivity at low cost is an everlasting goal in catalyst design and development. Activity refers to the rate at which a given reaction proceeds and it is often reported as turn over frequency (molecules converted per active center per unit time), even though also different ways, such as specific rate (rate divided by catalyst weight) and conversion after specified time (fraction of reactants converted per fixed time), are used. However, for continuous processes, activity is often expressed by space-time yield, i.e. the amount of product formed per unit time per unit volume of reactor [3, 4].

In addition to activity, the design of the catalytic process needs to consider selectivity towards the desirable products. In fact, selectivity is often the crucial criterion to decide if a particular catalytic process can be practicable. Selective reactions consume less reactant, avoid costly separations, and do not produce potentially polluting by-products.

Finally, a good catalyst must be stable. Ideally, catalysts are expected not to be consumed during the reaction, maintaining a constant level of performances. In the real situation, however, both catalytic activity and selectivity may decrease during the process. Thus, the lifetime of most industrial catalysts is finite, ranging from months to years. The most common reasons for catalyst deactivation include evaporation, washout, reduction, corrosion or other transformation of the active catalytic species during reaction, the formation of carbonaceous deposits (coking), the poisoning due to strong adsorption of impurities such as sulfur or carbon monoxide on the surface of the catalyst, and/or the coalescence of metal particles (sintering). If the process of deactivation is reversible the catalysts can be regenerated by a particular treatment, such as coke deposition burning off or other in situ chemical treatments. If deactivation is irreversible the replacement of the catalyst is needed [3].

In the last 20 years, the growing attention to environmentally concerns has focused the research efforts to the development of industrial processes named as sustainable and "green", with a special attention to bio and renewable resources. Sustainability was defined as "development that meets the needs of the present without compromising the ability of future generations to meet their own needs" at the Bruntland conference in 1987 [5]. This concept has acquired importance since the last twenty years and nowadays seems to be one of the main priorities for human future[6]. The

guideline principles which drove the development of environmentally benign products and processes can be embodied from the following twelve sentences:

1. Waste prevention instead of remediation

2. Atom efficiency

3. Less hazardous/toxic chemicals

4. Safer products by design

5. Innocuous solvents and auxiliaries

6. Energy efficient by design

7. Preferably renewable raw materials

8. Shorter syntheses (avoid derivatization)

9. Catalytic rather than stoichiometric reagents

10. Design products for degradation

11. Analytical methodologies for pollution prevention

12. Inherently safer processes

Industry segment	Product tonnage [a]	kg waste [b] /kg product
Oil refining	$10^6 - 10^8$	< 0.1
Bulk chemicals	$10^4 - 10^6$	< 1–5
Fine chemicals	$10^2 - 10^4$	5–> 50
Pharmaceuticals	$10 - 10^3$	25–>100

a) Typically represents annual production volume of a product at one site (lower end of range) or world-wide (upper end of range).

b) Defined as everything produced except the desired product (including all inorganic salts, solvent losses, etc.).

Table 1.2. The E factor [7].

Two useful measures of the potential environmental acceptability of chemical processes are the E factor, defined as the mass ratio of waste to desired product and the atom efficiency, calculated by dividing the molecular weight of the desired product by the sum of the molecular weights of all substances produced in the stoichiometric equation [7]. The E factor provides a mental idea of how wasteful is a process, and its ideal value is zero, while atom efficiency is a measure of "how much reactants remain in the final product" [8] and the best value is 100. However the drawback of E factor is the assumption we have to be made: in fact it disregards substances which do not appear in the stoichiometric equation.

In this view, heterogeneous catalysis plays a fundamental role in the development of new industrial processes, because it potentially possesses the requirements to achieve the objectives imposed by sustainable and green chemistry. Easy separation, easy recovery, no problem related with solubility and miscibility are the strengths of a heterogeneous system (respect to the homogeneous one) for reducing the cost of production and for developing environmentally benign processes [7, 9, 10].

In general an ideal catalyst for an industrial process must fulfill the following properties:

1. High activity per unit of volume in the eventual reactor
2. High selectivity towards the desired product, at high enough conversion, and the lowest possible selectivity to byproducts that generate waste problems
3. Sufficiently long life time with respect to deactivation
4. Possible regeneration, particularly if deactivation is fast
5. Simple and reproducible preparation
6. Sufficient thermal stability against sintering, structural change or volatilization inside the reaction environment (e.g. when steam is a byproduct of the reaction)
7. High mechanical strength with respect to crushing (e.g. under the weight of the catalyst bed or during the shaping process)
8. High attrition resistance (resistance to mechanical wear)

For these reasons, the most part of catalysts which give excellent activity and selectivity for a certain reaction at laboratory scale will not be successful catalysts in an industrial application [1], thus further efforts are necessary in the design of new heterogeneous catalysts suitable for a modern and clean chemistry.

Supported metal and metal oxides represent the larger class of heterogeneous catalysts and are widely employed in industrial processes, in particular in bulk and petroleum chemistry. Metal based catalysts, especially those containing transition metals, have proven particularly useful due to their ability in the easy activation of key molecules such as H_2, O_2, N_2, and CO as well as polyatomic organic molecules with C–H, C–O, C–N, and C–Cl bonds [3].

The use of metal (or metal oxides) as small particles gives the opportunity to take the most from simple inorganic compounds, otherwise poorly reactive if used in their bulk form. In fact, catalysis is a surface phenomenon, hence efficient catalysts have a large surface area implying that the active particles must be small, so it is not surprising that chemical reactions proceed more rapidly on a nanostructured material, due to the higher surface/volume ratio (Figure 1.1). Moreover, the maximization of surface/volume ratio of the active phase enables a decrease of the costs of some chemical processes or technologies, with obvious economical benefits, especially thinking about the

use of expensive metals, such as Pt, Ir or Rh. In fact, the higher fraction of active phase accessible for the reaction implies a lower amount of metal in order to have the same performances [3]. However small metal particles are often unstable and prone to sintering or leaching, particularly under conditions (pressure, temperature, interactions with reactants or side-products) typically used for catalytic reactions. Therefore, most heterogeneous catalysts used in industry consist of small particles on the surface and inside the pores of an inorganic matrix. Silica, alumina, titania, magnesia, zinc oxide, zirconia, as well as carbon can all be used as support materials [1, 11, 12].
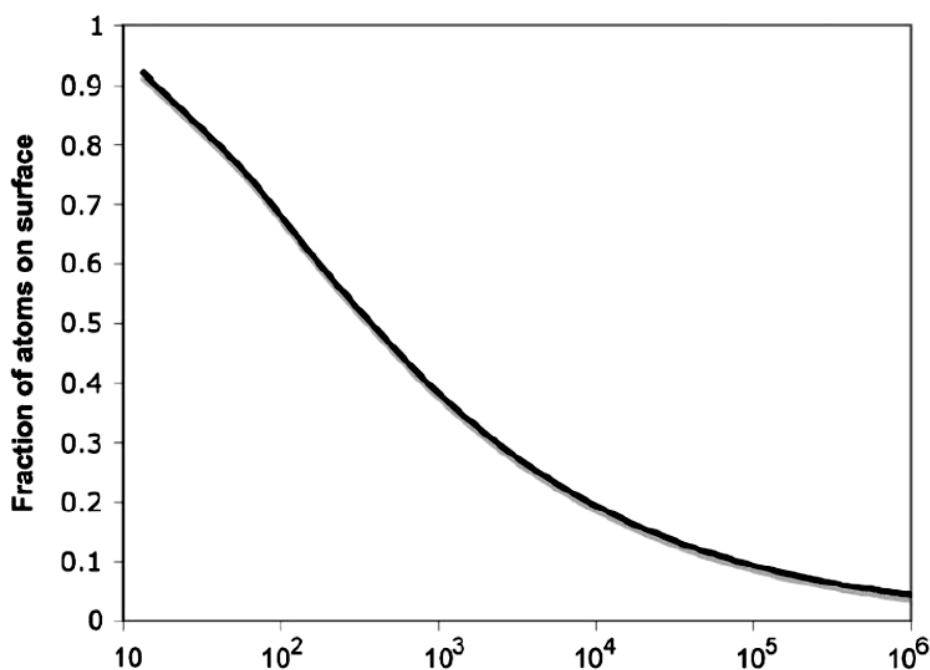
Figure 1.1. Fraction of atoms on the surface of cuboctahedral clusters of N atoms formed from a section o fan fcc lattice [11].

The choice of the support is primarily based on its surface area, but thermal and chemical stability, chemical properties, mechanical strength, and price also need to be considered [13]. Although most supports are primarily used to disperse a catalytic active phase and are considered as inert, they often show an effect on the overall chemistry of the catalytic process. In particular, supports with different acid-base or redox properties often have a marked influence on the active phase or directly on the reaction pathway, thus modifying catalytic behavior of the system. In addition supports with a regular structure and well defined pores (such as zeolites or ordered silica), because of the uniformity of their pores, can regulate the relative flows of the entering reactants, the leaving products and the transition states of the reaction based on their sizes, therefore determining the product distribution. Thus, the same active phase on different support can lead to different activity,

selectivity, stability and different product formation, not only because of the different surface area [3].

Notwithstanding the great advantage of nanostructured systems lies in their chemical features. The small particle size (and, as mentioned above, the interaction with the support) strongly affects the electronic state of the dispersed phase, and consequently its chemical properties: a highly dispersed metal (or metal oxide) is not merely a highly active surface system, but can express a completely different reactivity [12, 14-16]. A significant example of this behavior is represented by the use of gold as catalyst: for a long time this metal was considered far less active than other transition metals, but it is now well-known that there is a strong dependence of catalytic activity on the gold nanoparticle size, indeed very small Au nanoparticles (about 3 nm) exhibit extraordinary high performances in different reactions (Figure 1.2). At nanoscale dimension arises a quantum size effect which affects the properties of the metal particles, thus their catalytic activity [17-19].
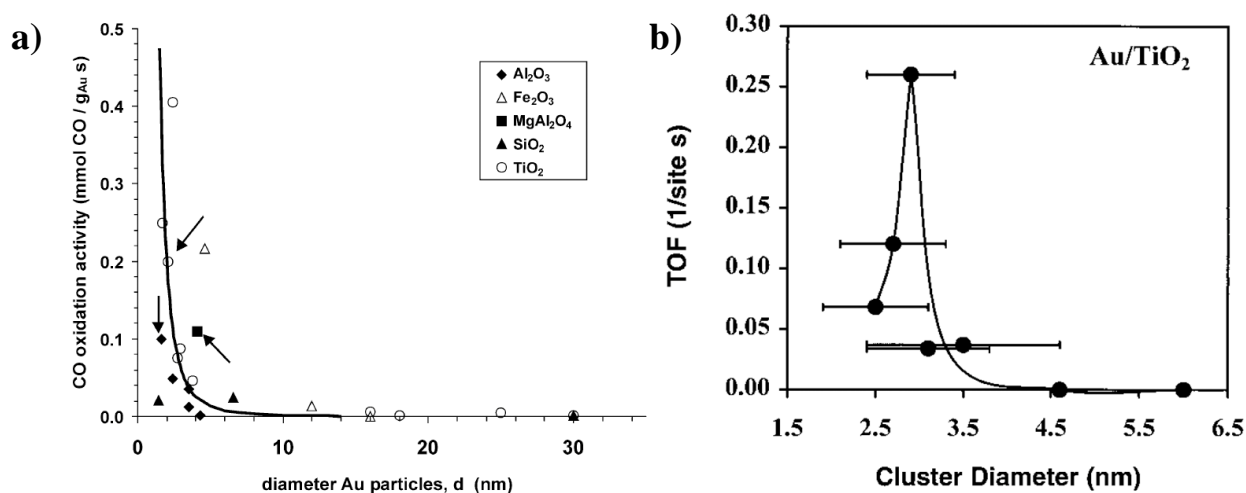
Figure 1.2. (a) Particle size effect in the CO oxidation reaction catalyzed by heterogeneous gold based catalysts on different supports. It is clearly evident that the CO oxidation rate for 2 to 4 nm particles is more than two orders of magnitude larger than for 20 to 30 nm particles. The dominant effect in the exceptional catalytic activity is the nanometric size of the particles, while other effects due to the support may have an additional, possibly important, but considerably smaller influence [17]. (b) TOFs increase as the diameter of the Au clusters is decreased until 3 nm. A further decrease in cluster diameter below 3 nm leads to a decrease in the activity of the Au [18].

Not only the size of nanocrystal reflects on the reactivity but also the atom coordination. For example, it is well known that densely packed oxide surfaces are largely inactive, while defects, particularly those associated with oxygen vacancies, provide sites where adsorbates may bind strongly. This means that structure and geometry of a surface play a dominant role with respect to its reactivity in adsorption and catalysis. In fact, coordinatively unsatured atoms, as well as low-

coordination and defective sites (kinks, steps or adatoms), generally show electronic and chemical properties that differ from flat surfaces and lead to higher activity [14, 20-24]. For the same reason high-index facets show higher catalytic activity than low-index ones (e.g. (730) vs (100)): in fact the former expose high densities of atomic steps. The general rule is that the more open the surface, the more reactive it is. The reactivity of a surface depends on the number of unsaturated bonds. An unsaturated bond is what is left from a former bond with a neighboring metal atom that had to be broken to create the surface [1]. But even at a flat exterior surface (typically the (111) face of a face-centered cubic (fcc) metal such as platinum), there are clearly three distinct adsorption sites - atop, bridge, and hollow - for small molecules such as carbon monoxide to be bound (Figure 1.3). Hence in general, solid heterogeneous catalyst, possess a spectrum of active sites each with their own energetics, activity, and selectivity [16].
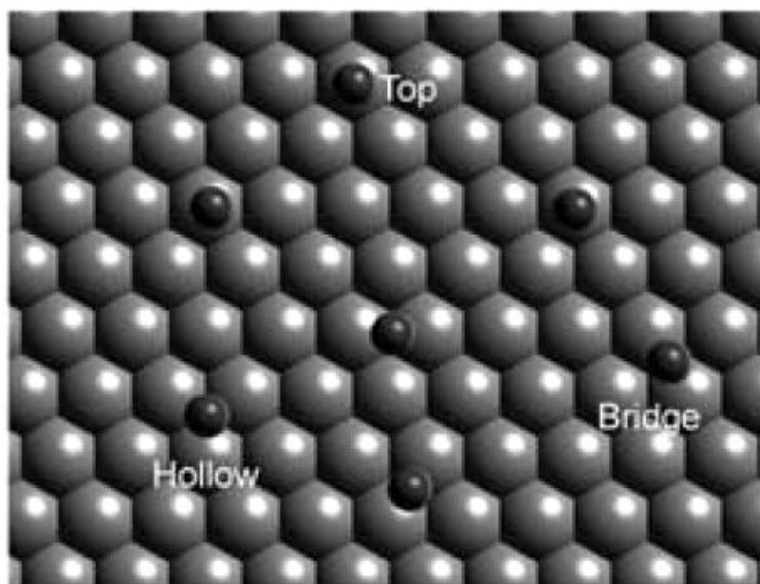
Figure 1.3. Even on a flat surface, such as the (111) face of platinum, there are three distinct sites for a molecule, such as CO, to be adsorbed [16].

In this view the ideal way to tune the catalytic properties consist in a fine control of the shape of catalyst nanoparticles that affects the distribution of different crystal planes, like (111), (100) and (110), and the relative proportion of the atom sites, such as faces, edges and corners.

However to understand structure/reactivity/selectivity relationships in heterogeneous catalysis is complicated by uncertainties in active site structure and in the percentages of surface structures which are catalytically significant [9]. Anyway, the uninterrupted improvements in the characterization techniques allow a better understanding of the catalytic system leading to a more rational approach in the design and preparation of new materials. Nowadays, the traditional

techniques employed in catalyst investigation, such as TEM, SEM, EXAFS-XANES, FT-IR, DRIFT, can be combined into in-operando systems which allow the real time study under working condition, thus providing important mechanistic insight into the active site and the related reaction mechanism [25].

Consequently, the synthesis of nanostructured materials supported on different matrixes is a well set and continuously pursued topic in heterogeneous catalysis. To find reliable and easy preparation techniques, enabling the preparation of robust and highly active materials still represents an important issue, particularly in the perspective of a wide application of catalysis to industrial purposes [1, 12, 16, 26, 27].

Copper Catalysts

Beside the preparation method a great importance falls on the choice of the active phase: noble metals show good catalytic properties but, usually, are also expensive, toxic and suffer of availability problems (Figure 1.4). For these reasons the research is moving toward the use of inexpensive and more available metals such as cobalt, iron, copper, nickel, manganese and others (Figure 1.5). Copper in particular is a low cost material and copper based catalysts are often preferred, with respect to other metal systems, as they offer similar activities and selectivities without toxicity problems, relevant in pharmaceutical chemistry and green chemistry where a contamination, also in traces, can affect the final product [7, 8] (see the exposure limits and concentration for different metals made by European Medicines Agency, Table 1.3).
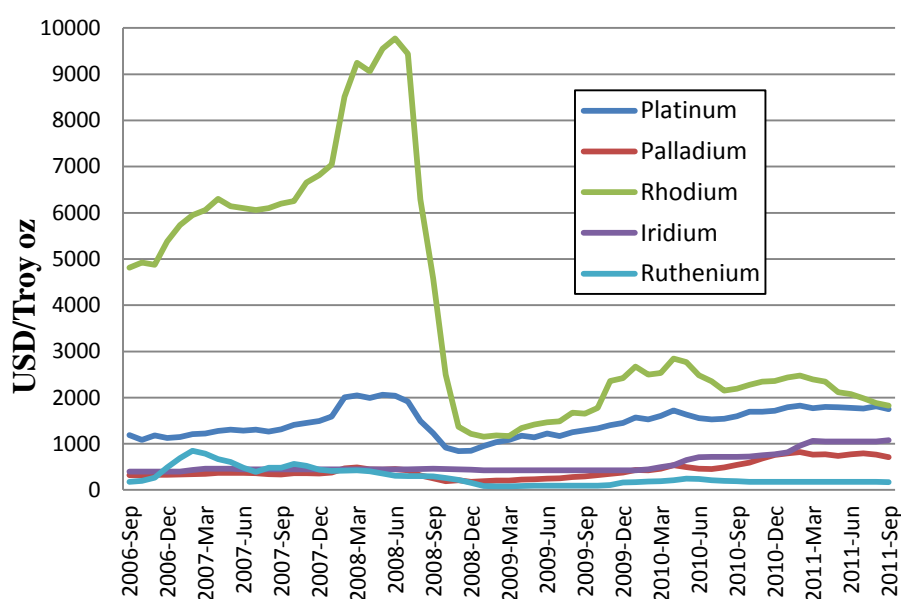
Figure 1.4. Noble metals price (last 5 years), http://www.platinum.matthey.com/.

The use of copper, copper oxide and salts in industrial catalysis is traditionally related with the use of systems with a very high metal content (up to 40%) for gas phase heterogeneous reactions, such as CO oxidation, conversion of syn-gas into methanol and water-gas shift [26, 28-32]. A typical example is embodied by copper chromites, that were found to be active in the hydrogenation of esters, ketones and aldehydes into alcohols, other than for methanol synthesis.

Generally the industrial scale hydrogenation processes are carried out with molecular H_2 in the presence of a catalyst (heterogeneous or homogeneous), rather than with an appropriate hydrogenation agent (e.g. metal hydride). The most used catalysts are based on noble metals (such as Pd, Pt, Rh, Ir and Ru) as well as non noble ones like Ni, Cr, Fe, Co and Cu.
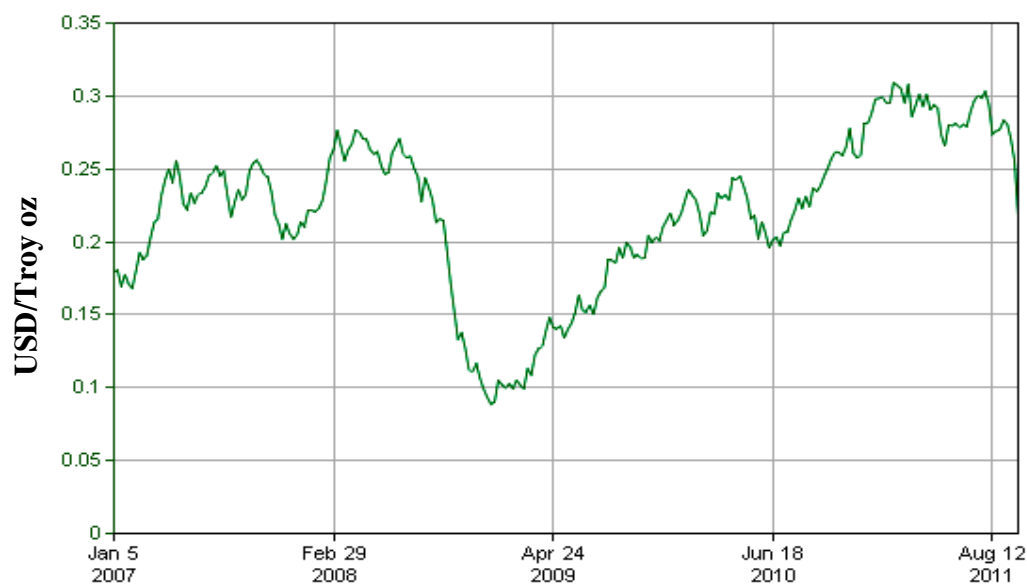
Figure 1.5. Copper price (last 5 years), http://www.infomine.com.

However, the leading role is traditionally up to noble metal based catalysts and Nickel ones, although the use of these systems often implies safety concerns and high costs.

Already in a paper published in 1931 copper chromite catalysts were used for the hydrogenation of different organic substrate, such as acetone, acetophenone, benzaldehyde, pyridine, nitrobenzene and more, with good result. Copper chromite catalysts reveal to possess certain advantages over nickel catalysts. They are not as sensitive as nickel to sulfur or halogen containing impurities in the compound to be hydrogenated and they show more resistance to deactivation [33]. Anyway, probably the most important characteristic is that copper chromite catalysts are selective toward the hydrogenation of the carbonyl group, leaving almost unaffected the C-C double bond: for that

14

reason these catalysts find important industrial application for the partial hydrogenation of vegetable oils and fatty acids. However deactivated copper chromite catalysts raise serious environmental concerns, and therefore they must either be recycled or reclaimed. This led to the development of inexpensive Cr free copper catalysts that could replace the traditional Cr-containing catalysts. Today the most studied heterogeneous copper catalysts consist of dispersed copper oxide (Cu (I) or Cu (II) eventually reduced through a pretreatment) on a support like silica, alumina, zeolites and more. Bimetallic system and the use of promoters are also reported in the literature. The nanodispersion allowed the minimization and optimization of the active phase and normally the amount of copper loaded on the support, without a negative effect on the particles dispersion, is up to 10 wt%.

Nevertheless, the spread of innovative preparation techniques for supported nanoparticles has enabled the application of copper catalysts to a wide variety of reactions due to the surprising properties provided by the high dispersion: nowadays Cu catalysts were employed not only for hydrogenation reaction, methanol production and water gas shift, but also for oxidation and epoxidation, etherification, dehydratation, epoxides alcoholysis and de-NO_x reactions.

Classification	Oral Exposure		Parenteral Exposure		Inhalation exposure
	PDE (µg/day)	Concentration (ppm)	PDE (µg/day)	Concentration (ppm)	PDE (ng/day)
Class 1A: Pt, Pd	100	10	10	1	Pt: 70
Class 1B: Ir, Rh, Ru, Os	100*	10*	10*	1*	
Class 1C: Mo, Ni, Cr, V Metals of significant safety concern	250	25	25	2.5	Ni: 100 Cr (VI): 10
Class 2: Cu, Mn Metals with low safety concern	2500	250	250	25	
Class 3: Fe, Zn Metals with minimal safety concern	13000	1300	1300	130	

* *Subclass limit: the total amount of listed metals should not exceed the indicated limit*

Table 1.3. Class exposure and concentration limits for individual metal catalysts and metal reagents made by European Medicines Agency; London, 21 February 2008; Doc. Ref. EMEA/CHMP/SWP/4446/2000

1.2 Aim of the thesis

The aim of the present Ph.D project is devoted to the optimization of heterogeneous copper catalysts made by Chemisorption-Hydrolysis method for hydrogenation and oxidation reactions. Different characterization technique (as XANES-EXAFS, FT-IR of CO and pyridine, TPR, TEM, XRD) were employed and different catalytic experiments were performed with the aim of investigate in the catalytic properties of studied materials.

As we will see in the next chapter, Chemisorption-Hydrolysis is a powerful, simple and versatile preparation technique able to give well dispersed small copper particles, different in nature depending on the support and pretreatments, even at high Cu loading. These features make CH method suitable to fulfill the requirement of a modern, green and sustainable chemistry.

The work is mainly focused onto different topics:

1. The copper catalysts preparation by Chemisorption-Hydrolysis and characterization of the obtained materials
2. The study of catalytic properties of Cu/SiO_2 depending on the atom site (hydrogenation/acid reactions)
3. The application of copper catalysts in the direct, gas phase epoxidation of propylene
4. The extension of the Chemisorption-Hydrolysis method to other metals, such as cobalt
5. The preparation of well defined Au NPs as futurable technique for catalyst preparation

1.3 References

[1] I. Chorkendoff, J.W. Niemantsverdriet, Concepts of Modern Catalysis and Kinetics, Wiley-VCH Verlag GmbH & Co. KGaA, Weinheim, 2003.

[2] Catal. Tod. 163 (2011) 3.

[3] R. B. King, Encyclopedia of Inorganic Chemistry, Second Edition, J. Wiley & Sons, Inc., 2005.

[4] G. J. Janz, S. C. Wait, J. Chem. Phys. 23 (1955) 1550.

[5] Our Common Future. 1987: United Nations.

[6] A. Gallo PhD Thesis, 2008.

[7] R. A. Sheldon, I. Arends, U. Hanefeld, Green Chemistry and Catalysis, Wiley-VCH Verlag GmbH & Co. KGaA, Weinheim, Germany, 2007.

[8] A. Lapkin, D. Constable, Green Chemistry Metrics. Measuring and Monitoring Sustainable Processes, Wiley-Blackwell, 2008.

[9] G. Centi, S. Perathoner, Cat. Tod. 77 (2003) 287.

[10] C. Pirovano PhD Thesis, 2009.

[11] J. A. Blackman, Metallic Nanoparticles, Elsevier, 2009

[12] N. Scotti, D. Monticelli, F. Zaccheria, Inorg. Chim. Acta (2011) doi:10.1016/j.ica.2011.10.001.

[13] B. Cornils, W. A. Herrmann, R. Schlögl, C. H. Wong, Catalysis from A to Z, Wiley-VCH, Weinheim, 2000

[14] C.-J. Jia, F. Schüth, Phys. Chem. Chem. Phys. 13 (2011) 2457.

[15] J. C. Park, H. J. Lee, J. U. Bang, K. H. Park, H. Song, Chem. Commun. (2009) 7345.

[16] J. M. Thomas, R. Raja, D. W. Lewis, Angew. Chem. Int. Ed. 44 (2005) 6456.

[17] N. Lopez, T. V. W. Janssens, B.S. Clausen, Y. Xu, M. Mavrikakis, T. Bligaard, J. K. Nørskov J.Catal. 223 (2004) 232–235

[18] M. Valden, X. Lai, D. W. Goodman, Science (1998) 281.

[19] M. Haruta, T. Kobayashi, H. Sano, and N. Yamada, Chem. Lett. 16 (1987) 405.

[20] J.-F. Paul, P. Sautet, J. Phys. Chem. 98 (1994) 10906.

[21] H. Lu-bing, D. Hui-qiu, H. Wang-yu, Trans. Nonferrous Met. Soc. China 16 (2006) 820.

[22] M. F. Haroun, P. S. Moussounda, P. Légaré, J.-C. Parlebas, Eur. Phys. J. B 78 (2010) 353.

[23] T. Ming, W. Feng, Q. Tang, F. Wang, L. Sun, J. Wang, C. Yan, J. Am. Chem. Soc. 131 (2009) 16350.

[24] K. Mori, T. Hara, T. Mizugaki, K. Ebitani, K. Kaneda, J. Am. Chem. Soc. 126 (2004) 10657.

[25] S. J. Tinnemans, J. G. Mesu, K. Kervinen, T. Visser, T. A. Nijhuis, A. M. Beale, D. E. Keller, A. M. J. van der Eerden, B. M. Weckhuysen, Cat. Tod. 113 (2006) 3.

[26] B. Delmon, J. Therm. Anal. Cal. 90 (2007) 49.

[27] M. Campanati, G. Fornasari, A. Vaccari, Catal. Today 77 (2003) 299.

[28] G. A. Olah, A. Goeppert, G. K. S. Prakash, Beyond Oil and Gas: The Methanol Economy, Second updated and enlarged edition, Wiley-VCH Verlag GmbH & Co. KGaA, Weinheim, 2009.

[29] Ullmann's Encyclopedia of Industrial Chemistry, Sixth Edition, Wiley-VCH, 1998.

[30] F. Severino, J. L. Brito, J. Laine, J. L. G. Fierro, A. L. Agudo, J. Catal. 177 (1998) 82.

[31] J. R. Mellor, N. J. Covllle, A. C. Sofianos, R. G. Copperthwaite, Appl. Catal. A: Gen. 164 (1997) 185.

[32] S. Lee, Encyclopedia of Chemical Processing, Taylor & Francis Group, New York, 2006.

[33] H. Adkins, R. Connor, J. Am. Chem. Soc. 53 (1931) 1091.

Chapter 2

Characterization of Cu catalysts prepared by CH

2.1 Introduction

Heterogeneuos copper catalyst preparation

In Chapter 1 the role of heterogeneous catalysts in a sustainable and modern chemistry was discussed, with particular attention to nanodispersed copper based catalysts. Several methods have been developed for the preparation of heterogeneous catalysts, but, as already mentioned, the current state-of-the-art cannot completely satisfy the demand of robust and active materials, in particular for industrial application. In this section, the main advantages and drawbacks of main catalysts preparation techniques are reported, taking also a look to the trends concerning copper catalysts.

Traditional coprecipitation and impregnation techniques are based on uncomplicated preparation steps employing simple and cheap precursors. As a drawback, catalysts prepared in this way present quite low dispersion, particularly for high metal loadings and lack in particle size control and uniformity. For example, coprecipitation techniques allow one to prepare supported, mixed and also single component catalysts, often in one step, but the process may be difficulty controlled and features low flexibility, as components in the starting homogeneous solution need to be simultaneously precipitated in a single material. Likewise, impregnation techniques are quite easy preparation procedures, but often lead to a large spectrum of catalytic sites, different in size, shape and support interaction [1, 2].

The general trend in new heterogeneous catalyst design has been driven towards the production of well defined and uniform active sites, in order to combine the advantages of homogeneous catalysts with an easy product separation, recover, recycling and a good stability of the catalyst [3-7]. The latest cutting-edge of single site hetereogeneous catalysis (SSHC) is nothing but the extreme expression of this strategy. This particular approach aims at the preparation of catalytic systems where the active sites are well-defined, isolated, evenly distributed entities (single sites) with defined chemical surroundings, as in conventional homogeneous catalysts or enzymes, while showing all of the advantages of heterogeneous systems [8, 9].

A simpler alternative to SSHC is chemical vapor deposition (CVD) and related methods. CVD is an useful technique for the preparation of well dispersed catalysts with quite high metal loadings, avoiding several steps of the traditional method, such as washing, drying, calcination and reduction [6, 10-12].

Unfortunately, preparation methods like SSHC and CVD, though affording the synthesis of highly active heterogeneous systems, frequently require sophisticated and tricky techniques or apparatus that lead to low reproducibility or scarce practical applicability, particularly when large scale productions are sought. The search for a particular morphology in the catalytic site calls for highly controlled conditions in the preparation method, as much as the use of elaborate, costly and unstable complexes as metal precursors [8, 9, 11, 13].

The preparation of colloidal metal nanoparticles and their deposition on a support is an alternative persecuted route. It usually allows a good control of the shape and size of the particles at the expenses of the handiness of the protocol. The synthetic procedure is frequently complicated, leading to the coverage of the colloid surface by organic polymers that can interfere with the catalytic activity of the system: moreover the removal of these polymers may affect the stability of the nanoparticles [3, 14].

As regards copper, today heterogeneous Cu catalysts are prepared with the more traditional techniques, like impregnation and cooprecipitation, but also by means of less conventional method.

Metal vapor synthesis (MVS) has been used to obtain copper catalysts with high metal dispersion, used for Ullman reactions [15] as well as for oxygen activation [16, 17].

A different approach has been employed in the precipitation-gel (PG) technique, involving the addition of aqueous NaOH to a solution of $Cu(NO_3)_2$ to form a precipitate, following by the addition of colloidal silica to the obtained suspension, in order to stabilize the microparticles of the precipitate and simultaneously to form a gel. These materials have been proposed for the glycerol hydrogenolysis into 1,2-propandiol [18].

Finally, a microwave assisted protocol introduced for noble metals has been successfully extended to copper catalysts and used for C-S coupling reactions [19].

Chemisorption-Hydrolysis

In the present thesis we report about the use of an unconventional technique, called Chemisorption-Hydrolysis (CH), which enables to obtain highly versatile copper based catalytic systems in an easy and reproducible way. Chemisorption-Hydrolysis represents a fruitful trade-off, as it combines the simplicity of impregnation techniques, both in terms of handiness (easy experimental procedure,

simple apparatus) and cheapness, with the high metal dispersion obtained by anchoring techniques. As previously discussed, the possibility to prepare highly dispersed samples smoothes the way to diverse applications of the metal oxide and in this context CH leads to different catalytic sites just by varying the inorganic matrix, while always keeping a remarkable dispersion. On the other hand reductive treatment allows one to switch from an acidic catalyst to an hydrogenation one [1].

The preparation steps of Chemisorption-Hydrolysis are:

1. Preparation of $[Cu(NH_3)_4]^{2+}$ complex by dropping aqueous NH_3 to a $Cu(NO_3)_2 \cdot 3H_2O$ solution until pH 9 has been reached

2. Addition of support powder to the $[Cu(NH_3)_4]^{2+}$ solution

3. Dilution of the cooled slurry (0 °C)

4. Filtration and calcination (350 °C, 4 h) of the solid to obtain CuO/support (Cu^{2+}) or CuO_x/support ($Cu^{\delta+}$, $+1 \le \delta \le +2$) catalyst

If required by reaction conditions, an eventual reduction pretreatment (directly with H_2) leads to Cu/support catalyst, where copper is totally or partially reduced.

The pH of the solution used in Chemisorption-Hydrolysis and Incipient Wetness methods plays a fundamental role [20]. Differently to traditional impregnation method, in CH the pH of the starting aqueous solution of $Cu(NO_3)_2$ is increased until 9, well above the zero charge point of the common supports employed (e.g. SiO_2 and TiO_2), by adding NH_4OH: hence the surface of the support is negatively charged, thus favoring the adsorption of copper cations and giving the observed high dispersion of the sample, while nitrate ions are removed by washing. On the other hand, in the case of impregnation methods the pH of the impregnating solution used is 3–4, thus below the zero charge point for supports. Therefore the surface is positively charged and adsorbs anionic species, i.e. copper nitrates. Moreover, as a consequence of the quite low pH of the impregnating solution some dissolution of the support is expected: through calcination both unsupported CuO and a disordered, amorphous surface layer, containing copper, titanium, oxygen, and nitrogen, will be produced. A phase retaining some nitrogen, in Cu/SiO_2 samples prepared by Incipient Wetness, has been observed also by Higgs and Pritchard [21]. Thus in the case of Chemisorption-Hydrolysis the copper deposition at the surface of support is the result of an ionic exchange reaction, while in the case of the catalyst obtained by Incipient Wetness a cupric nitrate solution simply fills the pores [20].

In 1997 Boccuzzi et al. reported a comparison between Cu/TiO_2 catalysts made by CH and Incipient Wetness (IW), by using different characterization technique (TEM, TPR, FT-IR) [20]. The results clearly illustrate that samples having the same chemical composition show very different properties, depending on the preparation method and on the thermal and chemical pretreatments. HR-TEM

micrographs (Figure 2.1) show different characteristics of the two calcined catalysts reduced by the electron beam: on IW samples the beam produces a large, amorphous layer covering the TiO_2 crystallites, while on CH samples small particles are formed. This behavior is ascribed to the different structures of the copper containing overlayer as seen above.
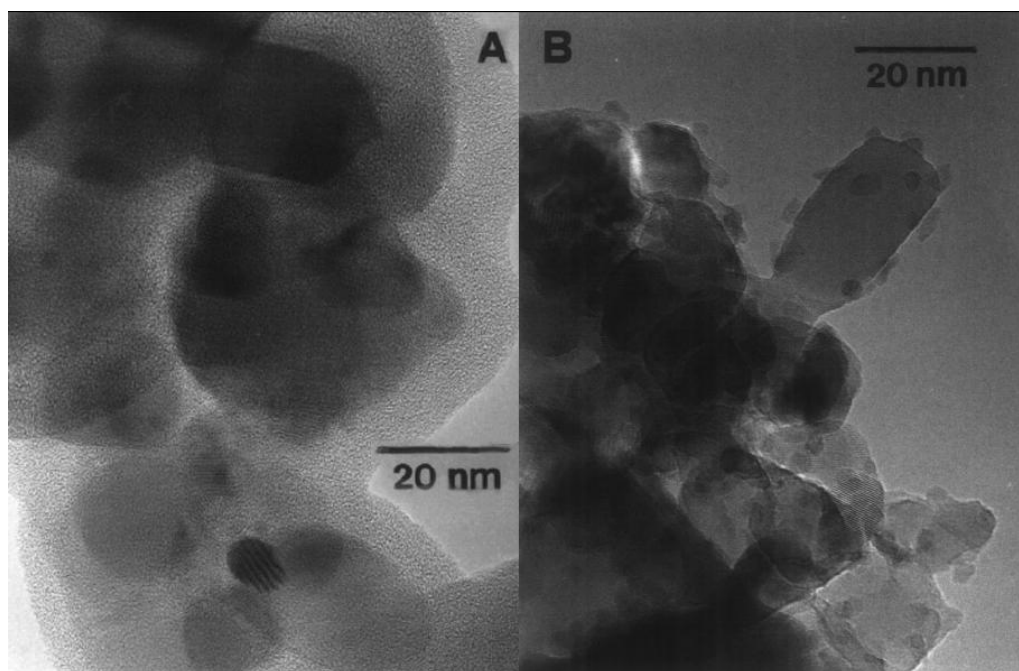
Figure 2.1. TEM images of CuO/TiO_2 samples after exposure to electron beam. (A) Cu/SiO_2 made by IW. (B) CuO/TiO_2 made by CH [20].

TPR profiles of CH and IW samples confirmed that the materials are completely different: a narrow peak in the range 180-230 °C is present for the former (reduction of CuO crystallites of different dimension), while a broad peak at 170–260 °C is seen for the latter (reduction of both unsupported CuO and a disordered phase containing copper and titania interdispersed at an atomic level, possibly with some residual anions). Finally, the interpretation of FT-IR spectra of adsorbed CO describes a situation in which isolated or two-dimensional clusters of copper are exposed on the surface of the catalyst made by Incipient Wetness, whereas the sample obtained by Chemisorption–Hydrolysis is composed by three-dimensional copper particles [20]. Therefore, it is not a coincidence that the two materials show a very different activity, e.g. in the hydrogenation of 1,3-cyclooctadiene, where the CH catalysts shows a turnover frequencies about 100 times greater than that prepared by IW [22].

Although the two papers wrote by Boccuzzi and coworkers pointed out, once again, the great influence of the preparation method on the catalytic properties of material nominally composed of

the same elements, the role of the support has not to be forgotten. Copper dispersed on SiO_2 or SiO_2-Al_2O_3 (13% of Al_2O_3) supports by Chemisorption-Hydrolysis method revealed to be very different in nature. On SiO_2, similarly to what happens also on TiO_2, the deposition of copper generates a CuO phase well reducible to metallic Cu, by means of a reductive pretreatment. The situation is markedly different when SiO_2-Al_2O_3 is used as support: in this case isolated copper species with oxidation state ranging from (II) to (I) were formed just after the catalyst preparation and the reduction only significantly decreases the amount of the Cu (II) species in favor of $Cu^{\delta+}$ (1 < δ < 2) and Cu (I). These differences were confirmed by a depth characterization (TPR, XPS, EXAFS-XANES and EPR) and, definitely, by catalytic experiments which show distinct behaviors depending on the support [23, 24].
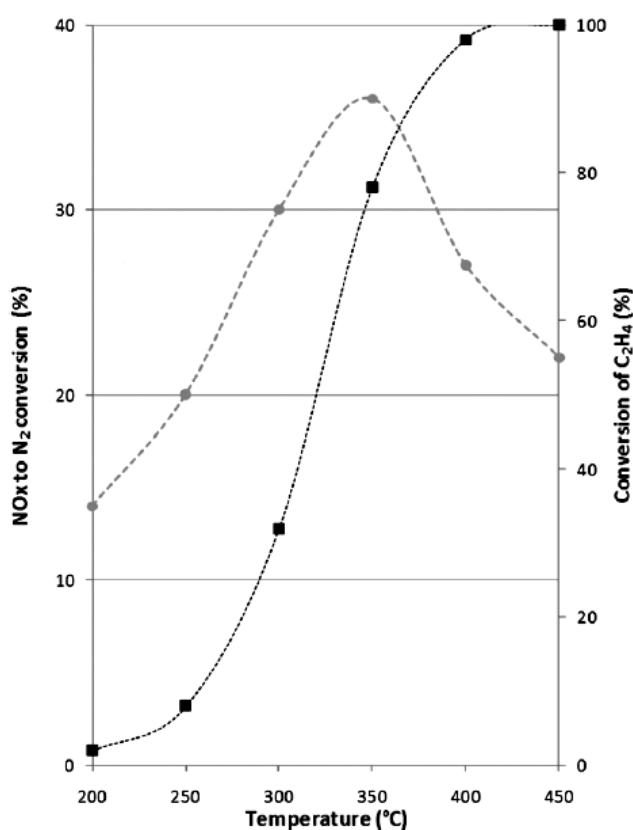
Figure 2.2. Conversion of NO_x to N_2 (gray dot) and conversion of C_2H_4 (black square) to carbon oxide as a function of reaction temperature in SCR (initial concentrations: ca. 1500 ppm of NO_x and of C_2H_4 and 15000 ppm of O_2) [1].

Even if the use of completely reducible Cu species is generally required on copper catalyzed hydrogenation reactions, the particular nature of the unreduced oxide obtained over silica alumina can conversely be exploited for several applications. Activity of $Cu/SiO_2-Al_2O_3$ in the carbene insertion coming from methyl phenyldiazoacetate, into one C-H bond of THF has been recently reported, thus constituting the first example of this reaction promoted by a purely inorganic catalyst [25]. In this synthetic application, $Cu/SiO_2-Al_2O_3$ leads to better results regarding yield and catalyst recovery than Cu/SiO_2, confirming that different redox properties of the supported Cu phase influence the behavior of the catalyst depending on the support. The particular electronic properties of the oxidic phase when dispersed over this silica alumina can be conveniently exploited for other catalytic applications than hydrogenation. In particular, the similarity with copper-exchanged zeolites prompted to test these systems in the Selective Catalytic Reduction in oxidizing atmosphere (HC-SCR) for NO_x [1, 23, 24]. According to Márquez-Alvarez at al., HC-SCR can be performed in any Cu-based system containing small cupric oxide particles and some acidity [26]. The catalyst preparation method is a critical factor for improving the de-NO_x activity of copper dispersed catalysts together with the choice of a suitable support with acidic properties and a wide surface to disperse the copper phase. The superior performances observed for copper-exchanged zeolites (particularly ZSM-5) compared to amorphous supported systems has been ascribed to the capacity of zeolites in disperding the active copper at atomic level [27]. On the other hand, desirable support properties are high mechanical and hydrothermal stability. Chemisorption-Hydrolysis has been revealed an adequate method to prepare nanodispersed copper catalysts supported over oxidic acidic support as $SiO_2-Al_2O_3$ to be used for this kind of catalytic application. Recently we reported a 35% of NO_x conversion to N_2 and 80% of C_2H_4 conversion to carbon oxides [1] (Figure 2.2). Comparable NO to N_2 conversions (41%) were reported over Cu-ZSM-5 at 250 °C [28].

A step forward in exploiting as much as possible the versatility of these kind of copper catalysts is represented by the use of dispersed copper oxide as an acidic catalyst, even if supported over non acidic matrixes. Acidic properties in heterogeneous catalysts usually derive from conventional acidic functions such as –OH groups in molecular sieves, or clays, or exchanged metal ions as Lewis acid [29]. Dispersed copper over a non acidic silica obtained with the Chemisorption-Hydrolysis technique can be used as a heterogeneous acid catalyst, by virtue of its high dispersion, while catalysts made by Incipient Wetness are completely inactive. In Table 2.1 are reported the result obtained by Zaccheria et al. is the alcoholysis reactions of epoxides with different alcohols catalyzed by CuO/SiO_2 catalyst. Good conversion and selectivity was reached with different alcohols, in general within 1 h. These results unravel the unexpected acidity of this material, where none of the partners shows acidic activity itself [30]. Although the use of Cu (II) salts as Lewis

Acids is known [31] reports on CuO are lacking. The reaction proceeds truly by a heterogeneous pathway, as clearly shown by the authors: if catalyst is filtrated from the reaction media, the reaction stops immediately. Moreover the use of chromatographic silica ensured the inertness of the support used under these conditions, in fact only SiO_2 did not lead to any reaction. On the other the sample prepared by traditional Incipient Wetness technique and with the same copper loading resulted to be almost inactive under the reaction conditions used, confirming the peculiar properties given by the particular preparation method used. Also bulk CuO resulted to be completely inert.

Alcohol	t (h)	Conv. (%)	Sel. (%)[b]
MeOH	8.5	97	92
EtOH	2	99	90
2-Propanol	0.75	100	83
	0.75	100	82[c]
2-Butanol	0.5	98	83
Isobutanol	0.5	100	81
1-Octanol	0.5	94	88
2-Octanol	0.5	100	87
Cyclohexanol	0.25	56	81
	0.5	100	78

[a] Alcohol as solvent (5 mL), 60 °C, N_2. [b] Main byproduct being phenylacetaldeide derived from the acid promoted epoxide isomerisation. [c] Reaction carried out under air.

Table 2.1. Styrene oxide alcholysis promoted by CuO/SiO_2 [30].

Summarizing, as we seen in this section, among the preparation methods used in heterogeneous catalysis, Chemisorption–Hydrolysis represents a powerful technique in order to combine high activity and handiness. This protocol is reliable and versatile, giving the opportunity to properly choose the support in order to tune the catalytic activity or selectivity, thus ranging over very different kind of purposes, aimed both to fine chemicals preparation and environmental remediation [32]. Thus, the same preparation technique leads to different catalytic sites just by varying the inorganic matrix, while always keeping a remarkable dispersion. On the other hand the reductive treatment allows one to switch from an acidic catalyst to an hydrogenation one. Moreover the use of a non noble, non toxic and non pyrophoric metal shelters from several economical and safety concerns.

Aim of the work

In this chapter preparation and characterization of different catalysts made by Chemisorption-Hydrolysis have been reported. The copper amount was chosen between 1 and 15 wt%. The preparation involved mainly two different support type: SiO_2 and SiO_2-Al_2O_3 with 13% of Al_2O_3. As regards to SiO_2, various silica with different surface area, pore diameter and pore volume were used as catalyst support. However the deeper characterization was focused mainly on silica Chrom catalysts. Other support taken into account were TiO_2, Al_2O_3, SiO_2-ZrO_2, SiO_2-TiO_2,…

Various techniques were employed for the characterization: AAS for the determination of copper loading, TPR, FT-IR of carbon monoxide, FT-IR of pyridine, EXAFS-EXANES, XRD and HRTEM.

On the basis of these analysis the differences between reduced and unreduced Cu/SiO_2 and Cu/SiO_2-Al_2O_3 catalysts prepared by CH and Cu/SiO_2 catalyst obtained by IW were debated. The knowledge acquired will be discussed, correlated and rationalized in the next chapters according to the catalytic data of the studied reaction.

Catalysts made with different preparation methods other than CH are always clearly marked (e.g. Cu/SiO_2 IW). If preparation method is not distinctly specified, Chemisorption-Hydrolysis should be implied.

Reduced catalysts are labeled as "Cu/support" (e.g. Cu/SiO_2), while unreduced ones as "CuO/support" or "CuO_x/support" (e.g. CuO/SiO_2 and CuO_x/SiO_2-Al_2O_3). However the label "Cu/support" can simply indicate a generic catalyst, or a class of catalysts (reduced or not), if in the specific context is not necessary to underline the pretreatment conditions (e.g. a general behavior).

2.2 Experimental

Chemicals

All reagents were purchased from Aldrich and used without further purification.

Supports

Supports were purchased and used without further purification. Table 2.2 reports specific surface area, pore volume and pore diameter of the main supports used in this work.

Support	SSA (m^2/g)	PV	DP_{av} (A)
SiO$_2$ 332	313	1.79	114
SiO2 Chrom	480	0.75	60
SiO$_2$ 360	564	0.99	35
SiO$_2$ MP04300	723	0.66	38
SiO$_2$ MP15300	297	1.29	156
SiO$_2$ MP25300	201	1.34	251
SiO$_2$ MP09300	478	1.04	86
SiO$_2$ MP20300	255	1.06	193
SiO$_2$ MI300	681	0.33	20
SiO$_2$ SP550-10022	330	1.2	-
SiO$_2$-Al$_2$O$_3$ 13 (13% of Al$_2$O$_3$)	485	0.75	37

Table 2.2. Features of main supports used in this thesis.

Preparation of copper catalysts

Chemisorption-Hydrolysis catalysts were prepared using the following procedure. The support powder was added to a $[Cu(NH_3)_4]^{2+}$ solution prepared by dropping aqueous NH$_3$ (28%) to a

$Cu(NO_3)_2 \cdot 3H_2O$ solution until pH 9 had been reached. After 20 min under stirring, the slurry, held in an ice bath at 0 °C, was slowly diluted in order to allow hydrolysis of the copper complex and deposition of the finely dispersed product to occur. Under these conditions, no dissolution of silica was detected. The solid was separated by filtration, washed with 0.5 L of water, dried in oven overnight at 120 °C, and calcined in static in air at 350 °C for 4 h. The amount of $Cu(NO_3)_2 \cdot 3H_2O$ was regulated in order to obtain, as each case required (as needed), a copper loading ranging between 1 and 15 wt%.

The Incipient Wetness sample was prepared by impregnating the support with a copper nitrate solution of proper concentration and volume in order to obtain a 8.5 % and 15% loaded catalyst.

AA Spectroscopy

Cu loading was determined by Atomic Absorption Spectroscopy (Atomic Absorption Spectrometer 3100 – PerkinElmer; flame: acetylene/air) and an external calibration methodology, after microwave digestion of about 20 mg of oxidized sample in 3 ml of HNO_3.

Temperature Programmed Reduction (TPR)

TPR profiles were recorded with a modified version of the Micromeritics Pulse Chemisorb 2700 apparatus equipped with a thermal conductivity detector (TCD). The samples (25 mg) were diluted with an equal amount of quartz, calcined at 500 °C under O_2 (40 mL/min) for 1 h and then reduced at 8 °C/min with a 8% H_2/Ar mixture at 15 mL/min. The rate of hydrogen uptake was measured by an HP 3396A integrator.

FT-IR of adsorbed CO

For FT IR studies, pure SiO_2 support, 9% and 15% Cu on silica Chrom powdered catalysts have been pressed in self supporting disks (average weight 30 mg), reduced in pure hydrogen (270 °C or 500 °C, 400 torr) and outgassed at the same temperature directly in the IR cell connected to a gas manipulation apparatus. CO adsorption was performed at liquid nitrogen temperature (-140 °C) by the introduction of a known amount of gas (around 10 Torr). FT-IR spectra have been recorded outgassing at increasing temperature in the range –130 °C/room temperature at decreasing CO coverage, until coverage = 0. The spectra were recorded with Nicolet Magna 750 and Nexus

instruments with a resolution of 4 cm^{-1}. Deconvolution spectra have been obtained using OMIC software (type of band Gaussian-Lorentzian, no fixed baseline, range 2230-2080 cm^{-1}).
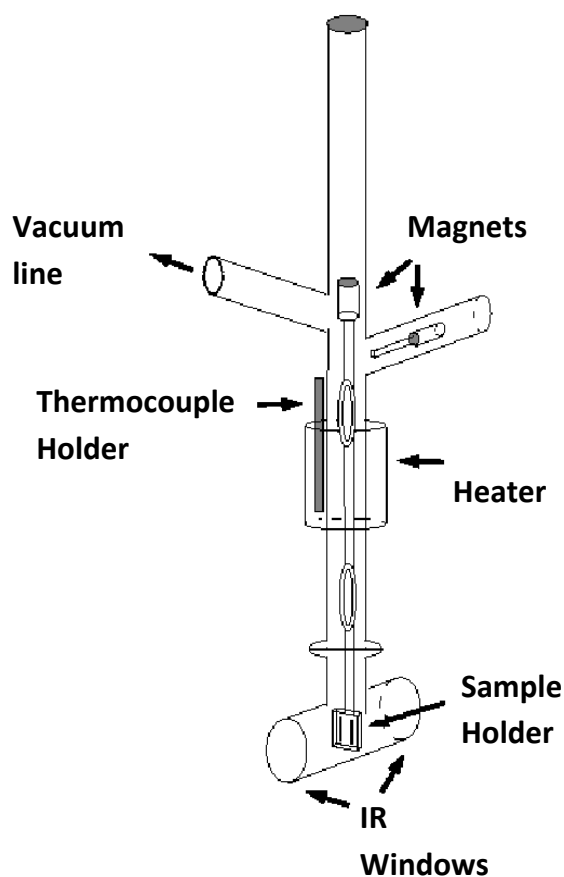
Figure 2.3. IR cell connected to a gas manipulation apparatus.

FT-IR of adsorbed Pyridine

The FT-IR studies of pyridine adsorption and desorption were carried out with a BioRad FTS40 spectrophotometer equipped with mid-IR DTGS detector.

The experiments were performed on sample disk (15-20 mg) after eventual pre-treatment (dehydration: 270 °C, 20 min air + 20 min vacuum; reduction: 270 °C, 20 min air + 20 min vacuum + 2 min H$_2$) and pyridine adsorption at room temperature. Following desorption steps were carried out for 30 min at various temperature (from room temperature to 250 °C). All spectra were recorded at room temperature after pyridine desorption at each temperature and one spectrum was collected before pyridine adsorption.

EXAFS-XANES analysis

Cu K-edge extended X-ray adsorption fine-structure (EXAFS) and near-edge X-ray adsorption structure (XANES) measurements were carried out at the XAFS beamline of the ELETTRA synchrotron (Basovizza-Trieste, Italy), in transmission goemetry using a Si(111) and Si(311) double crystal monochromator. EXAFS spectra, recorded over an energy range of 1 keV with a sampling step of 1 eV, have been measured at least three times, in order to perform the statistical analysis and to average the extracted EXAFS signals. XANES spectra have been recorded with a 0.25 eV energy sampling step. The ex-situ reduced samples were loaded under inert atmosphere inside the sample holders. The oxidized samples have been loaded in air inside the Little-type transmission EXAFS-cell for in-situ treatments under controlled temperature and gas flow and reduced in-situ in a 10ml/min H_2 flow at 543 K for 1 hour. The spectra have been recorded at ambient temperature in flowing N_2. Also the aged catalysts, transferred to the EXAFS cell under inert atmosphere at the end of an ex-situ catalytic run, has been measured before and after in-situ reduction.

EXAFS data analysis was performed with the Ifeffit software package. A copper metal foil was used for calibration and as reference for the Cu-Cu contributions, CuO and Cu_2O for the Cu-O contributions. Experimental phase and amplitude functions have been calculated from the back-Fourier-transformed filtered peaks of the references sample spectra. Theoretical phase and amplitude functions for each pair has been calculated with the FEFF8 program [Mus91]. For the metal-metal pairs, the program gives a good agreement with the experimental functions.

The EXAFS spectra have been analysed in the typical k range from 2.7 to 15.7 Å-1. The R intervals for the peak extraction are indicated for every sample. The best fits of the extracted $k^3\chi(k)$ signals of the filtered back-transformed peaks were determined by a least-squares spherical curve fitting procedure, where the maximum parameter number is determined by the expression $N_{par}<2\Delta k\Delta R/\pi +2$ [Len80]. The parameter error bars were calculated from the experimental standard deviation derived from the averaging of the extracted $\chi(k)$ function [Has91]. The F test [Joy87] was applied when necessary to distinguish between fits of similar quality.

HRTEM analysis

The morphology and distribution of the supported metal particles were evaluated by HRTEM. The powder samples were further ground and dispersed in toluene in an ultrasonic bath. A drop of the suspension was deposited on a perforated carbon film supported on a copper TEM grid. The specimen, after solvent evaporation under vacuum, was inserted in the column of a ZEISS LIBRA

200FE HRTEM. Pictures were taken spanning wide regions of several support grains in order to provide a truly representative map of the catalyst system. Distribution histograms of metal particle fraction versus diameter were evaluated from about 200 to 350 counts per sample.

XRD analysis

X-ray powder diffraction patterns were recorded within the range of 10° to 70° 2θ, with a step of 0.02° 2θ and counting time 1 or 4 sec/step on Philips PW-3020 powder diffractometer Ni-filtered Cu Kα radiation. The peak of CuO (111) at 2θ=35.5° was used for line-broadening determinations. Copper oxide crystallite sizes were estimated using the Scherrer equation.

2.3 Results and Discussion

TPR analysis

Temperature reduction profile of copper catalysts are reported in this section. The reduction peaks were assigned to $Cu^{2+} \rightarrow Cu^{0}$ one step reduction and to the reduction of strongly interacting with the support copper species with an oxidation state in the range between 1 and 2 [1, 33, 34].
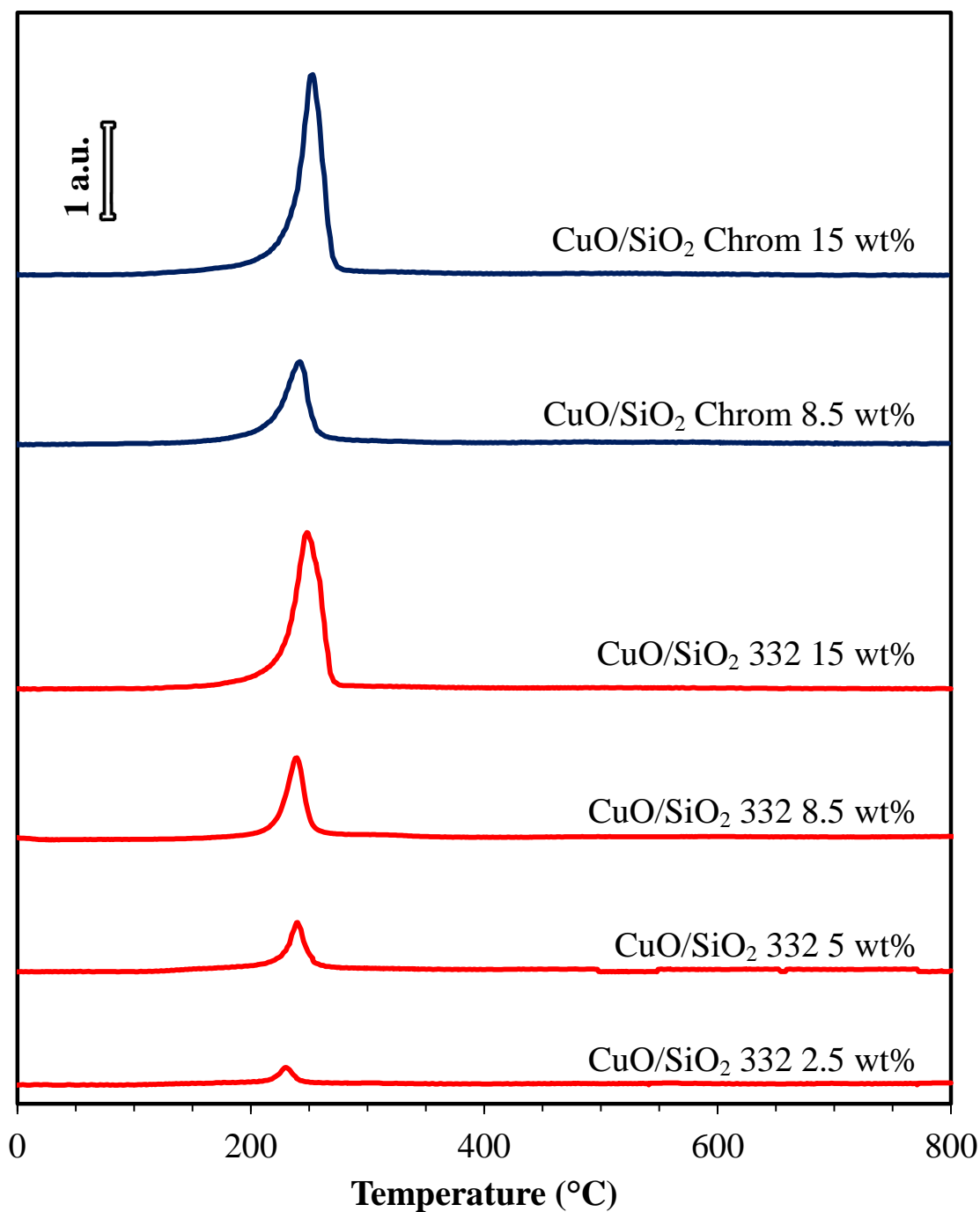
Figure 2.4. TPR profiles of CuO/SiO$_2$ Chrom and 332 with different copper loading made by CH.

Figure 2.4 reports the TPR profiles of Chrom and 332 copper silica based catalysts prepared by CH. TPR profiles of silica based catalysts show the presence of one single sharp symmetric peak centered around 240 °C. The increase of copper loading does not result in a significant shift in the peak maximum, that remains almost unchanged. On the other hand, as we expected, peak area increases. SiO_2 support does not have an important influence on copper reduction temperature, as shown by the comparison of TPR analysis of SiO_2 Chrom, SiO_2 332 (Figure 2.5) and other silica used (profiles not reported). Based on the literature, such a low temperature is diagnostic of the presence of a highly dispersed copper oxide phase in a single and reducible state, suggesting that small and well-dispersed CuO particles, easily reducible into metallic Cu small particles by treatment with H_2, are produced on catalyst surface after calcination. The reduction of CuO bulk starts indeed at low temperature (around 190 °C), with the maximum shifted to 276 °C due to the broadness of the whole peak, related to CuO dimension. On the contrary CuO/SiO_2 (IW) is less easily reducible (T_{max} = 332 °C) due to the presence of species strongly interacting with the support (Figure 2.6).
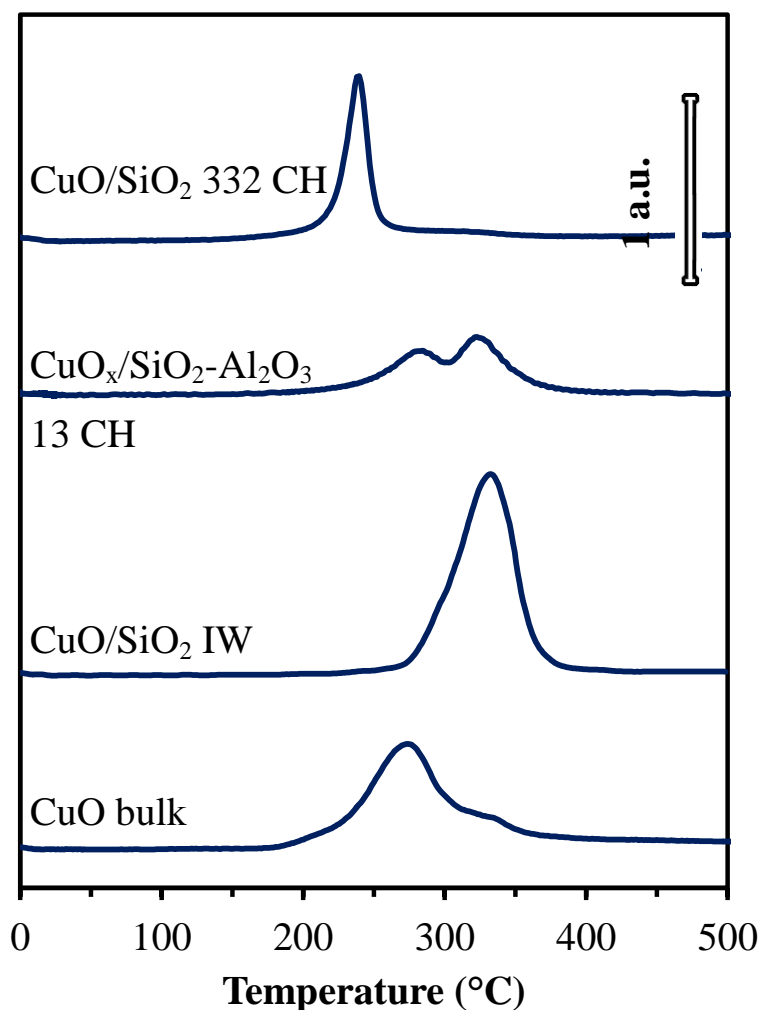
Figure 2.5. TPR profiles of different 8.5 wt% copper catalysts and CuO bulk.

The formation of a CuO phase was also confirmed by XRD (see further) and is well reported in literature [1, 35-37].
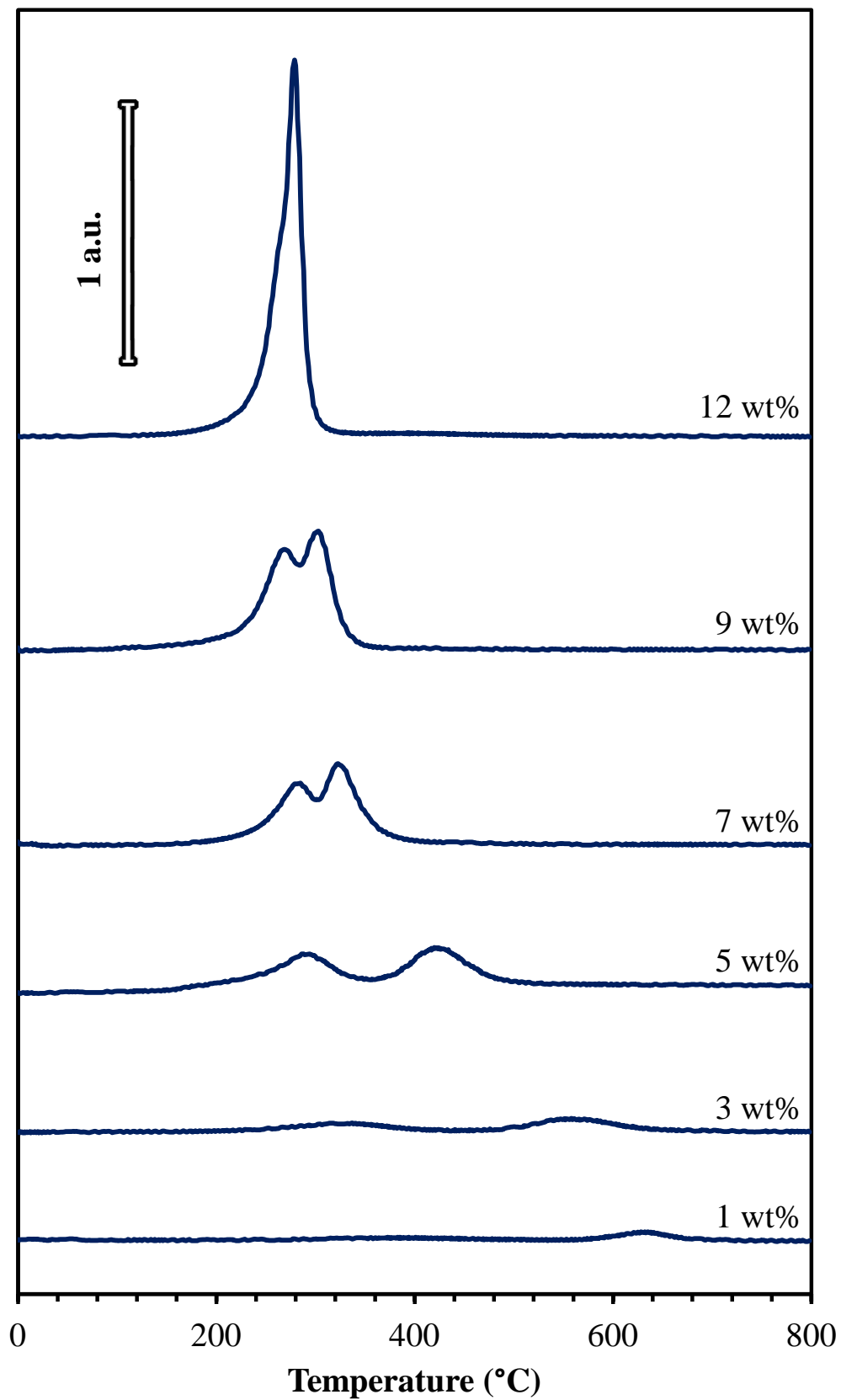
Figure 2.6. TPR profiles of different loading CuO_x/SiO_2-Al_2O_3 CH catalysts.

TPR profiles of Cu/SiO$_2$-Al$_2$O$_3$ 13 (Figure 2.6) indicate a very different situation. Low loading copper samples show high temperature reduction peaks (over 400 °C), hardly detectable because of the low copper content. However, in reduction profile of 5 wt% catalyst two broad peaks are clearly visible: one around 288 °C and another one around 422 °C. The peak referred to the higher temperature can be assigned to the reduction of CuO$_x$ in strong interaction with the support (Cu-aluminate-like phase), while low temperature one to the reduction of a Cu (II) species. The easy reducible fraction of metal increases with the amount of copper and CuO$_x$/SiO$_2$-Al$_2$O$_3$ 13 12 wt% shows a single narrow peak (with a small shoulder) centered at 277 °C. The TPR results are in good agreement with the literature, where oxidized 8 wt% CuO$_x$/SiO$_2$-Al$_2$O$_3$ is mainly composed of isolated copper species hardly reducible, with an oxidation state ranging from (II) to (I) [23], though this sight, in our case, appears more suitable for lower copper loading.

Therefore TPR analysis put in evidence distinctly that low loading silica and silica-alumina Cu catalysts expose a very different copper phase, while the differences were attenuated at high loadings. This was also confirmed by the different activity of the two materials. We reported, for example, the hydrogenation of 3-methylcyclohexanone to the corresponding alcohols. In this reaction 8 wt% Cu/SiO$_2$ catalyst reduced at 270 °C revealed outstanding performances (better rate and productivity) than the analogous on SiO$_2$-Al$_2$O$_3$ [1]. However similar TOFs per exposed metal site for the two catalysts were found. In fact, the proposed active site for the hydrogenation is Cu (0): as we expected, in the case of Cu/SiO$_2$-Al$_2$O$_3$ the metallic copper specific surface area measured by N$_2$O chemisorption is significantly lower than the one measured for Cu/SiO$_2$, as a consequence of the low reduction extent of copper on silica-alumina support.

EXAFS-XANES analysis

XANES spectra of CH reduced catalysts indicate the presence of metallic copper on the surface, while the spectra of fresh samples reveal the presence of a Cu (II) oxide phase. In Figure 2.7 are reported XANES measurements of two catalysts chosen as example (Cu/SiO$_2$ MP09300 15 w% and SP550-1002 8.5 wt% fresh and reduced). Table 2.3 reports the curve fitting results of the Cu K edge EXAFS data. The estimation of particle size on in situ reduced samples show that very small particles are formed on catalysts surface (size between 1.5 and 3.4 nm). Silica supports appears to have no influence on the formation of copper phase: all fresh catalysts expose CuO, whereas reduced ones Cu (0). The increase of copper loading has an effect only on copper nanoparticle size (e.g. Cu/SiO2 Chrom from 1.7 to 2.8 nm). These results are in agreement with the literature [38].

Catalyst	Shell	CN	R(Å)	$\Delta\sigma(\oplus)$	$\Delta E_o(\varepsilon\varsigma)$	D (Å)
Cu/SiO$_2$ 332 15 wt%	Cu	10.1±0.3	2.551±0.002	0.073±0.001	0.7±0.1	34
Cu/SiO$_2$ Chrom 15 wt%	Cu	9.6±0.3	2.551±0.002	0.074±0.001	1.1±0.1	28
Cu/SiO$_2$ MP09300 15 wt%	Cu	9.7±0.3	2.541±0.002	0.073±0.001	0.7±0.1	30
Cu/SiO$_2$ 332 8.5 wt%	Cu	8.6±0.9	2.549±0.015	0.078±0.013	-1.9±0.8	19
Cu/SiO$_2$ Chrom 8.5 wt%	Cu	7.6±0.1	2.560±0.001	0.074±0.001	-0.3±0.1	17
Cu/SiO$_2$ MP20300 8.5 wt%	Cu	10.1±0.3	2.551±0.002	0.073±0.001	0.7±0.1	34
Cu/SiO$_2$ MP25300 8.5 wt%	Cu	9.08±0.2	2.551±0.001	0.076±0.001	0.05±0.01	32
Cu/SiO$_2$ MI300 8.5 wt%	Cu	7.03±0.1	2.538±0.002	0.076±0.001	-1.8±0.7	15
Cu/SiO$_2$ SP550-10022 8.5 wt%	Cu	9.6±0.3	2.551±0.002	0.074±0.001	1.1±0.1	28
Cu/SiO$_2$ MP09300 8.5 wt%	Cu	8.02±0.3	2.550±0.002	0.074±0.002	0.05±0.2	18

Table 2.3. Curve fitting results of Cu K edge EXAFS data (at the end of in situ reduction, first Cu–Cu shell) of reduced Cu/SiO$_2$ CH catalysts.
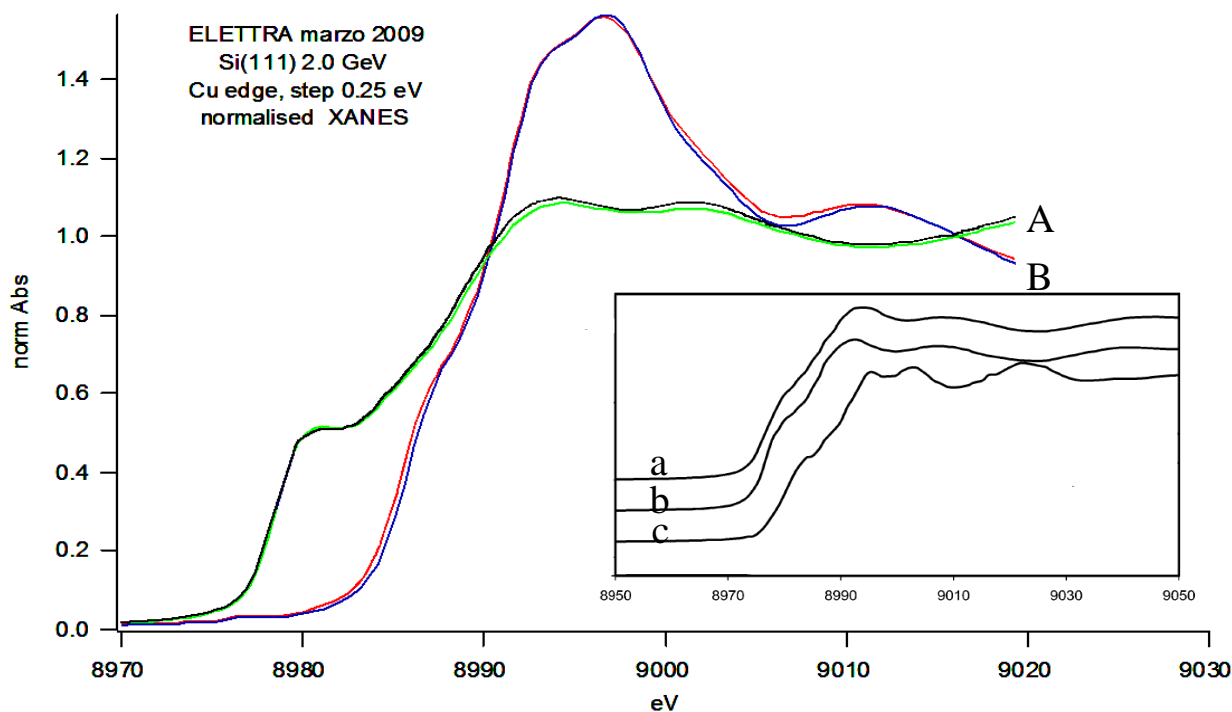
Figure 2.7. XANES spectra of CH catalysts: (A) CuO/SiO$_2$ MP09300 15 wt% - red, CuO/SiO$_2$ SP550-10022 8.5 wt% - violet; (B) Cu/SiO$_2$ MP09300 15 wt% - black, Cu/SiO$_2$ SP550-10022 8.5 wt% - green. Inset: (a) CuO; (b) Cu$_2$O; (c) Cu foil.

HRTEM analysis

HRTEM image (Figure 2.8) of 8.5 and 15 wt% CuO/SiO_2 Chrom were recorded. Related histograms are also reported (Figure 2.9).
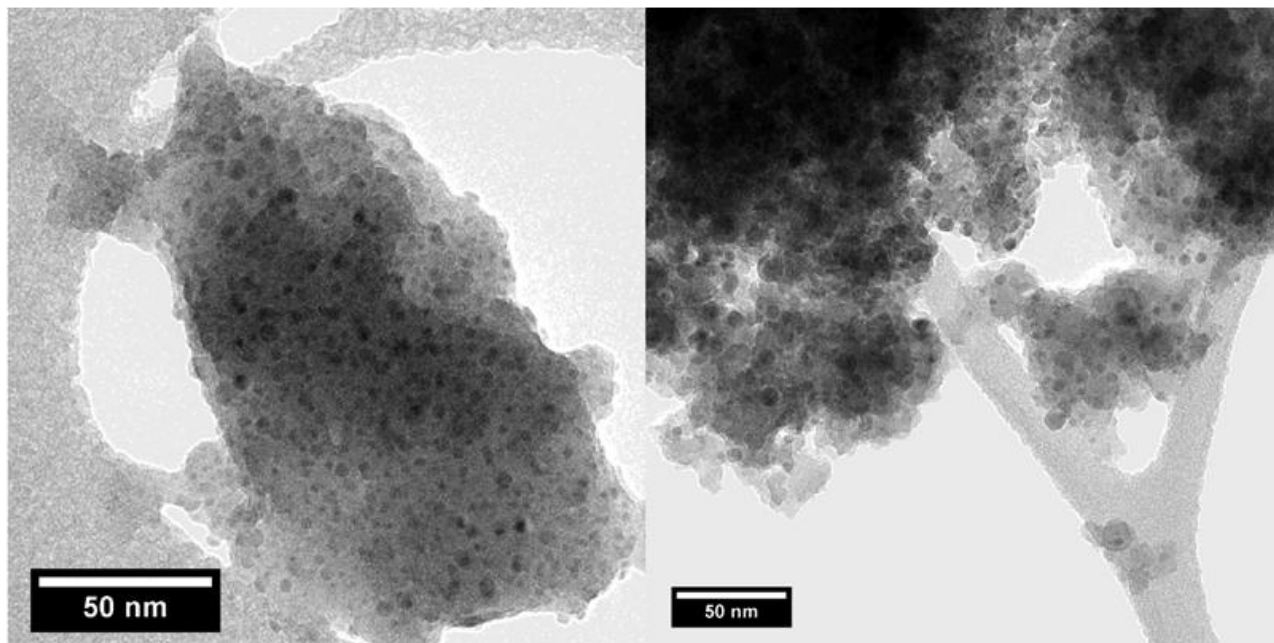
Figure 2.8. HRTEM of CuO/SiO_2: left – 8.5 wt%; right – 15 wt%.
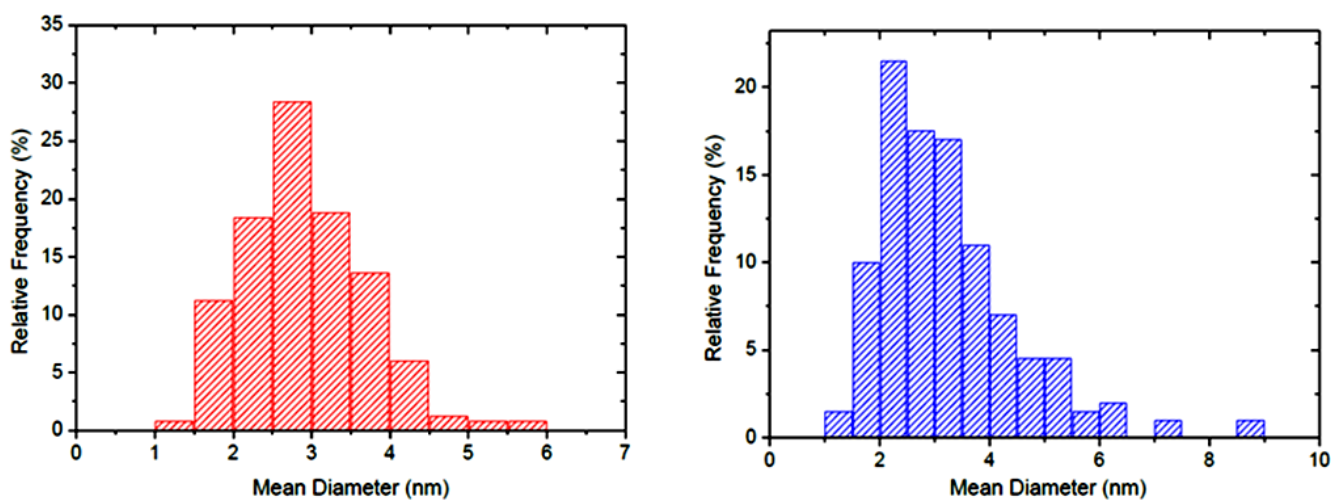
Figure 2.9. Histograms of CuO/SiO_2: left – 8.5 wt%; right – 15 wt%.

The mean diameter of nanoparticles is 2.9 nm for low loading samples and 3.2 nm for high loading one: these results differs from those estimated by EXAFS (1.7 nm and 2.8 nm), especially for the 8.5 wt% catalysts . We ascribe this fact to the different condition and intrinsic properties of two different analysis: before EXAFS measurements samples were reduced in situ under hydrogen

atmosphere at 270 °C, while during TEM the sample gets in contact with atmospheric air during the deposition on carbon film (thus fresh sample were used) and the reduction occurs under electron beam. Since the EXAFS reduction condition are closer to those used for the catalytic experiments (see in particular Chapter 3 and 4), we considered more trustworthy the size obtained from this analysis. Moreover very small nanoparticles can be most hardly detectable during TEM count, whereas EXAFS can provide a better estimation of smaller particles: it does not seem to be a coincidence that the size differs much more for the smaller crystals (8.5 wt% catalyst). Finally, as reported later, FT-IR spectra of adsorbed carbon monoxide suggests that the in situ reduced 8.5 wt% catalyst is composed mainly from zerovalent copper cluster (thus very small particles), instead of well structured particles. In any case, TEM measurements confirm the high dispersion of CH samples.

XRD analysis

XRD patterns of 15% CuO/SiO_2 Chrom IW indicates the reflections typical of CuO only for IW sample, while no significant reflections are registered in the spectrum of 15 wt% CuO/SiO_2 Chrom CH catalyst collected in same condition ($2\theta = 10°-70°$, 2θ step=0.02°, 1 sec/step), suggesting that either the structure of copper species is amorphous or their size is very small.
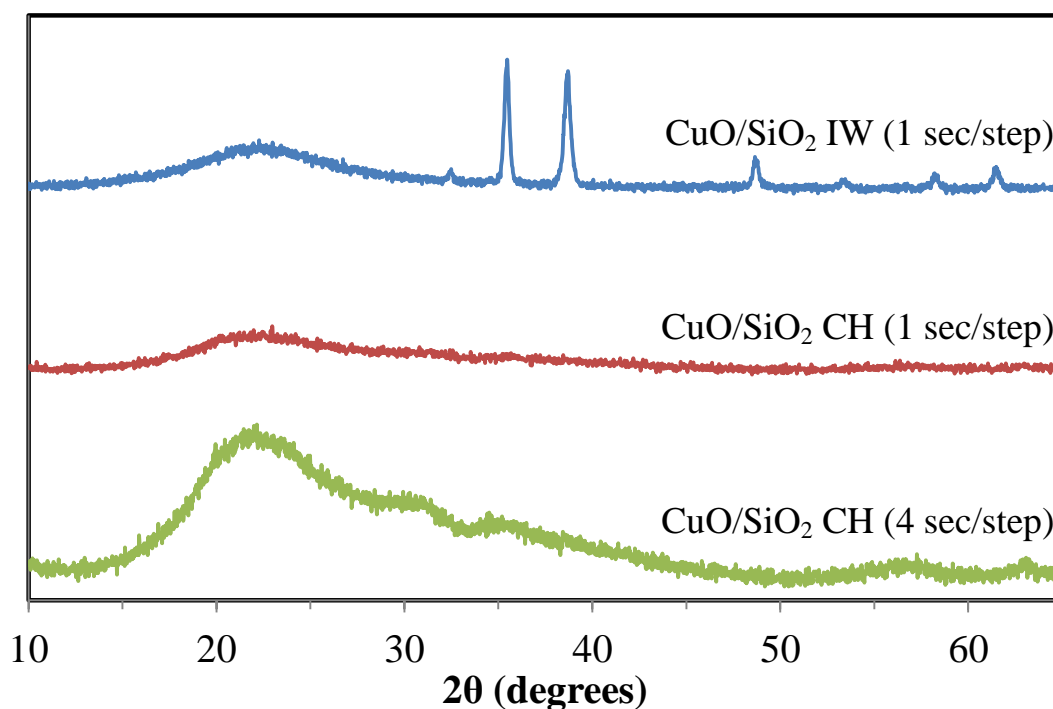
Figure 2.10. XRD spectra of 15 wt% CuO/SiO_2 Chrom catalysts.

However, an increase on the counting time (from 1 to 4 sec/step) results in a very broad signal, due to finely dispersion of copper on CH sample, in agreement also with TEM and EXAFS analysis.

On the other hand, the estimated mean particle size for IW catalyst is of 34 nm. From these results, we can assert that CH method allows to keep an high dispersion even at very high metal loading, while a classic impregnation method, such as IW, generates more than ten-times bigger particles. We performed XRD analysis also on other silica catalysts prepared by CH and IW obtaining similar results [39, 40].

FT-IR of adsorbed CO

The adsorption of CO molecule on reduced Cu/SiO_2 Chrom CH catalysts 8.5 and 15 wt% was studied. FT-IR spectra were recording starting form CO adsorption at −130 °C and following progressive warming until room temperature. In Figure 2.11 spectra of the surface species arising from CO adsorption over the reduced 8.5 wt% sample are reported (reduction temperature 500 °C).
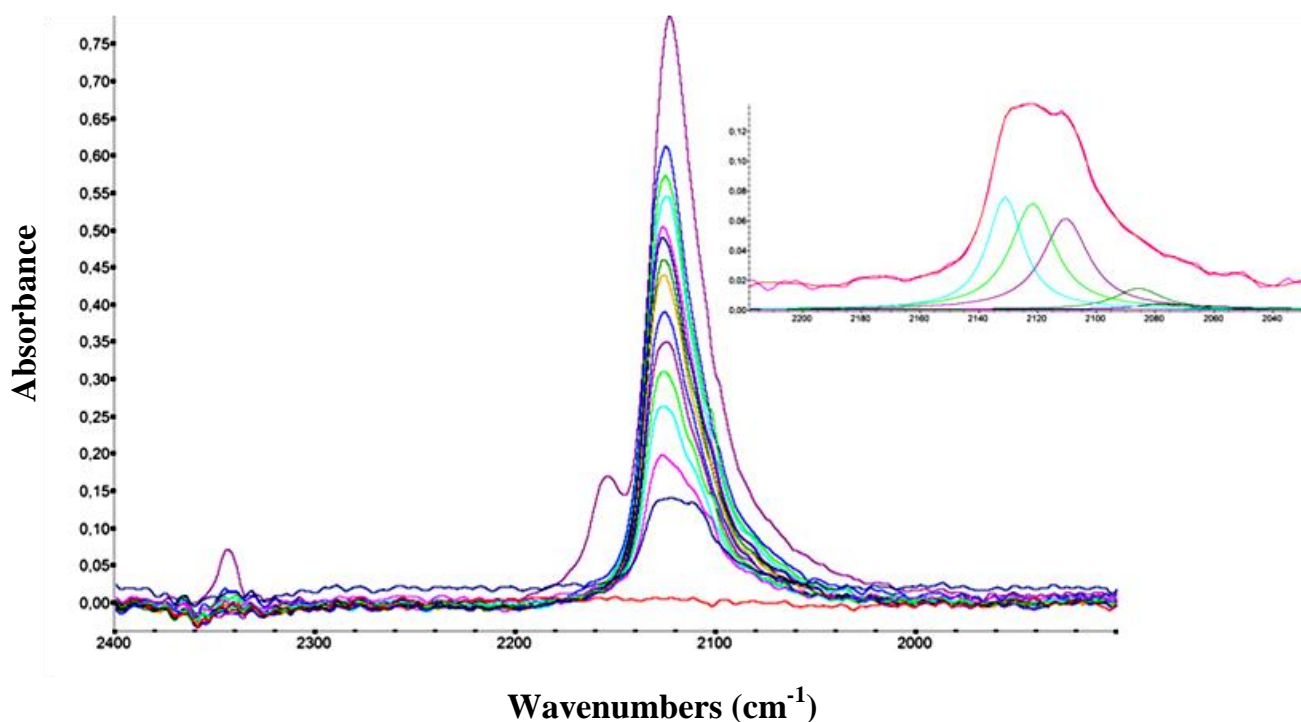
Figure 2.11. FT-IR spectra of Cu/SiO_2 Chrom 8.5 wt% reduced at 500 °C. Inset: deconvolution of the band at 2120 cm^{-1}.

All the bands disappear between 0°C and room temperature. At high CO coverage three main bands can be detected: one at 2354 cm^{-1} and strong one at 2120 cm^{-1} with a shoulder at 2154 cm^{-1}. The first band is certainly due to CO_2 physisorbed at the catalyst surface (OCO deformation mode). The

band centered at 2154 cm^{-1} can be assigned to CO interacting with the support OH groups, corresponding to a weak negative band in the subtraction spectrum in the OH stretching spectral region. Another possible assignation is to carbonyl species coordinated over residual Cu^{2+} ions, characterized by bands in the range 2180-2150 cm^{-1} [23, 41, 42]. Following outgassing this band disappears almost immediately, confirming its assignation to species weakly bound. At the same time, the band due to adsorbed CO$_2$ slightly increases, likely due to the CO oxidation from residual Cu ions [43].

The assignment of the band at 2120 cm^{-1} due to CO interacting with copper centers is more complex and widely discussed in the literature. Following results reported by several authors on CO adsorption over Cu-supported catalysts, the strong band centred at 2120 cm^{-1} asymmetric towards lower frequencies has been assigned to CO linearly bound to Cu^{+} centers [42, 43], but also to CO coordinated over Cu metal particles [44]. In particular, for Cu/SiO$_2$ and Cu/TiO$_2$ systems, Boccuzzi et al. suggested the attribution of the band at 2128 cm^{-1} to CO adsorbed over flat 2D Cu metal particles, strongly interacting with the support, on the basis of the decreased resistance to outgassing. Bands at lower frequencies (2100-2090 cm^{-1}) have been assigned by the same authors to CO adsorbed over metallic copper in more structured microparticles, exposing steps and well defined facets. Over alumina supported Cu catalyst, Escribano et al. assigned a strong band at 2115 cm^{-1} to carbonyls on copper ions or copper zerovalent clusters (which should correspond to the previously mentioned two dimensional metal cluster) and another component centred at 2100 cm^{-1} and tailing towards lower frequencies to terminal carbonyls on copper zerovalent particles [45]. This assignation has been supported also by the different stability of these species to outgassing: it is in fact well know that carbonyls on reduced Cu adsorbs weakly [46]. In the inset in Figure 2.11 we reported the deconvolution spectra for the band centered at 2120 cm^{-1}. Clearly, several components appear at 2130, 2121, 2109, 2086 cm^{-1} and even at lower frequency. Keeping in mind the literature data discussed above, we propose the following assignations: bands in the range 2130-2120 cm^{-1} characterizing carbonyls over Cu^{+} ions, in partial disagreement with Boccuzzi et al. [44], who proposed the assignation of all the band in this range to zerovalent copper clusters; band around 2100 cm^{-1} assigned to carbonyls over zerovalent Cu clusters, i.e. 2D particles strongly interacting with the surface, as reported by Dandekar et al. [42]; components below 2100 cm^{-1} to CO coordinated over zerovalent copper in structured microparticles. The detection of a component at 2086 cm^{-1} is in agreement with the presence of carbonyl species over metal Copper particles exposing (111) crystallographic planes.

The reduction of Cu/SiO$_2$ Chrom 8.5 wt% in hydrogen at lower temperature (270°C) leads to the detection of almost the same band pattern, although the intensity of the band at 2120 cm^{-1} is almost

halved (Figure 2.12). Furthermore, in the deconvolution spectra components below 2100 cm^{-1} are not evidenced, but the subtraction of the spectrum recorded at 0 °C to that one recorded at – 120 °C (Figure 2.12, inset) highlights a component at 2086 cm^{-1} (together with adsorption bands at frequencies higher than 2100 cm^{-1}) assignable to structured nanoparticles.

In Figure 2.13 spectra arising from CO adsorption over hydrogen reduced 15% Cu/SiO$_2$ sample are reported. A strong band centered at 2118 cm^{-1} and tailing toward lower frequencies is assigned to CO linearly coordinated over copper species. As discussed above, the deconvolution of this spectrum shows several components at 2125, 2115, 2104, 2093 and 2081 cm^{-1} corresponding to carbonyls adsorbed over residual Cu$^+$ ions, Cu zerovalent clusters (strongly interacting with the surface) and, below 2100 cm^{-1}, carbonyls over Cu zerovalent structured nanoparticles, mostly exposing (111) planes.
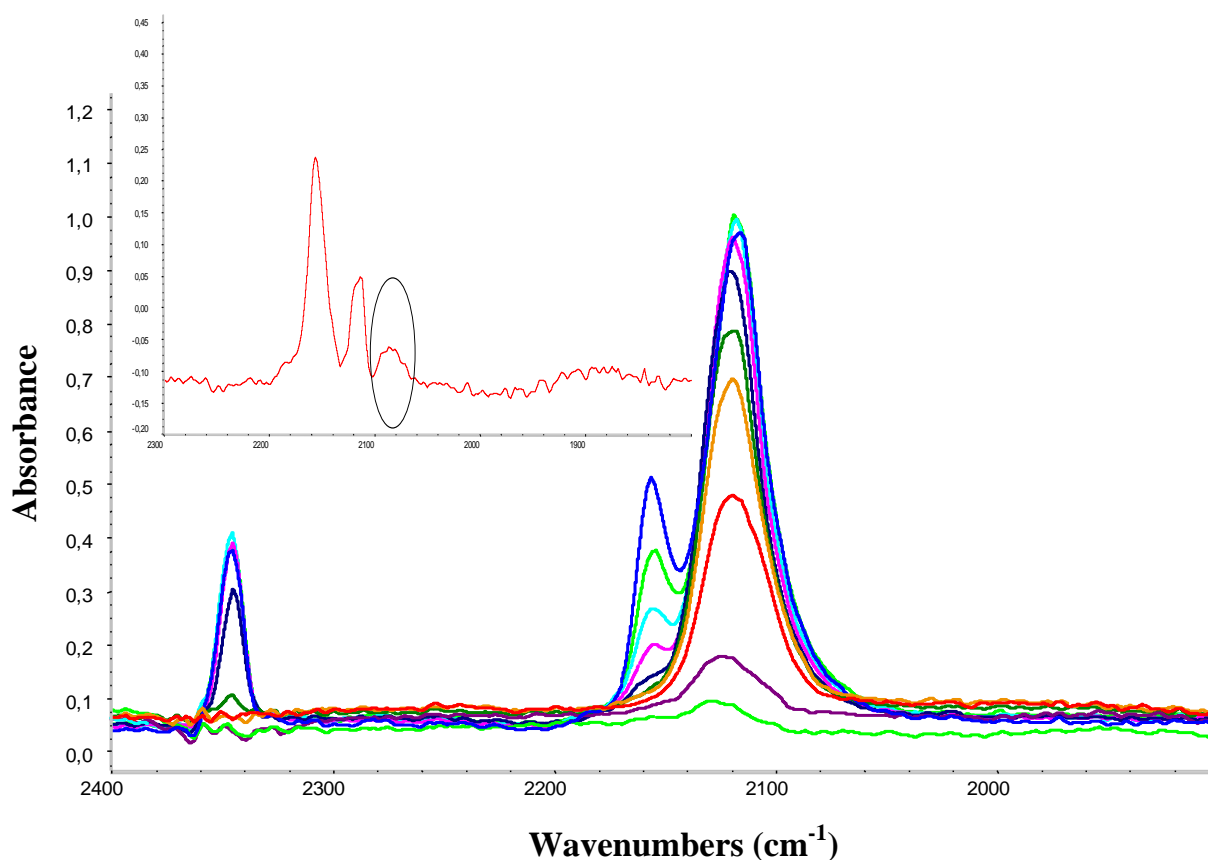
Figure 2.12. FT-IR spectra of Cu/SiO$_2$ Chrom 8.5 wt% reduced at 270 °C. Inset: subtraction of the spectrum recorded at 0 °C to that one recorded at – 120 °C.

From the comparison of reduced (T=270 °C) Cu/SiO$_2$ Chrom 8.5 and 15 wt% spectra appears that both the samples show the presence of residual Cu ions dispersed at the surface, zerovalent copper clusters and a fraction of more structured copper particles, exposing low index planes. However

structured particles are largely present on 15 wt% sample, whereas they are only hint on 8.5 wt% sample, which, instead, is composed mostly of zerovalent clusters. The reduction of low loading sample at 500 °C slightly increases the fraction of well-formed particles; this phenomenon can be due to the sintering of copper crystals. In any case in our catalytic tests, when needed, the catalysts were reduced at 270 °C.

Finally, FT-IR data, in accordance with previous analysis, confirm that, in spite of the high copper content in these samples, a very well dispersed metal phase has been obtained. Interestingly, the FT-IR spectra of CO on 8 wt% $Cu/SiO_2-Al_2O_3$ 13 present a main band at 2158 cm^{-1}, without adsorption below 2100 cm^{-1} [23].
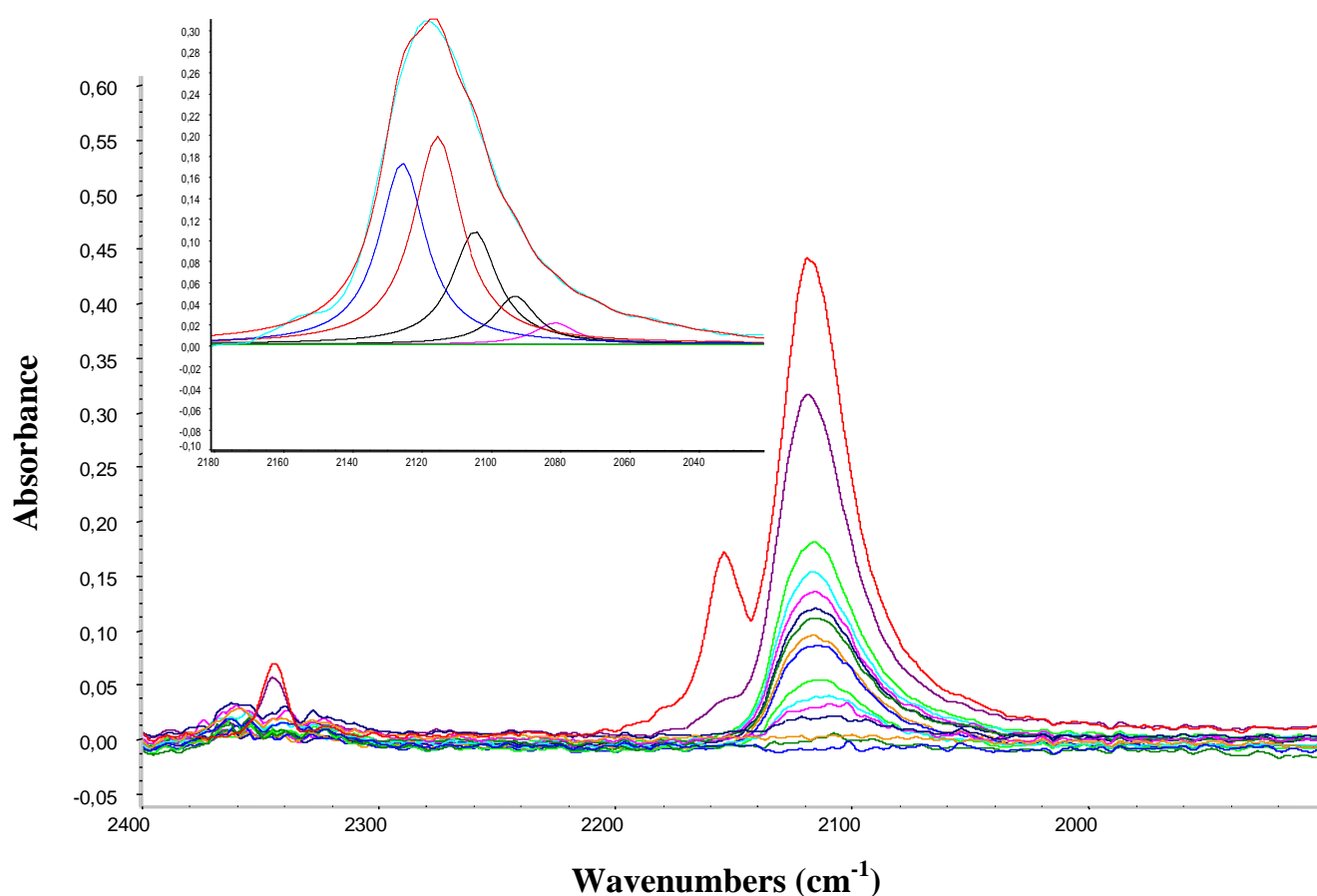
Figure 2.13. FT-IR spectra of Cu/SiO_2 Chrom 15 wt% reduced at 270 °C. Inset: deconvolution of the band at 2118 cm^{-1}.

FT-IR of adsorbed pyridine

Pyridine was chosen as probe molecule for the study of acid properties (detection of Lewis or Brønsted sites) of the studied material. In this investigation pyridine desorption spectra of the fresh

catalyst 15 wt% CuO/SiO$_2$ Chrom prepared by CH were compared with the spectra of dehydrated 15 wt% Chrom catalyst (vacuum at 270 °C) and of the reduced one (H$_2$ at 270 °C). Moreover we collected also spectra of bare SiO$_2$ Chrom support (fresh and dehydrated) and of 15 wt% CuO/SiO$_2$ Chrom made by IW.

As reported in the literature the FT-IR spectra of adsorbed pyridine show many peaks in the range of 1400-1700 cm^{-1}: bands around 1450 cm^{-1} and 1610 cm^{-1} can be assigned to pyridine bounded to Lewis acid sites, while absorption at 1550 cm^{-1} followed by other peaks near 1620 cm^{-1} and 1640 cm^{-1} is related to the presence of Brønsted acid sites. Finally a band around 1490 cm^{-1} is assigned to a combination of pyridine on Lewis and Brønsted acid sites. On the contrary, a weak interaction with the probe molecule (physisorption or hydrogen bond) results in an adsorption band in the range of 1440-1450 cm^{-1} followed by another one at 1580-1600 cm^{-1} [47-52].
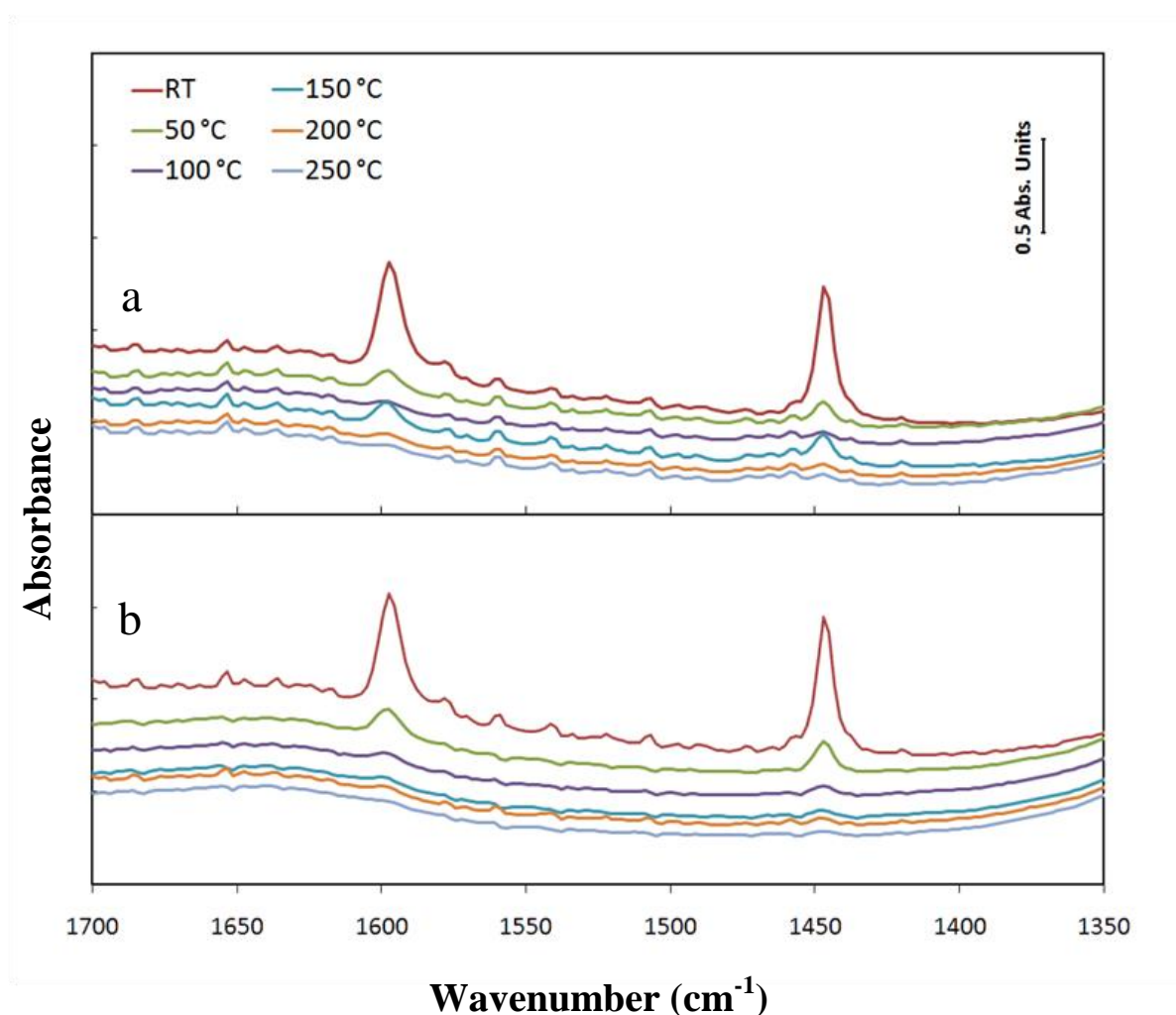
Figure 2.14. Desorption spectra of pyridine on: (a) fresh SiO$_2$ Chrom; (b) dehydrated SiO$_2$ Chrom.

The RT spectra of SiO_2 and dehydrated SiO_2 (Figure 2.14) show two characteristic peaks at 1447 cm^{-1} and 1598 cm^{-1} due to the physisorbed (or hydrogen bonded) pyridine to surface OH group of SiO_2 support. In fact, the outgassing at 50 °C leads to almost complete disappearance of this two bands, that are not clearly detectable at 100 °C, indicating only a weak interaction between the probe molecule and silica. Moreover, as clearly reported by Parry, the low shift of the band at 1440 cm^{-1} (present in free pyridine spectrum, ν_{19b}), to 1447 cm^{-1} is not large enough to indicate a Lewis interaction [53-55]. From the comparison of two spectra of SiO_2 Chrom we can observe that the dehydration does not result in any change in the pyridine absorption.
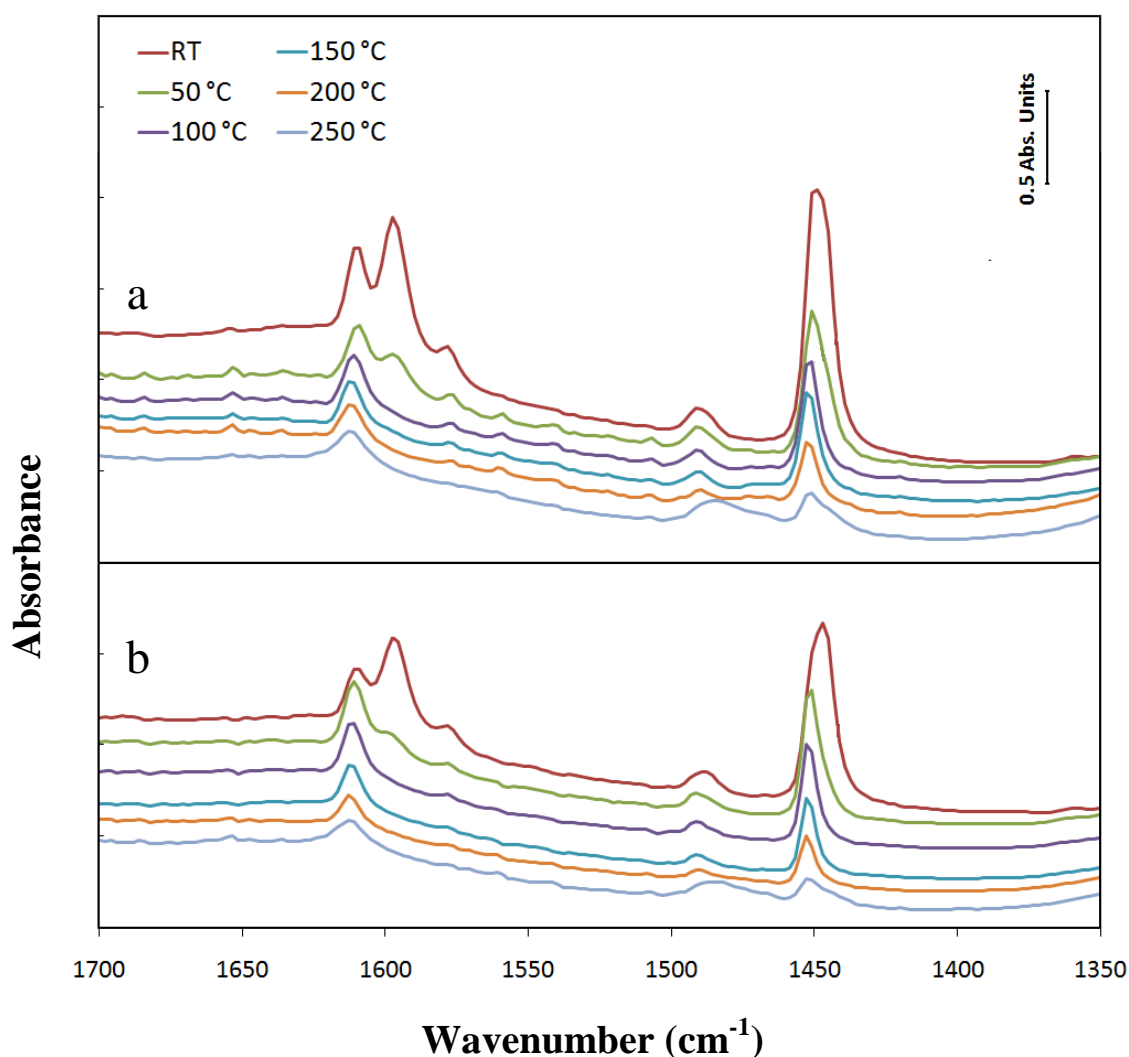
Figure 2.15. Desorption spectra of pyridine on: (a) fresh CuO/SiO_2 Chrom CH; (b) dehydrated CuO/SiO_2 Chrom CH.

Figure 2.15 shows the spectra of CuO/SiO_2 and dehydrated CuO/SiO_2 prepared by CH. The RT spectra show five main adsorption bands: an intense and broad one at 1449 cm^{-1}, two small peaks at

1488 and 1578 cm^{-1} and finally two intense peaks 1597 and 1610 cm^{-1}. The absorption at 1578 cm^{-1} is not very well characterized: Glen and Dumesic does not clearly distinguish this band between physisorbed pyridine or Lewis/Brønsted acid sites, while Parry assign an adsorption around these frequencies to a Lewis acid sites. On the other hand, as above mentioned, the band at 1488 cm^{-1} is not indicative of an specific acid site. By outgassing even at 100 °C the maximum of the broad band at 1449 cm^{-1} shifts to 1453 cm^{-1} indicating the presence of two component: physisorbed pyridine coming from the silica support (with maximum at 1446 cm^{-1}, as we seen before) and a strong absorption at 1453 cm^{-1}, due to the interaction with CuO. The evacuation results also in the desorption of the second physisorbed peak at 1597 cm^{-1}. Thus, in the spectrum recorded at 100 °C only bands at 1611 (slightly shifted respect to the same band at 1610 cm^{-1} at RT), 1488 and 1453 cm^{-1} are still present, both for fresh and dehydrated CuO/SiO$_2$. The bands at 1611 and 1453 cm^{-1} can be unambiguously assigned to pyridine adsorbed on Lewis acid sites, while peaks clearly corresponding to Brønsted acid sites are not visible (bands at 1550 cm^{-1}, 1620 cm^{-1} and 1640 cm^{-1} are totally absent). Moreover shape and adsorption frequencies of the CuO/SiO$_2$ spectra recorded at 100 °C (after physisorbed pyridine removal) resemble those of the spectrum of pyridine adsorbed on a classical Lewis acid (BH$_3$) presented by Yasuyuki at al. [56]. Again no important differences are seen for hydrated and dehydrated CuO/SiO$_2$ material.
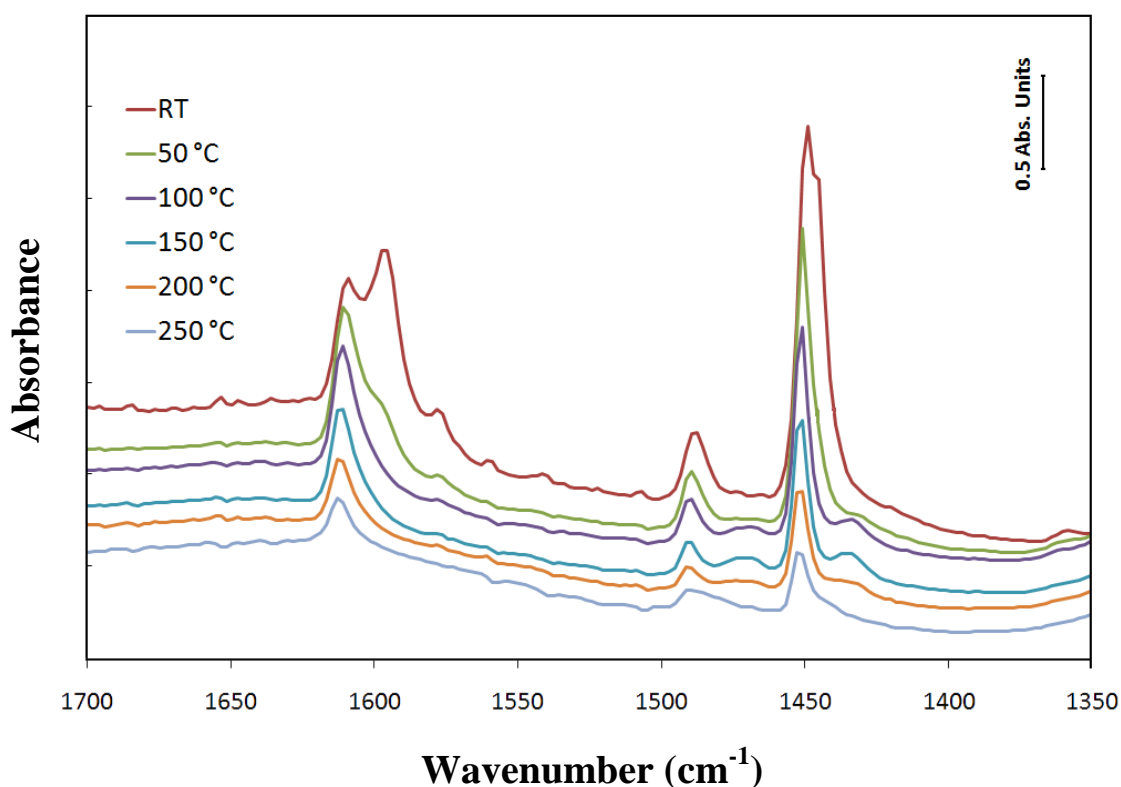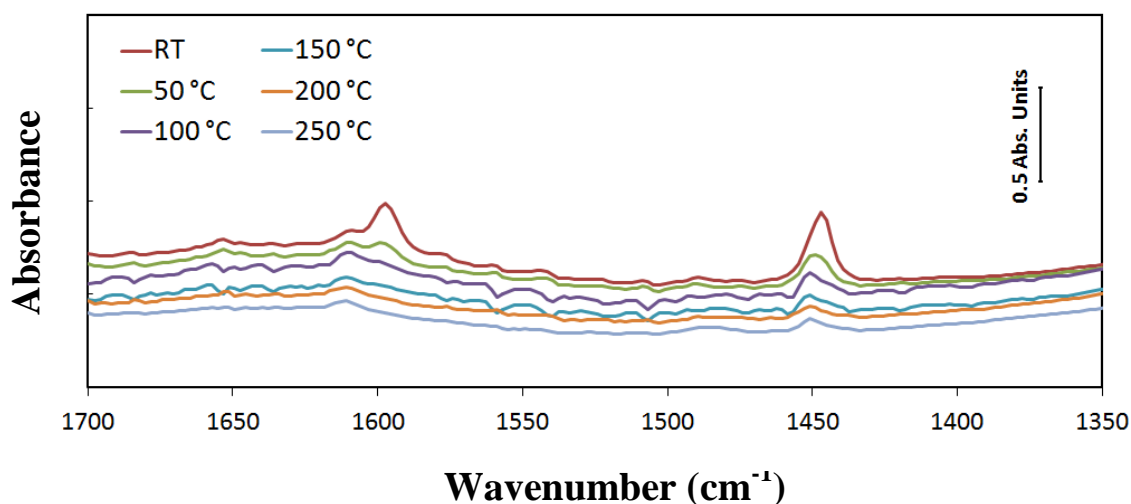

Figure 2.16. Desorption spectra of pyridine on reduced Cu/SiO$_2$ Chrom CH.

The spectra of reduced catalyst made by CH (Figure 2.16) does not show marked differences with fresh and dehydrate CuO/SiO_2 profiles: the adsorption bands kept after outgassing at 100 °C (or more) at 1453, 1488 and 1611 cm^{-1} are explainable with the presence of Lewis acid sites.

On the other hand desorption spectra of 15 wt% CuO/SiO_2 Chrom made by IW show only weak interaction with pyridine (Figure 2.17): the desorption is almost complete even at 100 °C, thus this sample does not show acidity. Figure 2.18 reports the comparison between pyridine desorption spectra (RT and 150 °C) of CH CuO/SiO_2, IW CuO/SiO_2 and SiO_2: this picture distinctly indicates how IW catalyst behaves like Chrom support.

The non-acid behavior of 15 wt% CuO/SiO_2 made by IW is attributed to the low dispersion of the material (as shown by XRD), while the high dispersion of the Chemisorption-Hydrolysis catalyst is responsible of the Lewis acidity. Very small CuO particles can be electronically unsatured in nature and/or the interaction with the support, even if weak, can influence the properties of copper phase. We further confirmed this surprising difference between CH and IW preparation method on 8.5 wt% copper silica catalysts obtained on different support other than Chrom (e.g. SiO_2 332, KIT and SBA, spectra not reported) [40].

Figure 2.17. Desorption spectra of pyridine on reduced CuO/SiO_2 Chrom IW.

If pyridine desorption analysis can again leave some doubts, in agreement with these experimental evidences we reported the acid catalyzed direct etherification of 4-methoxyphenylethanol with 2-propanol over CuO/SiO_2 CH catalysts [1]. Ether formation is traditionally performed with the Williamson reaction starting from an alcohol and a halide by using a strong base for the alkoxide formation. Nontheless, Brønsted acid catalysts are known to promote ether formation starting from the corresponding alcohols by means of a dehydration process [57]. In a recent communication, Sn-Beta has been reported as active heterogeneous Lewis acid for the asymmetric etherification of

benzylic alcohols and aliphatic ones [58]. The bare Chrom silica resulted to be completely inactive under the reaction conditions used (as confirmed also by pyridine desorption profile), whereas the unreduced copper catalyst supported over the same chromatographic silica is able to promote the condensation reaction with excellent selectivity and good activity (60% of conversion and 100% of selectivity after 5 h). The sample prepared by traditional Incipient Wetness technique with the same copper loading resulted to be almost inactive under the reaction conditions used, confirming the peculiar properties given by the particular preparation method used.

A similar behavior was recently reported, as previously discussed in the introduction of this chapters [30].

In conclusion, pyridine adsorption spectra clearly indicate the presence of Lewis acid sites on both CuO/SiO_2 and Cu/SiO_2, while the formation of Brønsted acid site can be excluded. The dehydration or the reduction do not appear to substantially modify the acidity of starting fresh material. Lewis acidity is attributed to high dispersion of the sample: low dispersed IW made material does not show any acid features. In the case of $Cu/SiO_2-Al_2O_3$ catalysts, the proper acidity of the support should not allows to separate the intrinsic acid character of small copper nanoparticles from that of $SiO_2-Al_2O_3$.
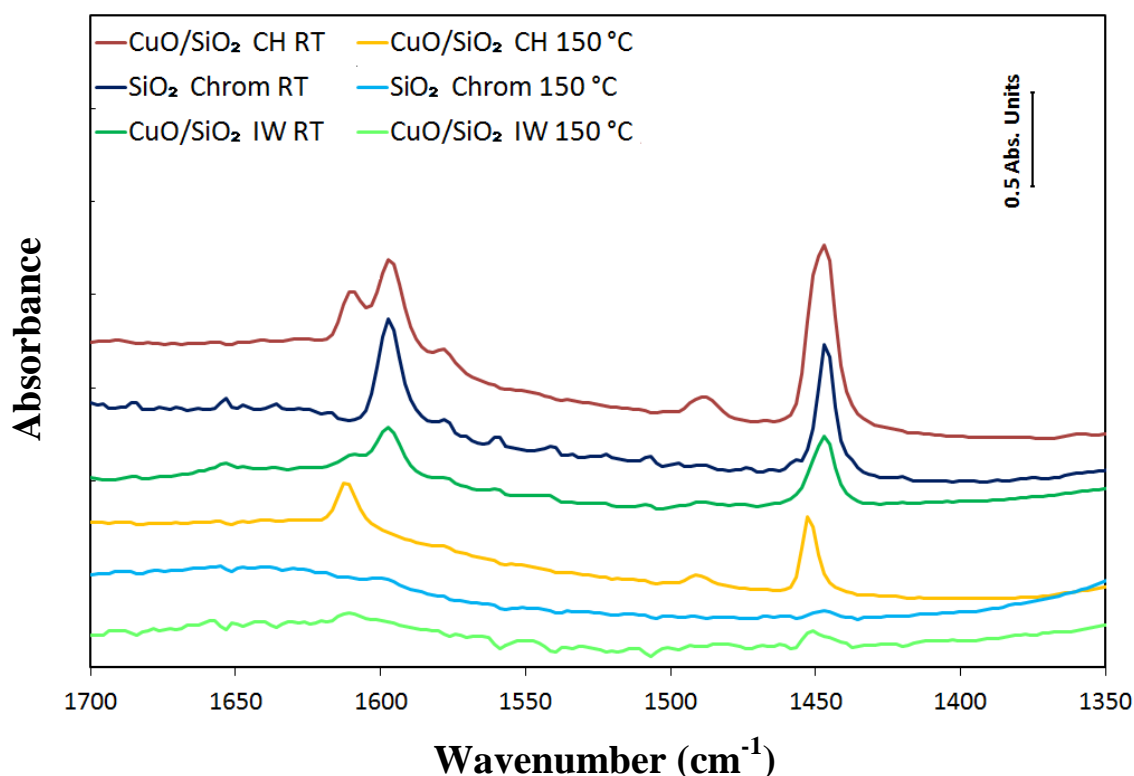
Figure 2.18. Desorption spectra of pyridine (RT and 150 °C) on CuO/SiO_2 CH, CuO/SiO_2 Chrom IW and SiO_2.

2.4 Conclusions

The behaviour Cu/SiO$_2$ catalysts can be outlined in Figure 2.19.
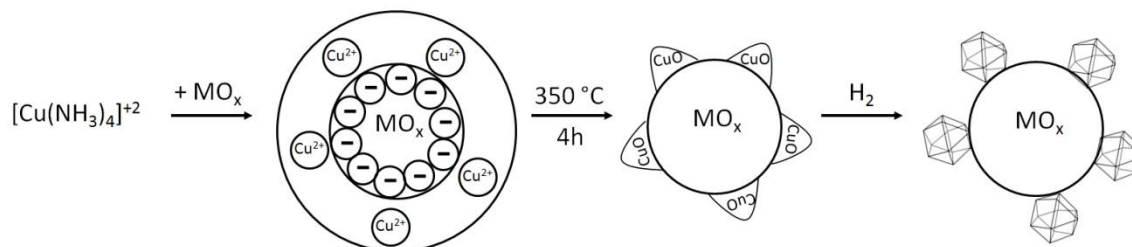
Figure 2.19. Cu/SiO$_2$ catalysts prepare by Chemisorption-Hydrolysis.

All the characterization technique agree with the formation of finely dispersed phase of CuO on silica, easily reducible to metal copper at any copper loading for CH samples. While unreduced silica catalyst shows acid properties, the metal copper nanoparticles formed after treatment with H$_2$ keep the acid feature but, as well reported in the literature, highlight also a good activity in hydrogenation reactions. The size of the particles, as estimated both by TEM and EXAFS analysis, is very small (between 1.5-3.5 nm) for all silica supports employed, even at high copper loading. Usually, literature reports that only low loading (1-5%) catalysts are active, because of the drop of dispersion as the amount of the metal increases. On the contrary Chemisorption-Hydrolysis method allows one to keep a great dispersion obtaining very small copper particles also to an high metal loading (up to 15%), with a potential beneficial effect on the productivity of the catalysts. The same catalyst prepared by Incipient Wetness presents very large copper crystals (34 nm as estimated by XRD). Lewis acidity appears to be truly a consequence of high dispersion: in fact materials made by IW does not show acid behavior both in pyridine adsorption and as catalyst in acid reactions. FT-IR spectra of adsorbed CO on reduced (270 °C) Cu/SiO$_2$ Chrom made by CH show the presence of well formed copper crystal exposing (111) facets on 15 wt% catalyst, while 8.5 wt% sample is composed mainly of small zerovalent clusters.

Cu/SiO$_2$-Al$_2$O$_3$ catalysts highlight a behavior which depends on the copper amount and influences catalytic properties: up to 5 wt% only hardly reducible Cu$^{\delta+}$ ($+1 \leq \delta \leq +2$) is formed on the catalyst, while after this loading a CuO phase easily reducible (at low temperature) to well formed Cu (0) crystallites begins to form on the surface.

2.5 Refereces

[1] N. Scotti, D. Monticelli, F. Zaccheria, Inorg. Chim. Acta (2011) doi:10.1016/j.ica.2011.10.001.

[2] I. Chorkendoff, J.W. Niemantsverdriet, Concepts of Modern Catalysis and Kinetics, Wiley-VCH Verlag GmbH & Co. KGaA, Weinheim, 2003.

[3] C.-J. Jia, F. Schüth, Phys. Chem. Chem. Phys. 13 (2011) 2457.

[4] M. Campanati, G. Fornasari, A. Vaccari, Catal. Today 77 (2003) 299.

[5] J. C. Park, J. U. Bang, J. Lee, C. H. Ko, H. Song, J. Mater. Chem. 20 (2010) 1239.

[6] M. A. Botavina, C. Evangelisti, Yu. A. Agafonov, N. A. Gaidai, N. Panziera, A. L. Lapidus, G. Martra, Chem. Eng. J. 166 (2011) 1132.

[7] G. W. Coates, Chem. Rev. 100 (2000) 1223.

[8] J. M. Thomas, R. Raja, D. W. Lewis, Angew. Chem. Int. Ed. 44 (2005) 6456.

[9] J. M. Thomas, R. Raja, Top. Catal. 40 (2006) 3.

[10] A. E. Aksoylu, J. L. Faria, M. F. R. Pereira, J. L. Figueiredo, P. Serp, J.-C. Hierso, R. Feurer, Y. Kihn, P. Kalck, Appl. Catal. A: Gen. 243 (2003) 357.

[11] H. O. Pierson, Handbook of Chemical Vapor Deposition, Second Edition, Noyes Publications/William Andrew Publishing, LLC Norwich, New York, U.S.A., 1999.

[12] C. Thurier, P. Doppelt, Coord. Chem. Rev. 252 (2008) 155.

[13] V. Dal Santo, F. Liguori, C. Pirovano, M. Guidotti, Molecules 15 (2010) 3829.

[14] X. Wang, P. Sonström, D. Arndt, J. Stöver, V. Zielasek, H. Borchert, K. Thiel, K. Al-Shamery, M. Bäumer, J. Catal. 278 (2011) 143.

[15] A. A. Ponce, K. J. Klabunde, J. Mol. Catal. A: Chem. 225 (2005) 1.

[16] G. Vitulli, M. Bernini, S. Bertozzi, E. Pitzalis, P. Salvadori, S. Coluccia, G. Martra, Chem. Mater. 14 (2002) 1183.

[17] C. Evangelisti, G. Vitulli, E. Schiavi, M. Vitulli, S. Bertozzi, P. Salvadori, M. Bertinetti, G. Martra, Catal. Lett., 116 (2007) 57.

[18] Z. Huang, F. Cui, H. Kang, J. Chen, X. Zhang, C. Xia, Chem. Mater. 20 (2008) 5090.

[19] C. Gonzalez-Arellano, R. Luque, D. J. Macquarrie, Chem. Commun., (2009) 1410.

[20] F. Boccuzzi, A. Chiorino, G. Martra, M. Gargano, N. Ravasio, B. Carrozzini, J. Catal., 165 (1997) 129.

[21] V. Higgs, J. Pritchard, Appl. Catal. 25 (1986) 149.

[22] F. Boccuzzi, A. Chiorino, M. Gargano, N. Ravasio, J. Catal. 165 (1997) 140.

[23] A. Gervasini, M. Manzoli, G. Martra, A. Ponti, N. Ravasio, L. Sordelli, F. Zaccheria, J. Phys. Chem. B 110 (2006) 7851.

[24] S. Bennici, A. Gervasini, N. Ravasio, F. Zaccheria, J. Phys. Chem. B 107 (2003) 5168.

[25] F. Liao, Y. Huang, J. Ge, W. Zheng, K. Tedsree, P. Collier, X. Hong, S. C. Tsang, Angew. Chem. Int. Ed. 50 (2011) 2162.

[26] F. Zaccheria, N. Ravasio, R. Psaro, A. Fusi, Tetrahedron Lett., 46 (2005) 3695.

[27] F. Zaccheria, N. Ravasio, R. Psaro, A. Fusi, Chem. Eur. J., 24 (2006) 6426.

[28] H. Yahiro; M. Iwamoto, Appl. Catal. A: Gen. 222 (2001) 163.

[29] A. Corma and H. Garcia, Chem. Rev. 103 (2003) 4307.

[30] F. Zaccheria, F. Santoro, R. Psaro, N. Ravasio, Green Chem. 13 (2011) 545.

[31] M. P. Sibi, G. R. Cook, Lewis Acids in Organic Synthesis, ed. H. Yamamoto, Wiley VCH, 2008, pp. 543–574.

[32] F. Zaccheria, N. Ravasio, in: B. Pignataro (Ed.), Tomorrow's Chemistry Today, 593 Wiley, VCH, 2008, p. 321.

[33] H. Tounsi, S. Djemel, A. Ghorbel, G. Delahay, L. C. de Menorval, B. Coq, React. Kinet. Catal. Lett. 81 (2004) 33.

[34] B. Bridier, N. López, J. Pérez-Ramírez, J. Catal. 269 (2010) 80.

[35] G.C. Bond, S.N. Namijo, J.S. Wakeman, J. Mol. Catal. 64 (1991) 305.

[36] G.C. Bond, S.N. Namijo, J. Catal. 118 (1989) 507.

[37] F.-W. Chang, W.-Y. Kuo, K.-C. Lee, App. Catal. A: Gen. 246 (2003) 253.

[38] F. Zaccheria, R. Psaro, N. Ravasio, L. Sordelli, F. Santoro, Catal. Lett. 141 (2011) 587.

[39] T. Tsoncheva, V. Dal Santo, A. Gallo, N. Scotti, M. Dimitrova, D. Kovacheva, App. Catal. A: Gen. 406 (2011) 13.

[40] M. Popova, M. Dimitrov, V. Dal Santo, N. Ravasio, N. Scotti, Catal. Comm. 17 (2012) 150.

[41] G. Busca, J. Mol. Catal. 43 (1987) 225.

[42] A. Dandekar, M. A.Vannice, J. Catal. 178 (1998) 621.

[43] N.Y. Topsoe, H. Topsoe, J. Mol. Catal. A:Chem. 141 (1999) 95.

[44] F. Boccuzzi, S. Coluccia, G. Martra, N. Ravasio, J. Catal. 184 (1999) 316.

[45] V. Sanchez-Escribano, L. Arrighi, P. Riani, R. Marazza, G. Busca, Langmuir 22 (2006) 9214.

[46] K. Hadjiivanov, T. Venkov, H. Knözinger, Catal. Lett. 75 (2001) 55.

[47] C. R. Reddy, G. Nagendrappa, B. S. J. Prakash, Catal. Comm. 8 (2007) 241.

[48] A. Gervasini, S. Bennici, A. Auroux, C. Guimon, App. Catal. A: Gen. 331 (2007) 129.

[49] Á. Szegedi, M. Popova, V. Mavrodinova, C. Minchev, App. Catal. A: Gen. 338 (2008) 44.

[50] D. R. Brown, C. N. Rhodes, Catal. Lett. 45 (1997) 35.

[51] G. Busca, G. Martra. A. Zecchina, Catal. Tod. 56 (2000) 361.

[52] V. Sánchez Escribano, C. del Hoyo Martínez, E. Fernández López, J. M. Gallardo Amores, G. Busca, Catal. Comm. 10 (2009) 861.

[53] E. P. Parry, J. Catal. 2 (1963) 371.

[54] R. Ferwerda, J. H. van der Maas, F. B. van Duijneveldt, J. Mol. Catal. A: Chem. 104 (1996) 319.

[55] M. Yurdakoç, M. Akçay , Y. Tonbul, K. Yurdakoç, Turk. J. Chem. 23 (1999) 319.

[56] M. Yasuyuki, H. Keiji, Y. Satohiro, J. Mol. Catal. 69 (1991) L19.

[57] J. G. Larsen, E. Lotero, M. Marquez, H. Silva, J. Catal. 157 (1995) 645.

[58] A. Corma, M. Renz, Angew. Chem., Int. Ed. 46 (2007) 298.

Chapter 3

Cu/SiO₂ CH Catalytic Activity: Atom Sites Influence

3.1 Introduction

Catalysis and Surface

Heterogeneous catalysis is a surface and interface phenomenon. The superficial atoms in the active phase of the catalyst have fewer neighbors than those in the bulk, hence are unsatured and can form new bonds with other molecules coming from the reaction environment (chemisorption). Thus, the new interaction perturbs the existing bonds, that can be modified or even broken (dissociative chemisorption). The surface species may therefore move from an atomic site to another, may react together to form new compound and finally desorbs [1, 2].

This is only a simplistic view of what happens on a catalyst, but immediately it becomes evident that when we talk about heterogeneous catalysis we should first focus our attention on the surface composition of the material of interest.
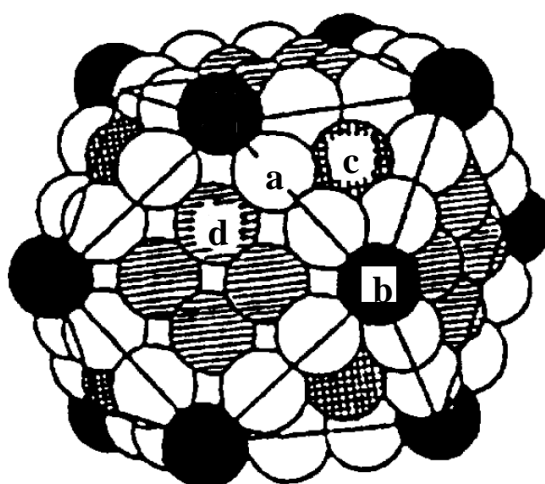
Figure 3.1. Cubooctahedron atom sites: (a), (b) low-coordination sites, edge and corner; (c), (d) high-coordination sites (terrace atoms, (111) and (100) [3].

For a metal crystal, the total atoms which compose the particle are divided in bulk atoms and surface atoms. The surface atoms are in turn composed of face atoms, edge atoms and corner atoms. Face (terrace) atoms are also called high-coordination-number atoms, on the other hand edge and corner represent the low-coordination number ones, since they are the most defective sites on the surface. Geometry and coordination number of the surface atoms reflect on their electronic, and catalytic, properties. Thus the different surface atoms (faces, edges and corners) are not all equivalent and may exhibit a different catalytic activity. A particular reaction can demand a specific arrangement of metal sites. The important fact is that the relative proportion of high and low coordination atoms with respect to the total number of surface atoms is well-known to vary with the metal particle sizes [3, 6]. Therefore the particle size influences not only the dispersion of the metal (surface versus total atoms), but also the ratio between high and low-coordination atoms, that increases with the size.

As a matter of fact, the same catalytic materials whit the same total number of exposed atoms but different crystal size can show different activity. A reaction whose turnover frequency depends on particle size is a structure sensitive reaction, while in the case of a structure insensitive reaction the TOF is relatively invariant with the crystallite size [7].
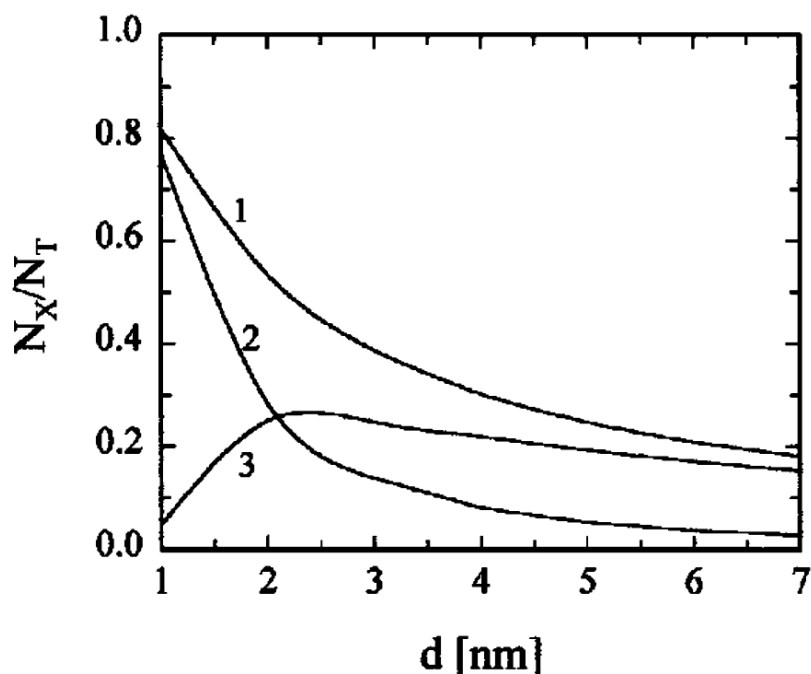
Figure 3.2. Variation of (1) surface atoms, (2) low-coordination atoms and (3) high-coordination atoms respect to the total atoms number with the size of the cubooctahedral crystal [5].

Examples of structure insensitive reactions are the ring opening of cyclopropane and the hydrogenation of ethylene over a wide variety of platinum catalysts, the hydrogenation of cyclohexene and the hydrogenation of carbon monoxide to produce methane on ruthenium catalysts. The explanation of the structure insensitivity of a catalytic reaction in generally complex. However this effect may be due to the presence of adsorbed species on the surface that either weaken the reactant-catalyst surface interaction or are inactive in the reaction, masking in both cases the surface structure of the catalyst [8].

A significant example of a reaction exhibiting a great structure sensitivity is the ammonia synthesis. This reaction is favored by roughness and open catalyst surfaces (usually Fe or Re).

Other structure sensitive reactions are those involving the formation and/or the breaking of carbon-carbon bonds, in which an increased activity of the supported catalyst with a decrease in particle size is observed. This behavior suggests that kinks and edges on the surface are accountable for the catalyst activity, since the concentration of these sites is expected to increase as the particle size decreases [8, 9].

In any case, a reaction can be also structure sensitive/insensitive depending on the experimental conditions. This occurs if the rate-determining step changes due to variations in the amounts and/or type of species on the surface [8].

Aim of the work

In this Chapter the structure sensitivity of two model reactions catalyzed by reduced Cu/SiO$_2$ Chrom CH catalysts was investigated. The former is the hydrogenation of 4-methoxyacetophenone to the corresponding alcohol, 1-(4-methoxyphenyl)ethanol. The second is the etherification reaction between two alcohols which involves 1-(4-methoxyphenyl)ethanol and 2-propanol.

The catalysts used are 8.5 and 15 wt% Cu/SiO$_2$ Chrom CH, with a mean particle size of 1.7 and 2.8 nm. With the hypothesis that the particles are truncated octahedral or cubooctahedral in shape is possible to calculate the total number of surface atoms and the fraction of high- and low-coordination sites. The structure sensitivity of the reactions was evaluated considering the TOF for the different atom sites lying on the surface of the particles.

The hydrogenation ability of copper catalysts is well reported in the literature, while the acidity, necessary for the etherification, of the reduced and unreduced Cu/SiO$_2$ Chrom CH catalysts was confirmed in Chapter 2 by pyridine adsorption spectra. The possibility to make the entire bifunctional process, starting from 4-methoxyacetophenone in presence of 2-propanol to obtain the corresponding ether, was already successfully explored by Zaccheria et al. [10]. Here the two

reactions involved were studied separately with the purpose to observe how the structure and the size of the catalyst particles can influence the hydrogenation and the acid reactions. The understanding of the catalysts attitudes is very important in order to tune their activity and selectivity. In particular the possibility to tune the acidity (non only by changing the support) and the hydrogenation power in function of copper particle size and, eventually, morphology would be a desired goal.

3.2 Experimental

Chemicals

All reagents were purchased from Aldrich and used without further purification.

Catalytic activity

The catalytic reaction were performed using reduced 8.5 and 15 wt% Cu/SiO_2 Chrom cayalyst CH. The catalysts (100 mg/50 mg) were prereduced in the reactor flask by heating at 270 °C under air for 20 min, under vacuum for other 20 min and finally by introducing H_2, at the same temperature. After cooling under H_2, 100 mg of reactant (4-methoxyacetophenone/1-(4-methoxyphenyl)ethanol) and 8 ml of 2-propanol were added under N_2; then 1 atm of H_2 was introduced and the reactor was placed into oil bath (50/60 °C). Conversion and products were determined by GC-MS.

3.3 Results and discussion

Atom sites calculation: generalities

The total number of atoms which compose a metal crystal is the sum between bulk atoms and surface atoms (Eq. 1). The surface atoms (N_S) are composed of face atoms, edge atoms and corner atoms (Eq. 2):

$$N_T = N_S + N_B \quad (1)$$
$$N_S = N_F + N_E + N_C \quad (2)$$
$$N_S = N_{HS} + N_{LS} \quad (3)$$

Face atoms are also called high-coordination-number atoms (**HS**), while edge and corner are defined as the low-coordination-number atoms (defective sites, **LS**). Thus, the N_S can be calculated equivalently by equation 2 and 3, where N_{HS} and N_{LS} are the number of high- and low-coordination atoms. The total number (N_T) of atoms for a copper nanoparticle for a f.c.c. crystal (as is the case of copper) can be calculated from:

$$d_{np} = 1.105 d_{at} N_T^{1/3} \quad (4)$$

where d_{np} is the average diameter of the catalyst nanoparticles derived from EXAFS measurement, d_{at} is the diameter of the copper atom (2.56 Å). The formula does not depend on particle shape [11, 12].

Two different models for the calculation of the different atom sites are reported in the literature. The first one starts from the assumption that the particles are truncated octahdra [11, 12], the second one approximates the shape of the crystals as cubooctahedral [3-5].

Atom sites equations: truncated octahedron model

Truncated octahedron is the shape that for any particular size has the shape closest to the sphere [11, 12]. Once the total number of atoms is calculated from equation (4), the edge length value (as atoms), **m**, for a f.c.c. lattice was obtained from eq. 5.

$$N_T = 16m^3 - 33m^2 + 24m - 6 \quad (5a)$$
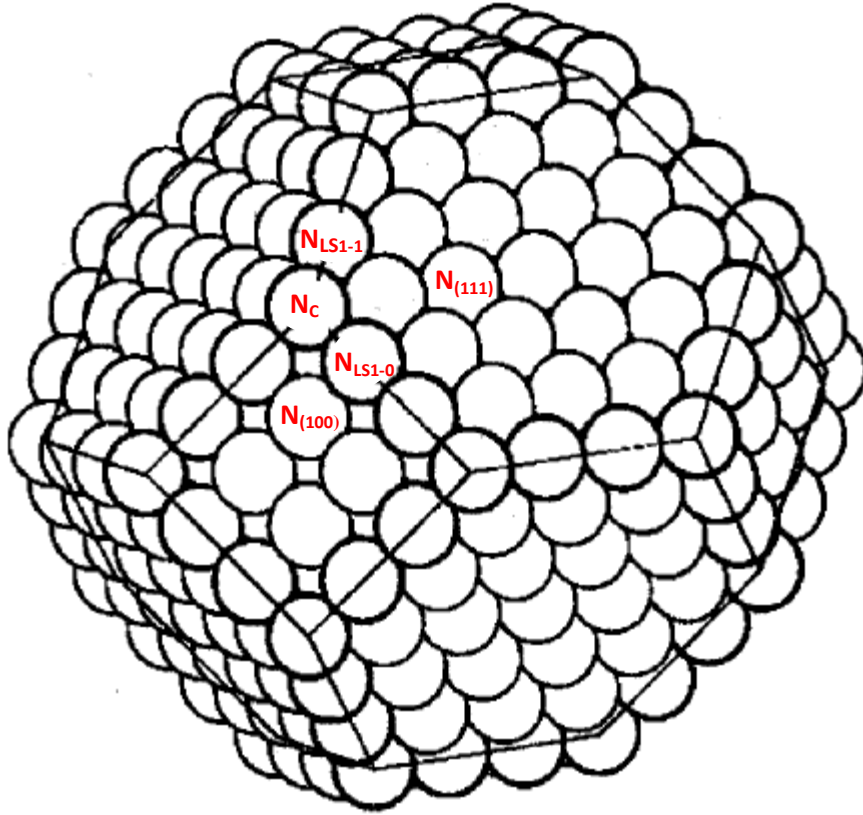
Figure 3.3. Truncated octahedron model, **m**=4.

N_S, N_{HS}, N_{LS} are given from equation 6, 7 and 8:

$$N_B = 16m^3 - 63m^2 + 84m - 38 \quad (6a)$$

$$N_S = 30m^2 - 60m + 32 \quad (7a)$$

$$N_{HS} = 6(m-2)^2 + 8(3m^2 - 9m + 7) \quad (8a)$$

$$N_{LS} = 24(m-2) + 12(m-2) + 24 \quad (9a)$$

Where N_B is the number of bulk atoms and N_{HS} is the sum of two parts: (111) atoms ($N_{(111)}$) and (100) atoms ($N_{(100)}$):

$$N_{HS} = N_{(111)} + N_{(100)} \quad (10)$$

$$N_{(111)} = 8(3m^2 - 9m + 7) \quad (11a)$$

$$N_{(100)} = 6(m-2)^2 \quad (12a)$$

N_{LS} is in turn made of three contributions: the corner atoms (24, N_C, the number does not depend on m), and the edge between an (111) and an (100) facets ($N_{LS\ 1\text{-}0}$) and two (111) ($N_{LS\ 1\text{-}1}$), equation 13a and 14a.

$$N_{LS\ 1-0} = 24(m - 2)\ (13a)$$
$$N_{LS\ 1-1} = 12(m - 2)\ (14a)$$

It should be noted that a truncated octahedron is bounded only by square (100) facets and hexagonal (111) facets. The representation of a truncated octahedron is reported in Figure 3.3.

Atom sites equations: cubooctahedron model

Assuming that the catalysts nanoparticles are cubooctahedral in shape with a f.c.c. structure, it is possible to calculate the number of different sites depending on the size of the nanocrystals [3-5]. Equation 5b allows one to calculate **m**, the length of an edge expressed as atom.

$$N_T = (10m^3 - 15m^2 + 11m - 3)/3\ \ (5b)$$

N_B (bulk atoms), N_S, N_{HS}, N_{LS} are given from equation 6b, 7b, 8b and 9b:

$$N_B = 16m^3 - 63m^2 + 84m - 38\ \ (6a)$$
$$N_S = 10m^2 - 20m + 12\ \ (7b)$$
$$N_{HS} = 6(m - 2)^2 + 4(m - 3)(m - 2)\ \ (8b)$$
$$N_{LS} = 24(m - 2) + 12\ \ (9b)$$

Also in this case N_{HS} is the sum of two parts: (111) atoms ($N_{(111)}$) and (100) atoms ($N_{(100)}$):

$$N_{HS} = N_{(111)} + N_{(100)}\ \ (10)$$
$$N_{(111)} = 4(m - 3)(m - 2))\ \ (11a)$$
$$N_{(100)} = 6(m - 2)^2\ \ (12b)$$

N_{LS} is in its turn made of two contributions: the corner atoms (12, the number does not depend on m), and the edge between an (111) and an (100) facets ($N_{LS\ 1\text{-}0}$), equation 13b.

$$N_{LS\ 1-0} = 24(m - 2)\ (13b)$$

It should be noted that a cubooctahedron is bounded only by square (100) facets and triangular (111) facets. The representation of a cubooctahedron is reported in Figure 3.4.
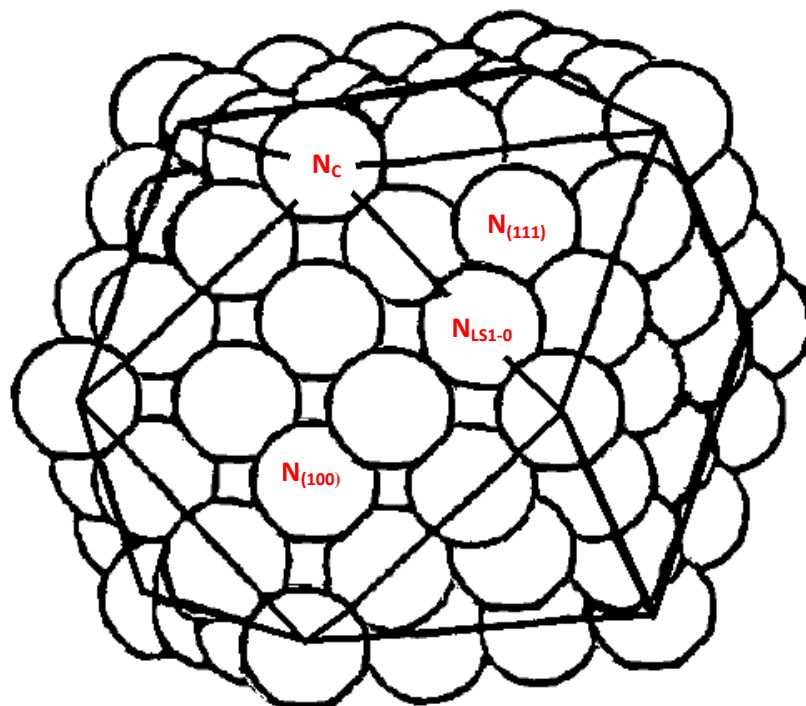
Figure 3.4. Cubooctahedron model, **m**=4.

Truncated octahedron vs cubooctahedron models: results and considerations

The surface compositions for 8.5 wt% and 15 wt% Cu/SiO$_2$ catalysts are reported in Table 3.1 and Table 3.2. The choice to estimate the mean size of nanocrystals from EXAFS analysis (instead from TEM) was clearly explained in Chapter 2 and primarily derives from the catalyst in-situ reduction pretreatment that is the same before both EXAFS analysis and catalytic experiments.

The choice of not to round the different atoms values to the unity was dictated by the fact that this numbers represent mediated values for all the surface particles.

Turnover frequencies were calculated using the equation 14:

$$TOF_x \ (h^{-1}) = \frac{n_{conv}}{t * n_X} \quad (14)$$

Where TOF_x is the turnover frequency normalized for a specific copper site (surface, high-coordination, low-coordination, (111), or (100) atoms), n_{conv} are the converted moles of the reactant, t is the time in hours and n_x are the moles of the specific atom site. The n_x values (n_S, n_{HS}, n_{LS}, $n_{(100)}$ and $n_{(111)}$) were calculated multiplying the fraction of a specific site on a single particle (N_x/N_T) for the total amount of copper (moles of Cu, n_{Cu}) present in the reaction (equation 15):

$$n_x = n_{Cu} * \frac{N_x}{N_T} \quad (15)$$

TOF ratios for a specific atom site were calculated dividing TOF_X of 8.5 wt% Cu/SiO_2 by a TOF_X of 15 wt% Cu/SiO_2.

The two crystal shape models used in this work (truncated octahedron and cubooctahedron) appear to be very similar: N_T are practically the same (217 for 8.5 wt% material and 970 for that with 15 wt% of copper), while N_B and N_S differ only of few atoms. This fact results in TOF values and, in particular, TOF ratios that are generally very similar for the two models (see the tables in the next two sections). However a marked difference can be noticed for $N_{(100)}$ and $N_{(111)}$ and corresponding TOFs and TOF ratios. This evidence is ascribable to the different shape of (111) facets on a truncated octahedron (hexagonal) and a cubooctahedron (triangular), leading to a different surface composition.

Truncated Octahedral model					
8.5 wt% Cu/SiO$_2$ Chrom			15 wt% Cu/SiO$_2$ Chrom		
Site	Number of Atoms	%	Site	Number of Atoms	%
N_T	217.02	100%	N_T	969.77	100%
N_B	87.65	40.4%	N_B	577.13	59.5%
N_S	129.37	59.6%	N_S	392.64	40.5%
N_{HS}	67.19	31.0%	N_{HS}	274.73	28.3%
N_{LS}	62.18	28.7%	N_{LS}	117.91	12.2%
$N_{(100)}$	6.75	3.1%	$N_{(100)}$	40.83	4.2%
$N_{(111)}$	60.44	27.9%	$N_{(111)}$	233.91	24.1%
$N_{(edge)}$	38.18	17.6%	$N_{(edge)}$	93.91	9.7%

Table 3.1. Truncated octahedral model: 8.5 and 15 wt% Cu/SiO_2 CH atoms composition.

Cubooctahedral model					
8.5 wt% Cu/SiO₂ Chrom			15 wt% Cu/SiO₂ Chrom		
Site	Number of Atoms	%	Site	Number of Atoms	%
N_T	217.00	100%	N_T	969.52	100%
N_B	92.94	42.8%	N_B	594.44	61.3%
N_S	124.07	57.2%	N_S	375.08	38.7%
N_{HS}	52.22	24.1%	N_{HS}	240.48	24.8%
N_{LS}	71.85	33.1%	N_{LS}	134.59	13.9%
$N_{(100)}$	37.31	17.2%	$N_{(100)}$	156.55	16.1%
$N_{(111)}$	14.90	6.9%	$N_{(111)}$	83.93	8.7%
$N_{(edge)}$	59.85	27.6%	$N_{(edge)}$	122.59	12.6%

Table 3.2. Cubooctahedral model: 8.5 and 15 wt% Cu/SiO₂ CH atoms composition.

Reduction of 4-methoxyacetophenone to 1-(4-methoxyphenyl)ethanol

The reduction of 4-methoxyacetophenone proceeded at 50 °C in presence of H_2, while no product formation was observed carrying out the reaction under N_2 atmosphere.

The TOFs normalized for the different atom sites (**n_S, n_{HS}, n_{LS}, $n_{(100)}$, $n_{(111)}$**) were calculated after 0.5 h of reaction (conversion less than 15 wt% for the two Cu/SiO₂ catalysts) and were reported in Table 3.3 and Table 3.4.
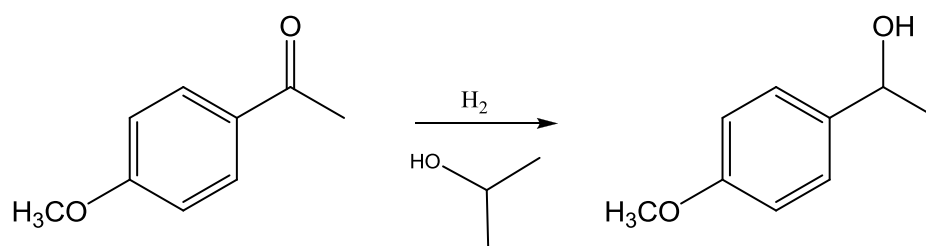
Figure 3.5. Scheme of the hydrogenation of 4-methoxyacetopehnone.

The two models used provide the same indication, that is that hydrogenation of 4-methoxyacetophenone is dependent on the particle size. If all the surface atoms of the copper nanoclusters act catalytically as the same active species for the reaction, the TOF values normalized to n_S are expected to be independent on the Cu nanocluster size [4]. As a result, larger nanoclusters gave higher TOF than smaller ones, indicating that not all the atoms have the same activity. On the other hand TOF values normalized for n_{HS} are independent on the particle size ($\mathbf{TOF_{HS}}$ ratio is about 1 in both cases): this means that high coordination atoms (terrace atoms) are the active sites in this reaction. Thus hydrogenation of 4-methoxyacetophenone is a structure sensitive reaction. A specific influence of the cubooctahedron facets, (100) or (111), on the reaction was not observed. It is reported that H_2 dissociation is favored on unsatured surface such as (110) facets of f.c.c. lattice or corner and edge atoms [2, 5, 13], therefore a low-coordination sites structure sensitivity would expected. The dependence on face atoms suggests that H_2 dissociation does not represent the rate determining step, in disagreement to what was found e.g. by Veisz and coworkers for styrene hydrogenation on Pd particles. Thus, it is possible that hydrogen dissociation occurs preferentially on low-coordination atoms (according to the literature) and that a slower reaction takes place preferentially on face atoms (the rate determining step, e.g. ketone adsorption to the catalyst, or alcohol desorption). Another hypothesis is that the hydrogenation could be faster on low-coordination atoms, but the overall process is slower on these sites because of a strong interaction between edges and corners and the adsorbed molecules present in the reaction environment (i.e. H_2, reactant, product, or solvent), which hardly desorb. A similar behavior has been already reported for NO-CO reaction [14].

4-Methoxyacetophenone Hydrogenation – Truncated Octahedral model

Site	TOF Name	8.5 wt% Cu/SiO$_2$ Chrom	15 wt% Cu/SiO$_2$ Chrom	TOF ratio
N_S	TOF$_S$	1.67	2.60	0.64
N_{HS}	TOF$_{HS}$	3.21	3.72	0.86
N_{LS}	TOF$_{LS}$	3.47	8.67	0.40
$N_{(100)}$	TOF$_{(100)}$	32.00	25.03	1.28
$N_{(111)}$	TOF$_{(111)}$	3.57	4.37	0.82

Table 3.3. TOFs and TOF ratios for the hydrogenation of 4-methoxyacetophenone - Truncated Octahedral model.

4-Methoxyacetophenone Hydrogenation - Cubooctahedral model

| Site	TOF Name	8.5 wt% Cu/SiO$_2$ Chrom	15 wt% Cu/SiO$_2$ Chrom	TOF ratio
N_S	TOF_S	1.74	2.72	0.64
N_{HS}	TOF_{HS}	4.14	4.25	0.97
N_{LS}	TOF_{LS}	3.01	7.59	0.40
$N_{(100)}$	$TOF_{(100)}$	5.79	6.53	0.89
$N_{(111)}$	$TOF_{(111)}$	14.49	12.17	1.19

Table 3.4. TOFs and TOF ratios for the hydrogenation of 4-methoxyacetophenone - Cubooctahedral model.

Obviously, the experimental error influences the TOFs ratio to a value that slightly differs from the unity. Indeed, the copper crystals present some defects with respect to the perfect shape and the particles are not monodispersed. Despite a certain degree of approximation due to its intrinsic imperfections the model was successfully applied in different case studies in the past and once again it provides a good description of the system [4, 5, 12, 15]. This consideration will be valid also for the next section.

Etherification of 1-(4-methoxyphenyl)ethanol with 2-propanol

The reaction was carried out under H$_2$ atmosphere only to prevent catalyst deactivation.
The TOF values for the different atom sites were calculated after 0.5 h, when the conversion were less than 25% for both 8.5 wt% Cu/SiO$_2$ and 15 wt% Cu/SiO$_2$ (Table 3.5 and Table 3.6).
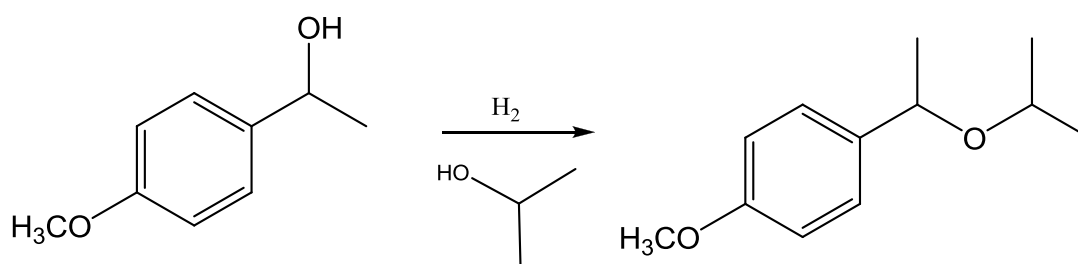
Figure 3.6. Scheme of the etherification of 1-(4-methoxyphenyl)ethanol with 2-propanol.

On the same grounds seen in the case of the hydrogenation of 4-methoxyacetophenone we can say that the reaction of etherification is structure sensitive. In fact the reaction appears to be dependent on particle size (TOF_S ratios other than 1), on the other hand it seems to be independent on high-coordination atoms. This remark results to be valid for both truncated octahedral and cuboctahedral model, though a deeper analysis of TOF ratios shows a value closer to unity for either (100) or (111) sites. The opposite results derived the fact that the $N_{(100)}/N_{(111)}$ ratio for a truncated octahedron increases with particle size, while in the case of a cubooctahedron decreases as particle size increase. In any case it is possible that a specific facet results to be (more) active with respect to another one and the results seem to lean towards this hypothesis. Between (111) and (100) facets the latter is the most unsaturated one and reasonably the acid character of the catalyst is enhanced on unsatured facets.

Since the aromatic substrates involved in the etherification are similar to those of the hydrogenation reaction, the apparent inactivity of low-coordination atoms can lie on the same reasons. The structure sensitivity of the etherification on high-coordination atoms, somehow, strengthens the idea that the hydrogen dissociation on the reduction of 4-methoxyacetophenone is not the rate determining step, while a slower reaction involving the aromatic molecules occurs on terrace.

The entire bifunctional process studied by Ravasio and coworkers [10] from ketone to the corresponding ether, through the alcohol formation and the subsequent reaction with the second alcoholic compound present in the reaction mixture, should be favored by the use of the catalyst with larger particles (15 wt% Cu/SiO_2), since both the reaction involved are enhanced by the presence of terrace atoms.

Etherification of 1-(4-Methoxyphenyl)ethanol and 2-Propanol – Truncated Octahedral model

Site	TOF Name	8.5 wt% Cu/SiO_2 Chrom	15 wt% Cu/SiO_2 Chrom	TOF ratio
N_S	TOF_S	4.61	8.64	0.53
N_{HS}	TOF_{HS}	8.88	12.34	0.72
N_{LS}	TOF_{LS}	9.60	28.76	0.33
$N_{(100)}$	$TOF_{(100)}$	88.45	83.05	1.06
$N_{(111)}$	$TOF_{(111)}$	9.87	14.50	0.68

Table 3.5. TOFs and TOF ratios for the etherification of 1-(4-methoxyphenyl)ethanol and 2-propanol - Truncated Octahedral model.

Etherification of 1-(4-methoxyphenyl)ethanol and 2-propanol - Cubooctahedral model

Site	TOF Name	8.5 wt% Cu/SiO$_2$ Chrom	15 wt% Cu/SiO$_2$ Chrom	TOF ratio
N_S	TOF$_S$	4.81	9.04	0.53
N_{HS}	TOF$_{HS}$	11.43	14.10	0.81
N_{LS}	TOF$_{LS}$	8.31	25.19	0.33
$N_{(100)}$	TOF$_{(100)}$	15.99	21.65	0.74
$N_{(111)}$	TOF$_{(111)}$	40.05	40.39	0.99

Table 3.6. TOFs and TOF ratios for the etherification of 1-(4-methoxyphenyl)ethanol and 2-propanol - Cubooctahedral model.

3.4 Conclusions

The results reported here show as both the hydrogenation of 4-methoxyacetophenone to the corresponding alcohol and the etherification reaction between 1-(4-methoxyphenyl)ethanol and 2-propanol, on reduced Cu/SiO_2 Chrom CH catalysts, are structure sensitive. The reactions are enhanced by the presence of terrace atoms, thus the catalyst with 15 wt% of copper, which shows larger particles, is the most active. The use of too small particles appears to be a disadvantages for these reactions. The terrace atoms dependence observed for both reactions may be due to a slow reaction (e.g. desorption) involving the aromatic substrate occurring preferentially on these sites.

Two different models were employed to calculate the number of different atom sites: one approximates the crystal shape as truncated octahedral, while another one considers the particle as cubooctahedra. The two models lead to similar observations and suggest that the acid promoted reaction of ether formation can be favored, in particular, by either (100) or (111) facets.

3.5 References

[1] G. Ertl, Angew. Chem. Int. Ed. 47 (2008) 3524.

[2] G. A. Somorjai, Introduction to Surface Chemistry and Catalysis, Wiley, New York, 1994.

[3] R. E. Benfield, J. Chem. Soc. Faraday Trans. 88 (1992) 1107.

[4] K. Mori, T. Hara, T. Mizugaki, K. Ebitani, K. Kaneda, J. Am. Chem. Soc. 126 (2004) 10657.

[5] B. Veisz, Z. Király, L. Tóth, B. Pécz, Chem. Mater. 14 (2002) 2882.

[6] J. Le Bars, U. Specht, J. S. Bradley, D. G. Blackmond, Langmuir 15 (1999) 7621.

[7] R. S. Rao, A. B. Walters, M. A. Vannice, J. Phys. Chem. B 109 (2005) 2086.

[8] G. A. Somorjai, J. Carrarza, Ind. Eng. Chem. Fundam. 25 (1986) 63.

[9] L. M. Falicov, G. A. Somorjai, Proc. Natl. Acad. Sci. USA 82 (1985) 2207.

[10] F. Zaccheria, R. Psaro, N. Ravasio, Tetrahedron Lett. 50 (2009) 5221.

[11] R. Van Hardeveld, F. Hartog, Surface Sci. 15 (1969) 189.

[12] R. Van Hardeveld, F. Hartog, Adv. Catal. 22 (1972) 75.

[13] Q. Sun, J. Xie, T. Zhang, Surf. Sci. 338 (1995) 11.

[14] Y. Li, E. Boone, M. A. El-Sayed, Langmuir 18 (2002) 4921.

[15] J. Le Bars, U. Specht, J. S. Bradley, D. G. Blackmond, Langmuir 15 (1999) 7621.

4.1 Introduction

Propylene oxide

Propylene oxide (PO, C_3H_6) is a very reactive substance and one of the most important and versatile chemical intermediate, used in the production of a large variety of valuable consumer products, such as polyurethane foams, polymers, propylene glycol, cosmetics, food emulsifiers, fumigants and insecticides. Ever since the early '50s the industrial importance of this epoxide has growth as well as its demand: in 1993 about $4.0 \cdot 10^6$ t were produced, in 1996 $4.9 \cdot 10^6$ t, in 2006 $6 \cdot 10^6$ t and nowadays over 8 million tons of PO are produced annually from propylene. About 10% of European propene is used for the production of propylene oxide [1-3].

Reactant	Product(s)	Structural formula
Polymerization (ROH as initiator)	polyether polyols	$R[-O-CH-CH_2]_n-OH$ $\quad\quad\quad\quad CH_3$
Water	monopropylene glycol ($n = 0$) dipropylene glycol ($n = 1$) tripropylene glycol ($n = 2$)	$CH_3-CH[-CH_2-O-CH]_n-CH_2$ $\quad\quad OH \quad\quad\quad\quad CH_3 \;\; OH$ (and isomers)
Alcohols and phenols (ROH)	propylene glycol ethers	$CH_3-CH-CH_2$ $\quad\quad OH \;\; OR$ (and isomers/highers)
Ammonia	isopropanolamine	$CH_3-CH-CH_2$ $\quad\quad OH \;\; NH_2$ (and isomers/highers)
Carbon dioxide	propylene carbonate	$CH_3-CH-CH_2$ $\quad\quad O \quad O$ $\quad\quad\quad C=O$
Isomerization	allyl alcohol acetone propanal	$CH_2=CHCH_2OH$ CH_3COCH_3 CH_3CH_2CHO

Table 4.1. Most important PO reaction [1].

Country	Producer	Location	Process [a]	Capacity, 10^3 t/a
America				
Brazil	Dow Quimica	Aratu	CH	150
Canada	Dow	Sarnia, Ont	CH-NaOH	60
United States	Arco Chemical	Channelview, TX	styrene	270
	Arco Chemical	Bayport, TX	TBA	550
	Dow Chemical	Freeport, TX	CH-NaOH	500
	Dow Chemical	Plaquemine, LA	CH-NaOH	200
	Olin	Lake Charles, LA	DO	5
Total				*1735*
Asia				
China	Zhangdian Petrochem.	Zibo/Shandong	CH	10
	Jinling Petrochem. Corp.	Zhongshan	CH	10
	Tianjing Dagu	Tianjing	CH	16
	Gao Qiao	Shanghai	CH	16
	NJ Zhongshan	Guang Dong	CH	16
India	Manali Petrochem.	Baroda, Madras	CH	12
	UB Petroproducts	Manali, Madras	CH	12
Japan	Sumi-Arco	Chiba	styrene	140
	Tokuyama Soda	Tokuyama City	CH	50
	Showa Denko	Kawasaki	CH	30
	Mitsui Toatsu	Nagoya	CH	36
	Asahi Glass Co.	Kashima	CH	100
Korea (South)	Yukong Arco Chemical	Ulsan, Yukong	styrene	100
Taiwan	Chiung Long Petrochem.	Linyuan/Kaohsiung	CH	15
Total				*563*
Europe				
Bulgaria	Neftochim	Burgas	CH	12
Czechoslovakia	Novacke Chemicke Zavody	Novaky	CH	5
France	Arco Chimie France	Fos-sur-Mer	TBA	200
Germany	Dow Deutschland Inc.	Stade	CH-NaOH	420
	Erdoelchemie	Koeln-Worringen	CH	150
	Bunawerke	Schkopau	CH	50
	BASF	Ludwigshafen	CH	90
Italy	Enichem	Priolo, Sicily	CH	60
Netherlands	Arco Chemie Nederland	Botleck	TBA	250
	Shell Netherland Chemie	Moerdijk	styrene	140
Poland	State	Rokita	CH	20
Romania	Oltchim	Rimnicu Vilcea	CH	12
	State	Midia	CH	60
Spain	Repsol Quimica/Arco	Puertollano	styrene	50
Former Soviet Union	State	Sumgait	CH	25
	State	Nizhnekamsk	styrene	50
Yugoslavia	Sodaso	Tuzia	CH	20
Total				*1614*
Total worldwide				*3912*

[a] CH = chlorohydrin PO process (using lime unless stated otherwise) ; DO = direct oxidation of propene ; styrene = styrene/PO process ; TBA = *tert*-butyl alcohol/PO process.

Table 4.2. World PO capacities in 1991 [1].

PO polarity and the strained three-membered epoxide ring cause the easily opening by reaction with a wide variety of substances. In addition, with respect to its analogous ethylene oxide, the number of possible derivatives is very large [1-3]. Most industrial reactions of PO are catalyzed, however it also reacts very fast directly with all compounds containing active hydrogen atoms (including the hydrogen halides), as well as chlorine and ammonia. The addition of PO to a compounds containing a labile hydrogen represents the most common reaction of propylene oxide, but it also may condense with substances not containing reactive hydrogen. From a commercial point of view, the violent polymerization of PO to form poly(ether polyols) in the presence of a catalysts (such as

bases, acids, or salts) is the most important reaction. For the polymerization, the chain initiators are active hydrogen atoms containing substances (e.g., water, glycols, phenols, amines, or carboxylic acids). PO forms mixed polyols with ethylene oxide, tetrahydrofuran, 3,4-epoxy-1-butene (butadiene monoxide), and carbon dioxide. It is hydrolyzed by water, without any catalyst, in a liquid phase reaction to give monopropylene glycol, dipropylene glycol, tripropylene glycol, and polyglycols. Propylene oxide reacts also with ketones or aldehydes to form cyclic ketals or acetals, and with carbon dioxide to form propylene carbonate. Hydrogen halides convert PO to propylene halohydrins, and ammonia gives mono-, di-, and triisopropanolamine. In the presence of alumina PO isomerizes to propanal and acetone, and over Li_3PO_4 catalysts to allyl alcohol. Hydrogenation with nickel catalyst leads to 1-propanol. Many other reactions are also possible, including reactions with natural products like starch or cellulose. Therefore the wide reaction pathways (see also Table 4.1) accounts for the industrial importance of PO. However, all the reactions involving PO may become violent and dangerous if not properly controlled, thus every possible applications should be investigated very thoroughly. Under pyrolytic conditions PO isomerizes to propanal, acetone, methyl vinyl ether, and allyl alcohol, while its decomposition does not result in hazardous products. In any case, PO is a stable compound under moderate conditions, but polymerization may occur on contact with highly active catalytic surfaces such as iron, tin, or aluminum chlorides, iron and aluminium peroxides, or alkali-metal hydroxides and clay-based absorbent materials [1].
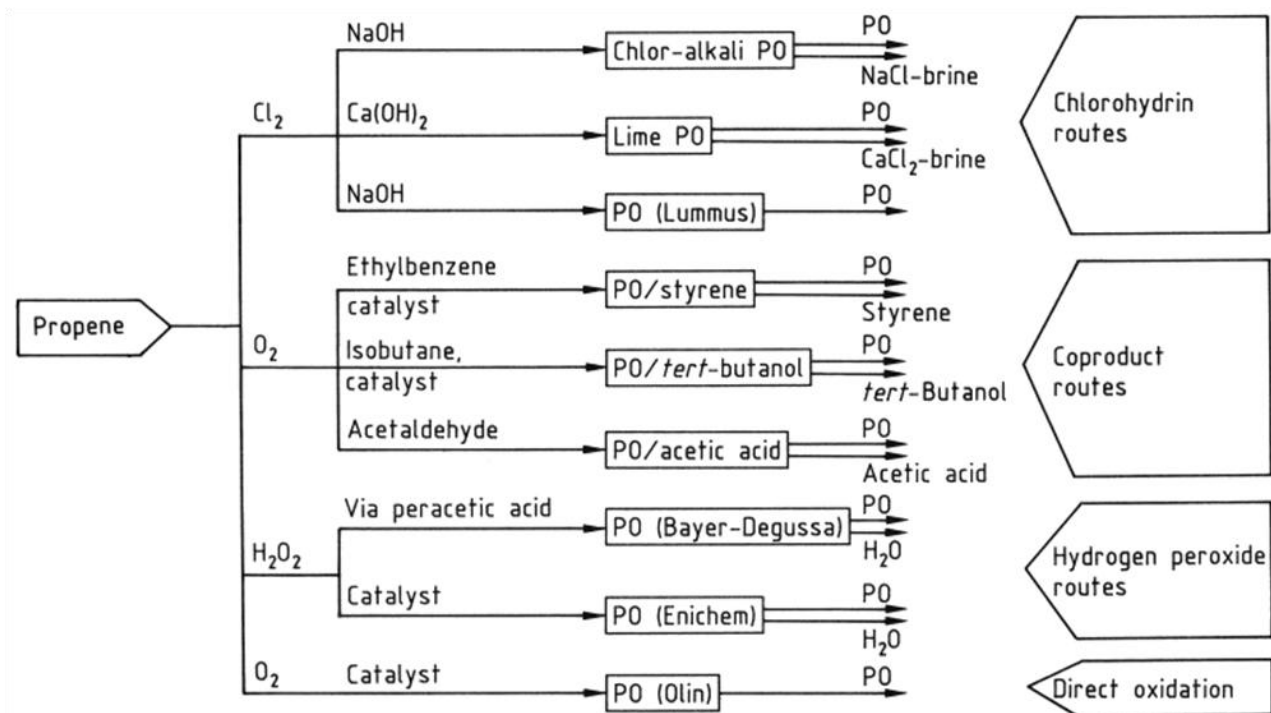

Figure 4.1. PO production routes [1].
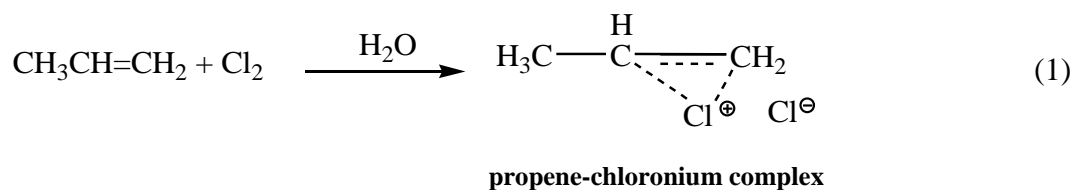
Propylene Oxide Production

The technologies which allow to produce PO can be divided into three categories (Figure 4.1):

- Chlorohydrin process
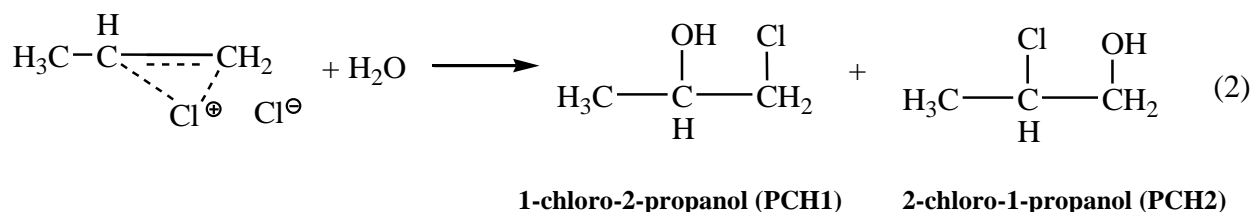- Indirect oxidation preccesses
- Direct oxidation processes

On an industrial scale only the first two (chlorhydrin and indirect oxidation) processes are practiced (hereinafter we will see the reason).

The chlorohydrin process is based on two main steps: the synthesis of propylene chlorohydrin (PCH) and the subsequent dehydrochlorination of PCH to PO. These steps are followed by PO purification and wastewater treatment.

Chlorine and propylene are mixed together in an aqueous solution for the synthesis of PCH. First a propene-chloronium complex is formed as an intermediate (Eq. 1).
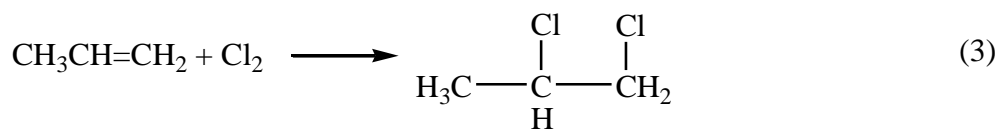
$$CH_3CH{=}CH_2 + Cl_2 \quad \xrightarrow{\ H_2O\ } \quad \underset{\textbf{propene-chloronium complex}}{H_3C{-}C\overset{H}{\cdots\cdots}CH_2 \atop \ \ Cl^{\oplus}\ \ Cl^{\ominus}} \qquad (1)$$

Then, this intermediate reacts with H_2O to give hydrochloric acid and the propylene chlorohydrin isomers: 1-chloro-2-propanol (90 %) and 2-chloro-1-propanol (10 %) (Eq. 2).

$$\underset{\ \ Cl^{\oplus}\ \ Cl^{\ominus}}{H_3C{-}C\overset{H}{\cdots\cdots}CH_2} + H_2O \longrightarrow \underset{\textbf{1-chloro-2-propanol (PCH1)}}{H_3C{-}\underset{H}{\overset{OH}{C}}{-}\overset{Cl}{CH_2}} + \underset{\textbf{2-chloro-1-propanol (PCH2)}}{H_3C{-}\underset{H}{\overset{Cl}{C}}{-}\overset{OH}{CH_2}} \qquad (2)$$
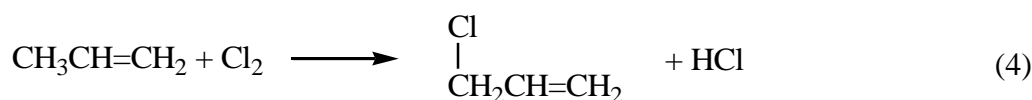
The formation of propene-chloronium complex is followed by two gas phase side reactions between chlorine and propylene. The first one results in the main side product of the process, 1,2-dichloropropane (DCP, Eq. 3), while the second one gives 1-chloropropene (allyl chloride) (Eq. 4).
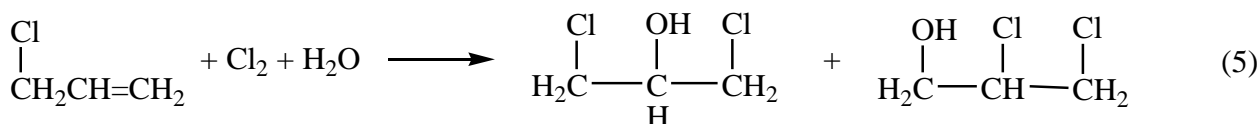
1-chloropropene reacts with Cl_2 and H_2O to give the two dichlorohydrin isomers: 1,3-dichloro-2-propanol and 2,3-dichloro-1-propanol (DCH1 and 2DCH, Eq. 5).

$$CH_3CH=CH_2 + Cl_2 \longrightarrow \underset{\overset{|}{H}}{H_3C-\overset{\overset{\textstyle Cl}{|}}{C}-\overset{\overset{\textstyle Cl}{|}}{CH_2}} \tag{3}$$

1,2-dichloropropane (DCP)

$$CH_3CH=CH_2 + Cl_2 \longrightarrow \overset{\overset{\textstyle Cl}{|}}{CH_2CH=CH_2} + HCl \tag{4}$$

1-chloropropene

$$\overset{\overset{\textstyle Cl}{|}}{CH_2CH=CH_2} + Cl_2 + H_2O \longrightarrow \underset{\overset{|}{H}}{H_2C-\overset{\overset{\textstyle OH}{|}}{C}-\overset{\overset{\textstyle Cl}{|}}{CH_2}}Cl \quad + \quad H_2C-\overset{\overset{\textstyle Cl}{|}}{CH}-\overset{\overset{\textstyle Cl}{|}}{CH_2}OH \tag{5}$$
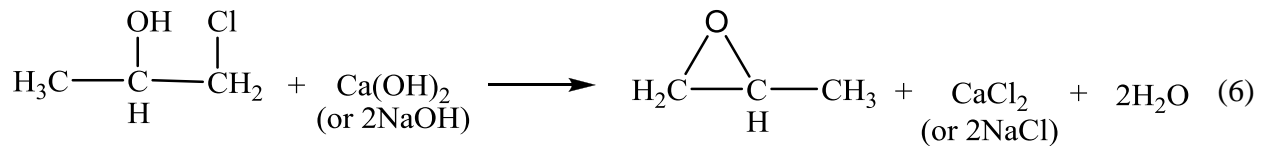
1,3-dichloro-2-propanol   **2,3-dichloro-1-propanol**

(DCH1)   **(DCH2)**

In aqueous solution the chloronium ion can also react with chloride ion leading to the formation of DCP, or with PCH to form 2,2'-dichlorodiisopropyl ether (DCIPE).

In addition, other chlorinated compounds (e.g., monochloroacetone) are produced, but in very small amounts. The modern industrial plants for chlorohydrin PO process give a PCH yield of 88-96%, while DCP, the main side product, varies between 3 and 10%. Small amounts of other side product are also produced: DCH 0.3-1.2%, DCIPE 0.2-0.8%, other 1% maximum. An excess of water has a positive effect on the process: H_2O reduces the concentration of PCH inside the reactor enabling a lesser production of DCP and DCIPE and prevents the formation of a liquid organic phase where chlorine and propylene can react together to give more DCP.

The second step of chlorohydrin process is the dehydrochlorination (also called epoxidation/saponification, Eq. 6) of PCH in the presence of a base, either lime, $Ca(OH)_2$, or caustic soda, to form crude PO and a dilute $CaCl_2/NaCl$ brine stream. The reaction of PO formation is fast and the optimum of conversion requires a slightly excess of alkalinity. Half base is necessary to neutralize the HCl produced in the chlorohydrination step.

$$\underset{H}{\overset{\overset{\displaystyle OH}{|}\quad\overset{\displaystyle Cl}{|}}{H_3C-C-CH_2}} + \underset{(or\ 2NaOH)}{Ca(OH)_2} \longrightarrow \underset{H}{\overset{\overset{\displaystyle O}{\triangle}}{H_2C-C-CH_3}} + \underset{(or\ 2NaCl)}{CaCl_2} + 2H_2O \quad (6)$$

Moreover, during saponification process some organic impurities are removed from the aqueous saline solution, before the final purification step of the epoxide [1].
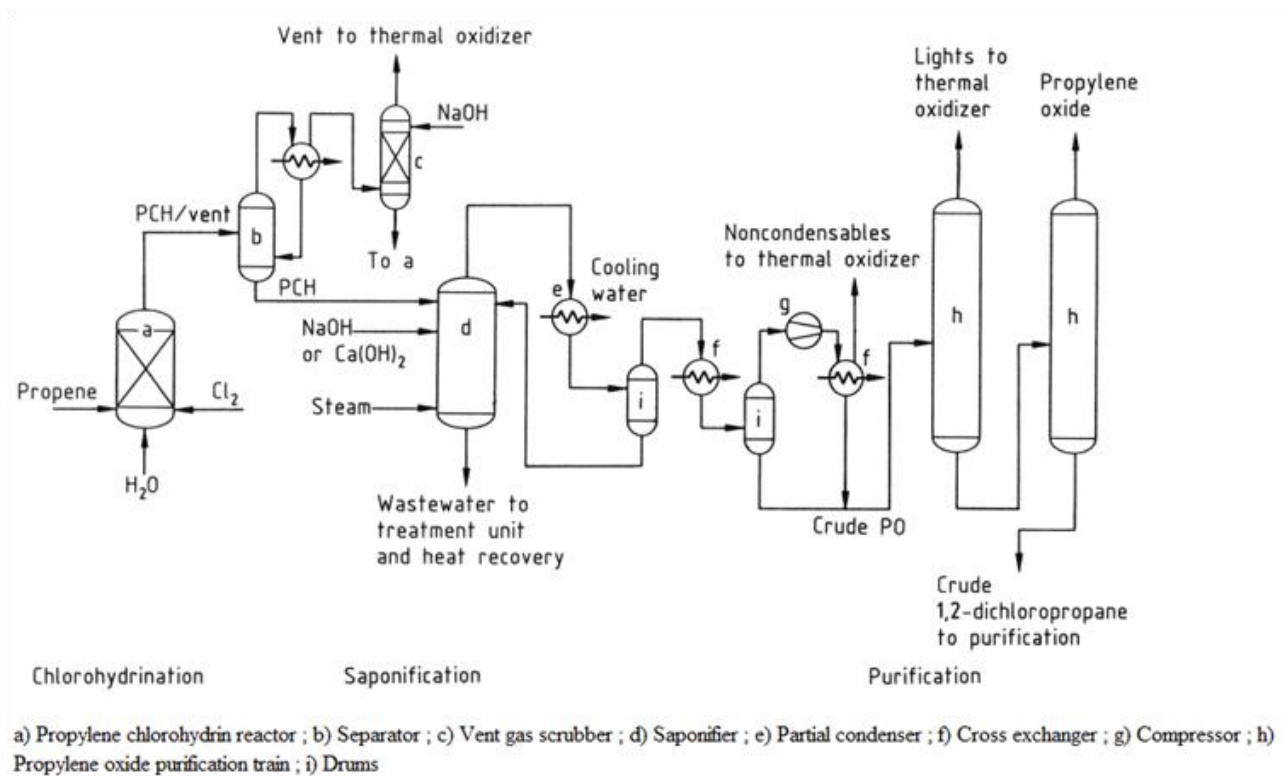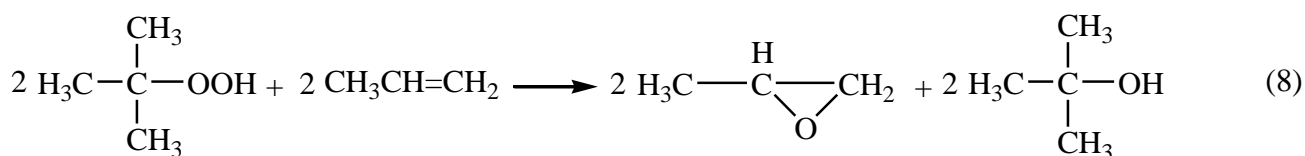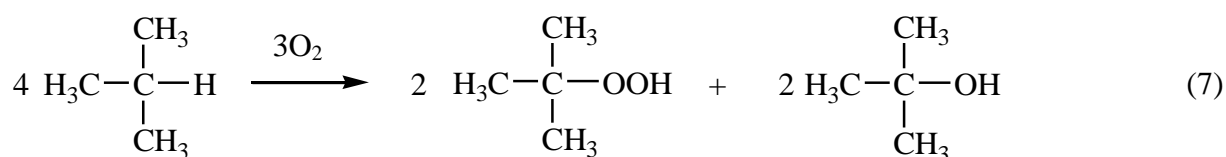

Figure 4.2. Diagram chlorohydrin plant for PO production [1].

Also the indirect oxidation route is a two steps process:

1. Formation of hydrogen peroxide or an organic peroxide from a suitable alkane, aldehyde, or acid

2. Conversion of the peroxide to water, or the corresponding alcohol or acid by epoxidation of propene to propylene epoxide.

The most common oxidants employed in the reaction are hydrogen peroxide, performic acid, perphthalic acid, permaleic acid, perpropionic acid, peracetic acid, tert-butyl hydroperoxide and ethylbenzene hydroperoxide. However, the use of H_2O_2 has two main drawbacks that are the hazard potential associated with its concentrated solution and the high cost [1, 2]. On the other hand, tert-

butyl hydroperoxide and in particular ethylbenzene hydroperoxide are widely used in industry as the reaction of PO formation leads, at the same time, to the synthesis of other coproducts with considerable economic value (these processes are called coproduct processes). Unfortunately, the presence of these coproducts can also become a disadvantage if the demands for PO and the respective coproduct are not properly balanced [4]. On the other hand, chlorohydrine process is free of these considerations. In the indirect processes the hydroperoxide is generated towards a catalytic oxidation of the appropriate substrate with oxygen or air.

Equation 7 and 8 report the main reactions involved in the processes with tert-butyl hydroperoxide.

$$4\ H_3C-\underset{\underset{CH_3}{|}}{\overset{\overset{CH_3}{|}}{C}}-H\ \xrightarrow{3O_2}\ 2\ H_3C-\underset{\underset{CH_3}{|}}{\overset{\overset{CH_3}{|}}{C}}-OOH\ +\ 2\ H_3C-\underset{\underset{CH_3}{|}}{\overset{\overset{CH_3}{|}}{C}}-OH \tag{7}$$

$$2\ H_3C-\underset{\underset{CH_3}{|}}{\overset{\overset{CH_3}{|}}{C}}-OOH + 2\ CH_3CH{=}CH_2\ \longrightarrow\ 2\ H_3C-\overset{\overset{H}{|}}{\underset{\underset{O}{\diagdown\diagup}}{C}}{-}CH_2\ +\ 2\ H_3C-\underset{\underset{CH_3}{|}}{\overset{\overset{CH_3}{|}}{C}}-OH \tag{8}$$

Isobutane is converted by mean of oxygen into tert-butyl hydroperoxide (120-140 °C, 25-35 bar), which partially decomposes to tert-butyl alcohol (Eq. 7). The reaction takes place in the liquid phase and does not require a catalyst. However, additives can be used to optimize reaction conditions. Isobutane conversion is ca. 48% with a selectivity of 50% relative to hydroperoxide and 46% relative to tert-butyl alcohol. Tert-butyl alcohol can be dehydrated to isobutene and then converted to methyl tert-butyl ether (MTBE), which find important application as a fuel additive for lead-free gasoline.

On the other hand, the crude peroxide solution is used for the epoxidation of propene (Eq. 8). It consists of a mixture of tert-butyl hydroperoxide, tert-butyl alcohol, and smaller amounts of aldehydes and ketones. The solution is mixed to the homogeneous catalyst, then dissolved in toluene. The catalyst is typically an organometal soluble in the reaction mixture. The metal center can be tungsten, vanadium, or molybdenum. Molybdenum complexes with napthenates or carboxylates grant the best combination of selectivity and reactivity. Finally, propene is added and the mixture is fed to the epoxidation reactor system, composed of up to five consecutive reactors. Not all the peroxide reacts to form PO and the selectivity, calculated with respect to the converted peroxide to PO is ca. 80%, with a 10-fold excess of propene. Alternatively tert-butyl hydroperoxide

can decompose without transferring oxygen to propene. At the end of the process the reaction mixture contains tert-butyl alcohol, catalyst, and medium- and high-boiling components, other than the desired product, thus crude PO is distilled. However crude PO contains impurities such as hydrocarbons, carbonyl compounds, and ethylene oxide, therefore further purifications are required [1, 4, 5].
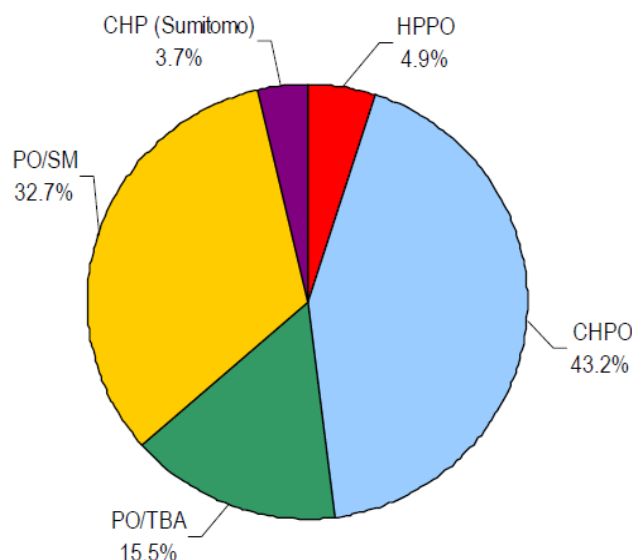
**Figure 4.3.** Propylene oxide capacity share by technology in 2008 [4].

Notwithstanding, the most diffused coproduct process employs ethylbenzene hydroperoxide (and not tert-butyl hydroperoxide) as oxidant agent, with the concomitant production of styrene. Likewise the previous technology, the hydroperoxide is produced by a direct oxidation with air, thus the ethylbenzene hydroperoxide is converted to the corresponding alcohol in the epoxidation reaction with propene and finally dehydrated to styrene. Obviously, the core of the process is the catalyzed epoxidation reaction: the homogeneous catalyst is based on molybdenum, tungsten, or titanium and an organic acid, such as acetate,napthenate, stearate, while the heterogeneous catalysts consist of titanium oxides on a silica support [1, 4, 5].

Unfortunately the actual propylene oxide production routes are inefficient from several point of view. In general they are not atomically economic, since they produce a large amount of by-products and wastes which have brought serious environmental problems [6].

The chlorohydrin process suffers, in particular, from environmental liabilities and large capital investment requirements. The process produces a great amount of wastewater, so extensive water treatment facilities are required, and the salt load means that an environmentally acceptable

geographical location (close to the sea) is desirable. In contrast the coproduct routes present safety concerns: fire and explosion risk are significantly greater than in the case of a chlorohydrin facility. Moreover the product flexibility is considerably more limited with a coproduct plant than with a stand-alone process [1, 4, 5].

Current PO routes (both chlorohydrins and indirect oxidation) are also unsuitable from an energetic point of view: PO production is one of the most demanding process in terms of energy requirement, as showed by high GER value (Figure 4.4). GER (Gross Energy Requirement) indicates the total primary energy consumption of the entire process chain to manufacture a chemical product. This value includes energetic consumption, which in chemical processes is largely represented by the process energy, and non-energetic consumption, namely the direct use of fossil energy sources, such as crude oil [7].
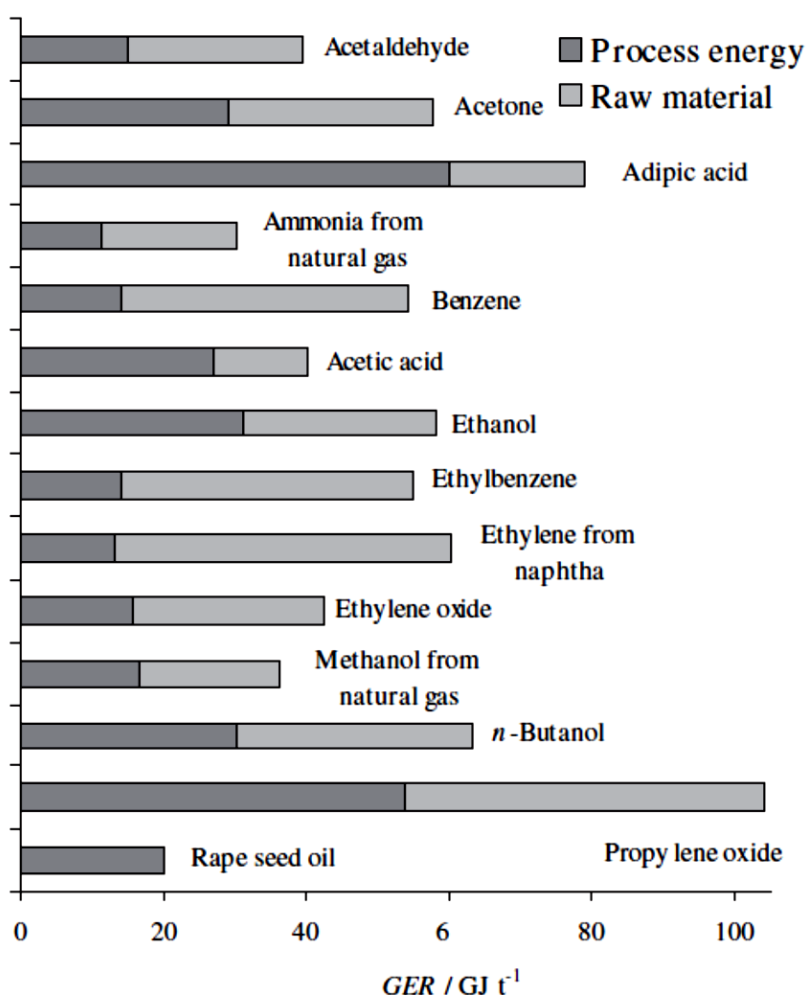
Figure 4.4. Gross energy requirements (GER) for important base chemicals [7].

Direct epoxidation routes

Since the inefficiency of the current PO production processes to found a direct and green epoxidation route, environmentally friendly and economically viable becomes urgent. Many studies have been devoted to the direct C_3H_6 epoxidation using a proper catalyst combined with an appropriate oxidant. Oxidant such as H_2O_2, O_2/H_2 gas mixture and N_2O, in the presence of an appropriate catalyst, can provide excellent PO selectivities at reasonable propene conversions, but these oxidants are still expensive. It is clear that the ideal oxidant for the epoxidation of propylene is oxygen or air [6]. Unfortunately, the direct formation of PO from a mixture of propene and oxygen is a very complicated reaction, due to easy formation of allyl species (by hydrogen abstraction), from the propylene molecules adsorbed on the catalyst surface. Then, by reaction with oxygen the allyl species lead to total combustion. For that reason the heterogeneous silver catalyst, successfully used in large-scale direct epoxidation of ethene (with a selectivity around 85%), is totally inefficient in the homologous epoxidation of C_3H_6, with a selectivity of just 5% [8].

In 1998 Haruta and coworkers brought to the attention the possibility to directly obtain propylene oxide, in high selectivity, from a mixture of C_3H_6, O_2, H_2 using gold catalysts dispersed on TiO_2 or TiO_2/SiO_2 supports [9]. The results were very promising despite the low conversion reached (around 1%), necessary to ensure high selectivity to the epoxide. The reaction takes places in accordance with the following equation:

$$CH_3CH=CH_2 + O_2 + H_2 \longrightarrow \quad H_3C-\underset{H}{\overset{O}{\underset{|}{C}}}\overset{\diagup\ \diagdown}{-}CH_2 \quad + H_2O \tag{9}$$
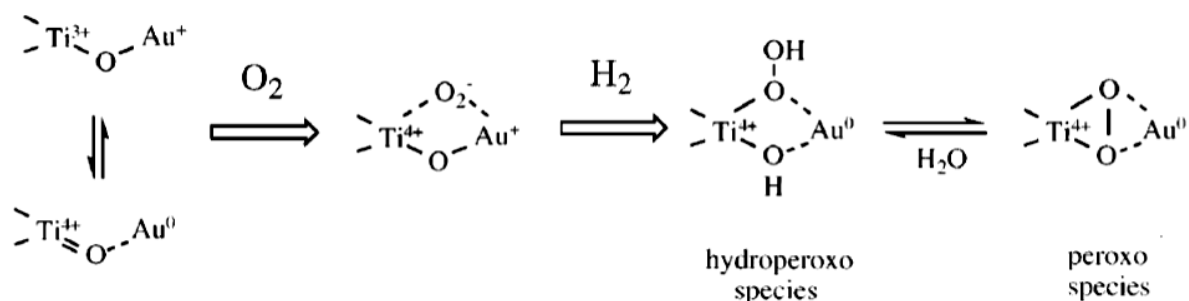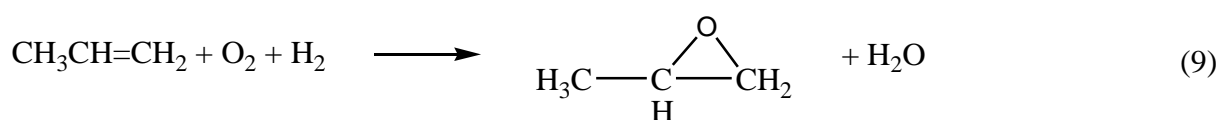
Figure 4.5. A probable pathway for the formation of an active oxygen species on Au/TiO_2 catalyst [9].

Since neither titanium oxide nor gold alone exhibit catalytic activity between 30 °C and 300 °C, it is clear that the combination of the two species is mandatory to give the selective oxidation of C_3H_6. Reasonably, hydrogen reacts with oxygen to form an active species (likely a peroxo species, formed on cationic Ti site, between gold particles and TiO_2 support, Figure 4.5) able to selectively oxidize propene adsorbed on Au particles to PO. The identified side products of the reaction are acetone and carbon monoxide. Without hydrogen the oxidation proceeded only at temperature above 200 °C and produced only CO_2 and water. Interestingly, while the conversion of propene was always very low (as already mentioned), the H_2 consumption to give water resulted to be much larger than the one calculated from the stoichiometry of Eq. (9). For example, at 80 °C this value was about 1.4 times as the stoichiometric amount required to produce PO. This fact implies that the selective partial oxidation may principally proceed via Eq. (9): O_2 is transformed by reduction with H_2 to an active species which has the ability to selectively oxidize C_3H_6 to PO. However the ratio of H_2 consumption to oxygenate formation increased with reaction temperature, indicating that the combustion of H_2 with O_2 is more enhanced than the partial oxidation of C_3H_6 at high temperature. Obviously, from the economical point of view, it is necessary to minimize the ratio of hydrogen consumption towards the theoretical value of 1, by limiting the reaction of H_2 with O_2 to form H_2O. When TiO_2 support is replaced with TiO_2 dispersed on SiO_2 (TiO_2/SiO_2) the optimum of reaction temperature is shifted to higher value, but a good selectivity toward the epoxide is preserved. This shift can be related to a decrease of catalytic activity towards H_2 oxidation, however it is also likely that the separation of active sites over the SiO_2 surface allows high temperature reaction maintaining a good selectivity to the epoxide. In any case, it is clear that there is an optimum temperature region for each gold catalysts for the epoxidation of propylene; on the other hand H_2 combustion monotonously increases with the reaction temperature.

Different supported metals (such as Pd, Pt, Cu and Ag on TiO_2) have been tested, however only gold based catalysts prepared with deposition-precipitation technique resulted in important PO selectivity. The combination of Au with other metal oxides, such as Al_2O_3, SiO_2, ZnO, ZrO_2, Fe_2O_3 e Co_3O_4, did not lead to the partial oxidation of propene but conduced only to complete combustion. Using metals like Pd and Pt supported on TiO_2 the main reaction was the hydrogenation of alkene to C_3H_8, with traces of acetone. On the other hand Cu/TiO_2 and Ag/TiO_2 did not catalyze neither such reaction nor the partial oxidation of propene.

It is now recognized that gold catalysis is strongly dependent on particle size (see also Chapter 1). In this view the catalyst preparation method plays a key-role: in fact with the classic impregnation only large gold particles were generated on support surface (with a diameter larger than 10 nm) and

during the reaction PO was not observed. Nevertheless also gold loading is an important parameter which generally affects the size of the nanoparticles.

Catalyst	Metal loading,[a] wt%	Reaction temperature, K	Reaction[b] conditions	Conversion, %		Selectivity,[d] %				PO yield,[f] %	PO formation rate	
				C_3H_6[c]	H_2	PO[e]	Acetone	C_3H_8	CO_2		mmol/hr/g-cat	mmol/hr/g-Au
Au/TiO$_2$	0.98	323	A	1.1	3.2	>99	-	-	-	1.1	0.2	20.0
Au/TiO$_2$[g]	1.0	353	A	0.2	8.9	-	-	<10	>70	-	-	-
Au/TiO$_2$	3.2	303	B	0.3	2.5	93	7	-	-	0.3	0.27	8.4
		323	B	0.6	4.2	96	4	-	-	0.6	0.54	16.7
Au/TiO$_2$/SiO$_2$	0.20	393	C	2.5	2.6	93	-	-	7	2.3	0.21	102.7
Pd/TiO$_2$	1.0	298	A	57	98	-	0.4	98	1	-	-	-
Pt/TiO$_2$	1.0	298	A	12	87	-	2	92	6	-	-	-
Cu/TiO$_2$	1.0	393	A	<0.2	2.7	-	-	-	>99	-	-	-
Ag/TiO$_2$	1.0	393	A	<0.1	<0.1	-	-	-	-	-	-	-

[a] Actual metal loadings determined by X-ray fluorescence analysis.
[b] A: Feed gas, $C_3H_6/O_2/H_2/Ar = 10/10/10/70$; flow rate, 2000ml/hr; catalyst, 0.5g; B: Feed gas, $C_3H_6/O_2/H_2/Ar = 10/10/10/70$; flow rate, 2000ml/hr; catalyst, 0.1g; C: Feed gas, $C_3H_6/O_2/H_2/Ar = 5/10/40/45$: flow rate, 2000ml/hr; catalyst, 0.5g.
[c] Conversion of propylene = 100 (moles of all products detected by GC analysis)/(moles of propylene fed); moles of CO_2 formed divided by three.
[d] Selectivity = 100 (moles of each product detected directly by GC analysis)/(moles of all products detected directly by GC analysis); moles of CO_2 formed divided by three.
[e] PO = propylene oxide.
[f] PO Yield = 100 (moles of PO detected directly by GC analysis)/(moles of propylene fed).
[g] Prepared by impregnation method.

Table 4.3. Epoxidation of propene on different heterogeneous catalysts [9].

Haruta and coworkers compared gold catalysts prepared with the same method, but with different particle size due to different metal loading (from 0.98 to 0.02%, Table 4.4). Catalysts with a gold amount of 0.98% and 0.39% were active in the epoxidation of propylene (with the formation of PO and CO_2 as side product), while samples with a gold amount lower than 0.10% catalyzed the formation of C_3H_8. Both PO and C_3H_8 were competitively produced for a metal loadings of 0.20 wt% and 0.10 wt%, but for latter catalyst C_3H_8 tend to exceed PO. Characterization indicated that in the case of 0.98 wt% and 0.39 wt% Au samples gold particles had hemispherical shape and were homogeneously dispersed with a mean diameter (determined by TEM) of 2.4 and 2.2 nm. On the other hand, a great difference in particle size was observed when gold loading decreased from 0.39 to 0.20 % (mean diameter 2.2 versus 1.5 nm). Finally, below 0.20 wt% of gold the particle size of Au/TiO$_2$ catalysts did not change so much. From the correlation between reactivity and TEM analysis the authors primarily concluded that gold particles larger than 2 nm are responsible for the formation of PO, whereas those below 2 nm catalyze the formation of C_3H_8. Gold particles smaller than 2 nm can be oxidic in nature due to the presence of O_2 or, in other word, can be partially positively charged, whereas Au particles larger than 2 nm might be still metallic. The positively charged state of Au may have electronically some similarities to that of Pt metal and can catalyze hydrogen dissociation and then hydrogenation. It is probable that Au can remain oxidic only in presence of oxygen and therefore O_2 is necessary for hydrogenation over Au/TiO$_2$. However, these

results showed by Haruta at al. indicated that the reaction pathway switches over from oxidation to hydrogenation over Au/TiO_2 catalysts depending on the particle size [9].

The reaction was successively improved by adding trimethylamine (10-20 ppm) to the reagent gas stream. The base can significantly improve the performance of the gold catalysts in terms of catalyst lifetime, catalyst regeneration, PO selectivity and H_2 efficiency. Trimethylamine is a strong Lewis base (pK_a= 9.9) and it can act by poisoning the Lewis acid site present on the support surface (mainly isolated Ti^{4+} centres). In fact, the acid sites are responsible for the side reactions of oligomerization, cracking and isomerization that forms PO byproducts and cause catalyst deactivation. Moreover the adsorption of the base on gold surface can suppress H_2 combustion to produce water, which results in an improved hydrogen efficiency [10].

Au loadings,[a] wt%	Yield of products,[b] %			TEM observaiton			
	Propane	Propylene oxide	CO_2	Total number of Au particles	Mean diameter, nm	Most frequent diameter, nm	Standard deviation, %
0.98	—	0.61 [0.109][c] (11.1)[d]	0.08 [0.014] (1.4)	446	2.4	2.2-2.4	25
0.39	-	0.56 [0.100] (25.6)	0.20 [0.036] (9.2)	258	2.2	2.2-2.4	30
0.20	0.33 [0.059] (29.5)	0.54 [0.096] (48.0)	0.05 [0.009] (4.5)	393	1.5	1.2-1.4	25
0.10	1.9 [0.346] (346)	0.1 [0.018] (18.0)	-	35	1.8	1.0-1.2	36
0.05	3.1 [0.554] (1108)	-	-	79	1.5	0.8-1.0	25
0.02	2.5 [0.446] (2230)	-	-	80	1.7	1.4-1.6	25

[a] Actual Au loadings determined by X-ray fluorescence analysis.
[b] Reaction conditions: feed gas, $C_3H_6/O_2/H_2/Ar = 10/10/10/70$; flow rate, 2000ml/hr; catalyst, 0.5 g; temperature, 353K.
[c] Formation rate (mmol/hr/g-cat) is given in parenthesis [ ].
[d] Formation rate (mmol/hr/g-Au) is given in parenthesis ( ).

Table 4.4. Size dependent catalytic behavior of Au/TiO_2 catalysts [9].

Gold is not the only metal active in epoxidation of propene. A series of surface studies carried out on Ag and Cu single crystal, under ultrahigh vacuum conditions, showed as low index copper facets, like (110) and (111), are more selective than those of Ag in the epoxidation of olefins, such as styrene and methylstyrene. In particular superior activity is pointed out for copper (111) facets, with respect to (110) [3, 11-15]. Further investigation extended these results to the epoxidation of propene [8, 16].
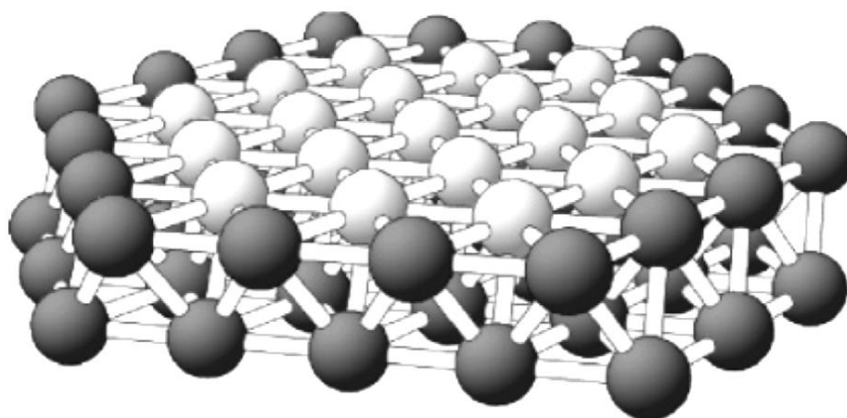
**Figure 4.6.** Cu cluster simulating the Cu(111) surface [14].

The investigation carried out on silver crystal showed that oxygen can adsorb on the metal surface both in molecular and atomic (O_a, oxygen adatoms) way. It is just the oxygen adatoms which is responsible for all the catalytic activity (both combustion and epoxidation reaction), while O_2 is merely a spectator. However Ag catalysts drive the reaction towards total combustion of propene.

Not only oxygen but also the alkene needs to be adsorbed in the appropriate chemical state. On Ag, ethene adsorbs with minimal rehybridisation of the olefinic π bond, thus oxygen insertion to yield the epoxide is therefore possible. In contrast, on Ni and Pt surfaces, for example, the alkene is present as a di-σ-bonded species: in this case the possibility of epoxidation is eliminated, whatever the state of the adsorbed oxygen. The adsorption of alkene on copper surface resembles that on silver and under appropriate conditions the O_a can be formed: so there are all the condition necessary to have the epoxidation of terminal olefins [8, 11, 17]. The accepted reaction mechanism, proposed by Linic and Barteau, is illustrated in Figure 4.7:
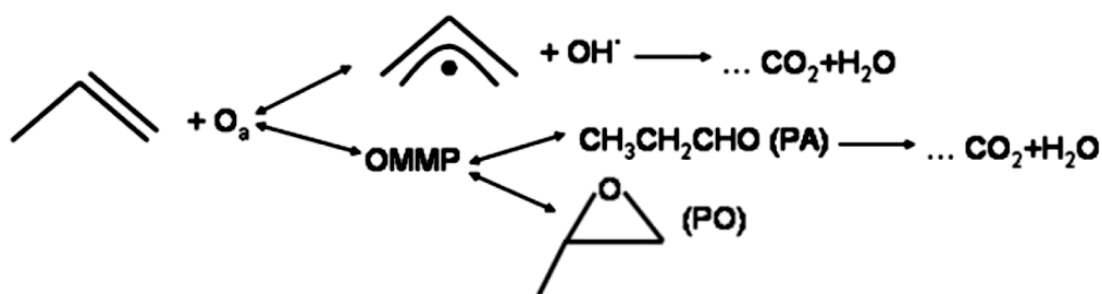
Figure 4.7. Reaction mechanism for propylene oxidation [8].

The reaction between oxygen adatoms and C_3H_6 on metal surface can lead, by removal of allylic hydrogen, to the dehydrogenation of alkene with the formation of hydroxyl and allyl species (the precursors of combustion). Alternatively a propylene oxametallacycle can be formed (OMMP, Figure 4.8). This intermediate is analogous to the one proposed for the direct epoxidation of ethane, named OMME. The OMMP intermediate can rearrange to give propylene oxide or propanal, the latter eventually leading to combustion. A strong basic character of O_a disfavors the epoxidation, driving the reaction towards the removal of allylic hydrogen and, thus, to the combustion. On the other hand, a low basic character of the oxygen adatoms favors the formation of oxametallacycle and then the propylene oxide production. However it has also hypothesize that other species other than (or in addition to) O_a are generated by oxygen dissociation: these are O^-, O_2^- and O^{2-}. O^{2-} is a nucleophilic species, whereas O^- and O_2^- are the electrophilic ones. If these compounds are present in the reaction system they may also have a role in the oxidation pathway. In fact, O^- can attack the C=C double bond of propylene to form PO, while O_2^- can react with the carbon double bond of propylene to form unstable peroxy complexes and causes the break of C=C bond and the total oxidation of propylene. Finally O^{2-} may attack the allylic C–H bonds anion to form acrolein and acrylic acid. In any case propylene epoxidation on silver is strongly disfavored because of the markedly basic character of O_a [18, 19]. In contrast, the lower basicity of copper favors metallacycle formation instead of the epoxide production. Theoretical estimates of epoxidation selectivity are in good agreement with experimental data for both silver and copper catalysts. These calculations shows that on Cu (111) the OMMP formation is favored with respect to the allylic hydrogen abstraction: around 220 °C the selectivity towards the epoxidation intermediate is around 60%, while under the same conditions around 99% of the adsorbed propylene molecules will undergo allylic hydrogen-atom abstaction on Ag (111). In the second reaction step about 99% of OMMP should undergo cyclization to PO, whereby the total selectivity for the entire process on copper surface should be more than 50%, as confirmed by catalytic experiments [8].

The styrene epoxidation reaction on copper can be further improved by the addition of Cs, as it has been shown by single crystals studies. A small amount of Cs (a submonolayer) enhances the olefin uptake and the styrene epoxide yield, without affecting the reaction selectivity. The proposed explanation is that the added metal reduces the oxidized copper sites, that are catalytically inactive, to active metallic copper sites. Thus cesium avoid the formation of great quantities of copper oxide, hence the passivation of the catalyst surface. Clearly under continuous reaction conditions this process would become certainly ineffective, because of the consequent oxidation of Cs, but these results pointed out the apparent crucial role of metallic copper [17].
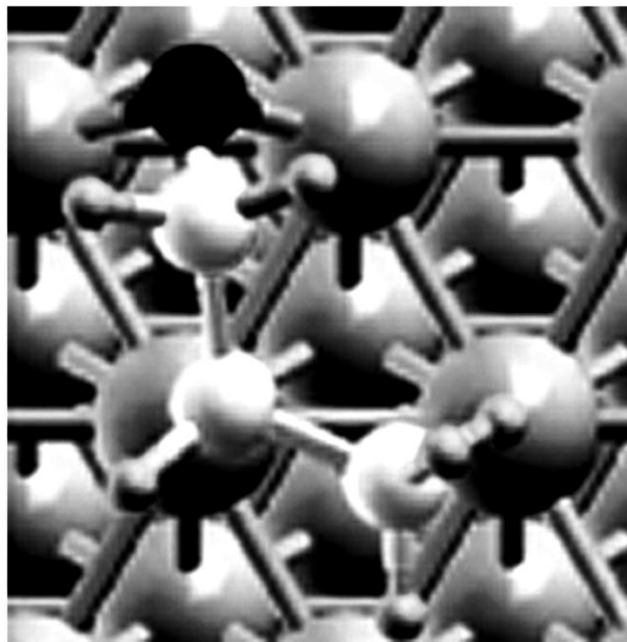
Figure 4.8. A propylene oxametallacycle (OMMP) on a (111) metal surface (C white, H small gray, O black, metal large gray) [8].

From theoretical single crystal studies the attention has been shifted to the investigation of a potential heterogeneous copper catalyst. In 2005 the first Cu/SiO_2 catalyst active in the epoxidation of propylene was reported [16]. This Cu/SiO_2 catalyst gave PO selectivity of 55% at about 1% of reagent conversion, under conditions suitable for the survival of metallic copper. Hence the performance of copper based catalyst were comparable with those of Ag/TiO_2, but differently to the latter, the former not requiring the hydrogen co-feed (an evident economical benefit).

After the reduction treatment of the catalyst in hydrogen stream, the reaction was carried out in a fixed-bed reactor in the presence of C_3H_6, O_2 and He (5%/5%/90%) between 220 and 380 °C (Figure 4.9). The main reaction products were PO, acrolein, combustion products (CO, CO_2, H_2O) and traces of acetone and acetaldehyde. In order to understand the mechanism of side products formation, the reaction of propylene oxide was carried out at 225 °C. Without oxygen the major products were propanal (75%), acetone (13%), acetaldehyde (3%) and CO_x (9%). In the presence of oxygen, acrolein became the main organic product (21%), followed by acetaldehyde, propanal and acetone (14%, 12% and 5%), while CO_x were 48%. Hence, when O_2 is present propanal undergoes an oxidative dehydrogenation to give acrolein. Thus it appears that production of acrolein during propene oxidation is at least partly due to the formation and further reaction of propylene oxide. Rodriguez et al. reported in situ XRD studies of the oxidation state of copper, as a function of temperature, under similar conditions of O_2 partial pressure used by Lambert and coworkers in their

catalytic experiments. They found that Cu^0 was the predominant species at temperatures below 250 °C, followed by Cu_2O at intermediate temperatures, with an onset of CuO formation at ~350 °C [20].
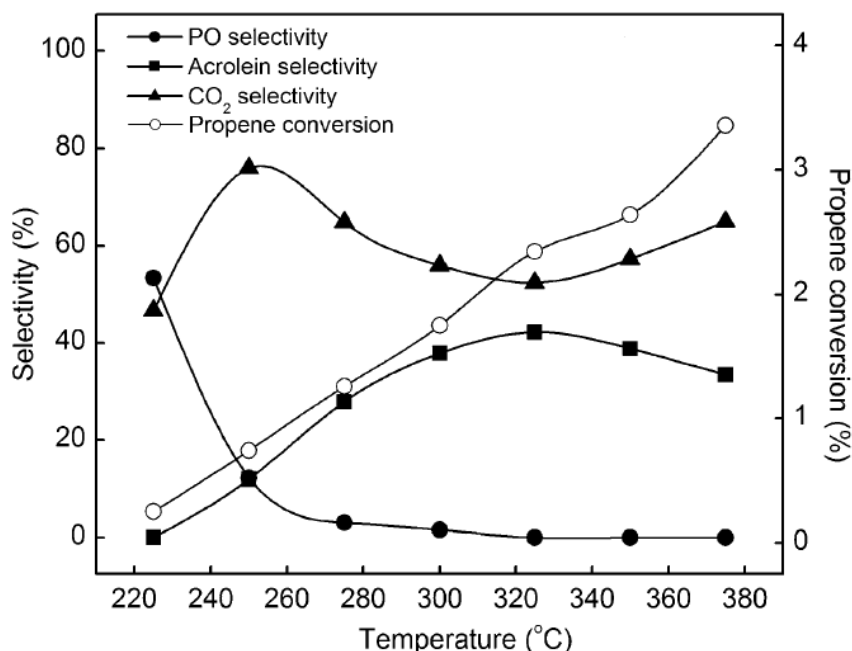
Figure 4.9. Effect of temperature on selectivity to major products and propene conversion for the oxidation of propene. Gas feed 5% C_3H_6, 5% O_2, 90% He; total flow is 50 mlmin^{-1}; 0.1 g catalyst [16].

During the reaction on Cu/SiO_2 catalyst, the selectivity to PO was greatest at 225 °C (at C_3H_6 conversion of 0.25%) and fell down quickly to a negligible value at about 270 °C (C_3H_6 conversion, 1.26%). From 225 °C to 325 °C the selectivity towards acrolein increased, while the combustion process was active all the time and the CO_2 selectivity, even if depending on the temperature, resulted always to be higher than 40%, with a decrease between 250 °C and 320 °C followed by a growth. The results, compared with XRD data, suggest that CuO catalyses propene combustion, whereas Cu_2O favors partial oxidation to acrolein (similar conclusion were also reported by Reitz and Solomon [21]). Anyway, our attention should be focused on the resistance of metallic copper in the temperature range within PO is formed. This is an important indication that the active site for the epoxidation reaction is associated with Cu^0. Moreover, as reported also for the epoxidation of methylstyrene and styrene, the oxidation of copper inhibits the PO production [12, 17].

Furthermore the complete characterization of Cu/SiO_2 catalyst suggested that the active species for propene epoxidation consists of a highly dispersed nanoscopic metallic phase with an electronic

structure, and thus chemical properties significantly different from those of mesoscopic or macroscopic copper [16].

The paper published by Lambert et al. in 2005 raised great attention by scientific community and further studies have been performed from different research group. Despite the evidences reported in support of metallic copper, the nature of the active site is still debated.

In 2006 Wang and coworkers proposed a silica copper based catalyst modified with potassium (K^+-modified CuOx/SBA-15), obtaining high PO selectivity (15-50%) at important conversion of C_3H_6 (1-12%), in the direct epoxidation of propene [22]. Interestingly they found as the active species an oxidized form of copper: Cu (II) or more likely Cu (I). Thus, the catalyst was oxidized in oxygen flow at 550 °C before the reaction and was not subjected to any reductive treatments. The reaction tests were performed using a fixed-bed reactor and a gas flow containing, other that C_3H_6 and the carrier gas, an high partial pressure of O_2. H_2 was not co-feeded. In absence of K^+ promoter (Fig cc) the propylene conversion was higher, whereas PO selectivity was low (only 6.9% at 0.77% of conversion, 225 °C) and the major product of partial oxidation was acrolein. In presence of K^+ PO, not acrolein, raised up and became the main product of oxidation, with a selectivity of 59% and 46% at 0.40% (225 °C) and 0.95% (250 °C) of C_3H_6 conversion. The condition of PO formation suggests that highly dispersed and oxidized copper species (Cu^{2+} or Cu^+), modified with K^+, are responsible of the epoxidation in the presence of O_2. In particular, it seems more likely that Cu (I), which may be formed on the surface of the catalyst during the reaction, plays a pivotal role in C_3H_6 epoxidation. In fact an electrophilic-type oxygen species generated from O_2 is required for epoxidation, and Cu(I) may activate O_2 to such an oxygen species.
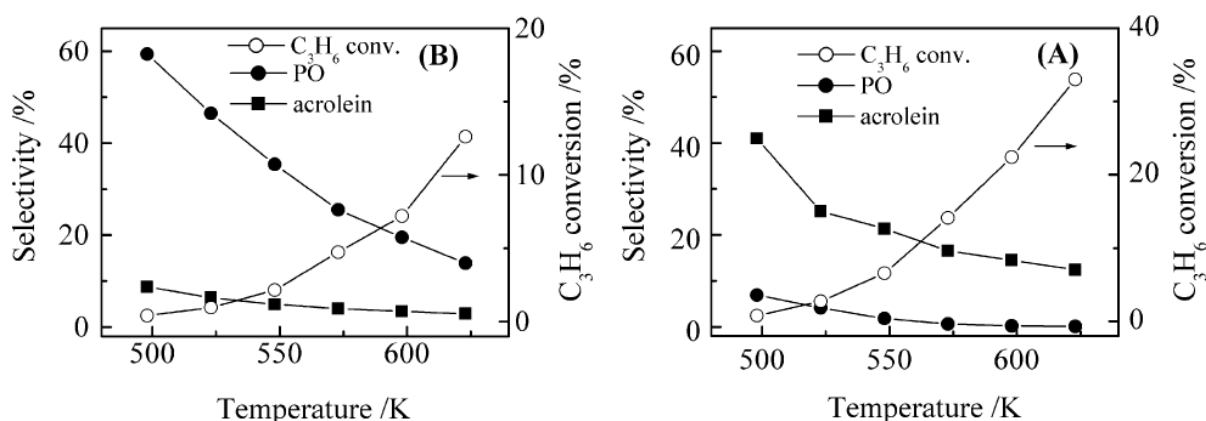
Figure 4.10. Temperature dependences of catalytic behaviors of the 1 wt% CuOx/SBA-15 (A) and the K^+–1 wt% CuOx/SBA-15 (K/Cu = 0.7) (B) for the oxidation of C_3H_6 by O_2. The other products were mainly CO and CO_2. Catalyst, 0.2 g; $P(C_3H_6)$, 2.5 kPa; $P(O_2)$, 98.8 kPa; total flow rate, 60 mLmin^{-1} [22].

The addition of K^+ led to different results depending on the potassium precursor employed; however the metal cation appears to shift the reaction pathway from acrolein to propylene oxide formation, with different possible mechanisms. One possibility is that K^+ may favor the formation of Cu(I) species on the surface or stabilize this species during the reaction. K^+ also may stabilize the electrophilic-type active oxygen species, such as peroxide or superoxide, responsible for the epoxidation on the catalyst surface.

At last, using different copper loading the authors observed that propylene conversion increased until 3 wt% of Cu, then decreased rapidly for further addition of metal. Finally the best K/Cu ratio for better selectivity to PO appeared to be 0.7 (with a Cu loading of 1%) [6, 22, 23].

Recently bimetallic or trimetallic copper based system (Ru-Cu(111) surface, $CuAu/SiO_2$ and RuO_2-CuO-$NaCl/SiO_2$) and the role of different promoters (VO_x, Na^+, Cl^-) have been investigated [2, 24-27].

Aim of the work

In this chapter different copper silica and silica-alumina catalysts have been tested in propylene epoxidation reaction, in the presence of C_3H_6, O_2 and He (carrier gas), without the co-feeding of H_2. The different nature of copper phase on CuO/SiO_2 and CuO_x/SiO_2-Al_2O_3 13 (as we elucidate in Chapter 2) and different pretreatment conditions provided some important tips about the active site of the reaction. In particular the activity of Cu^{2+}, $Cu^{\delta+}$ ($+1 \leq \delta \leq +2$) and Cu^0 were compared. Reaction products were analyzed by on-line mass quadrupole and the PO partial pressure (p_{PO}) was taken as the marker of catalytic activity. Moreover a FT-IR study of adsorbed styrene with the aim to investigate the interaction between catalyst surface and the C=C double bond involved in the epoxydation reaction was presented.

New catalytic tests, analyzing the product with a proper GC system, are currently in progress in collaboration with Professor Sels research group in Leuven University. New data will allow to provide a full quantification of the side-product together with conversion and selectivity values.

4.2 Experimental

Chemicals

Styrene was purchased from Aldrich and used without further purification, gases were purcheased from Siad.

Catalytic tests

The reaction of epoxidation of propene was carried out in fixed-bed reactor at atmospheric pressure with a gas flow of C_3H_6, O_2 and He (7.5 ml/min, 3.75 ml/min, 38,75 ml/min), space velocity= 55000 h^{-1}, between 180-300 °C (2.5 °C/min). The products were analyzed by quadrupole mass Thermo Fischer Scientific VGQ. As marker of catalytic activity we have reported a propylene oxide partial pressure (p_{PO}). All gas lines and valves between the exit of the reactor and the mass spectrometer were heated in order to prevent condensation of the products.
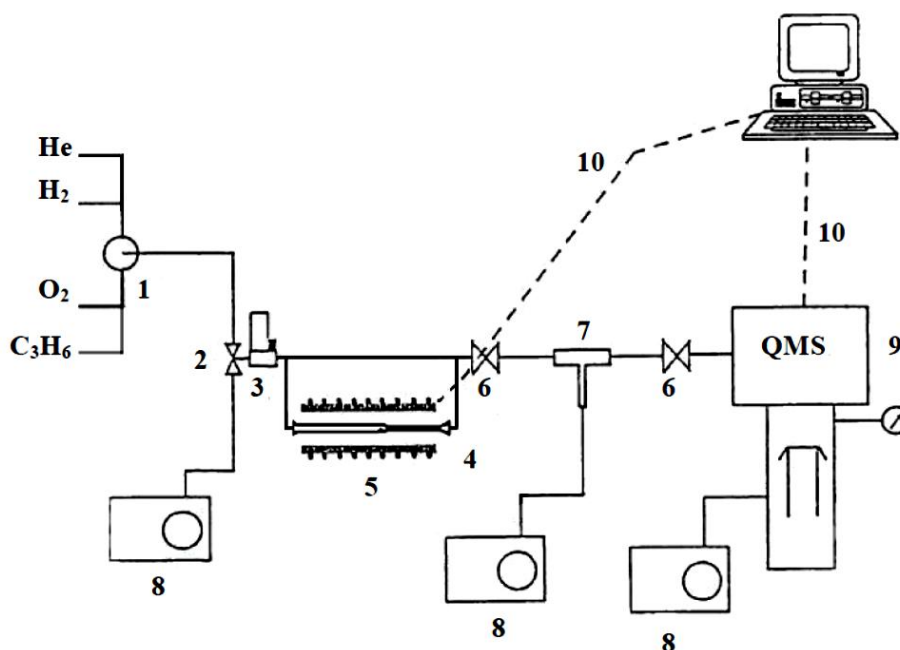
Figure 4.11. Diagram of the reaction system: 1) Gas selector; 2) Gas/vacuum valve; 3) Flow regulator; 4) Reactor; 5) Oven; 6) High vacuum valve; 7) Jet separator; 8) Mechanical pump; 9) Mass spectrometer; 10) PC connection.

Before reaction the catalyst was pretreated (reduction or simply dehydration) in situ in the quartz reactor. Reduction pretreatment consisted of an heating in He flow from RT to 270 °C (10 °C/min), then helium was fluxed for 20 min and finally hydrogen was fluxed for 10 min. Alternatively, for

the dehydration, catalysts was heated in He stream until 270 °C (10 °C/min) and left at 270 °C on He for 20 min. After the pretreatment catalyst was purged and cooled down in He flow until 180 °C, then the reactant flow (C_3H_6, O_2 and He) was introduced into the reactor and the reaction started. Identified side products were: propylene oxide, acrolein, acetaldehyde (traces), CO, CO_2 and H_2O.

FT-IR of adsorbed styrene

For FT-IR studies of adsorbed styrene 15 wt% Cu/SiO$_2$ Chrom powdered catalysts have been pressed in self supporting disks (average weight 30 mg), reduced in pure hydrogen (270 °C, 400 torr) and outgassed at the same temperature directly in the IR cell connected to a gas manipulation apparatus. The sample was cooled down and styrene was adsorbed (4-6 torr). Further heating and styrene adsorption were done, as needed. A spectra of pure styrene gas was also registered in same condition. The spectra were recorded with Nicolet Magna 750 and Nexus instruments with a resolution of 4 cm^{-1}. Result were present as a subtraction of reduce 15 wt% Cu/SiO$_2$ CH spectrum to the spectra of adsorbed styrene on catalyst surface. A spectrum of pure liquid styrene on KBr disk was recorded as reference.

4.3 Results and Discussion

Propene epoxidation: role of copper phase

According to the literature $CuO_x/SiO_2-Al_2O_3$ made by CH are mainly composed of isolated copper species with oxidation state ranging from (II) to (I). Reduction at 270 °C results in a significant decrease in the amount of the Cu (II) species in favor of $Cu^{\delta+}$ $(1 < \delta < 2)$ and Cu (I) ones, with a consequent very limited production of metal particles, as showed mainly by EXAFS-XANES spectra reported by Gervasini and coworkers [28, 29]. Thus, copper on $SiO_2-Al_2O_3$ resembles to the ones on ZSM-5 exchanged zeolite [30]. However, as deeply discussed in Chapter 2 reduced copper silica-alumina catalysts expose more or less reducible copper phase depending on the copper loading: up about 5 wt% only $Cu^{\delta+}$ $(+1 \leq \delta \leq +2)$ strongly resistant to reduction is formed on the catalyst surface, while after this loading a CuO phase easily reducible to well formed Cu(0) crystallites begins to form on the surface. This peculiar behavior makes reduced $Cu/SiO_2-Al_2O_3$ 13 catalysts the ideal materials for the study of active site in the propylene epoxidation. In fact, the mild reduction condition (270 °C, 10 min) is sufficient to reduce Cu (II) species (if present) to metallic copper, leaving almost unchanged the $Cu^{\delta+}$ present. In Figure 4.12 we report the PO partial pressure obtained in the epoxidation reaction on $Cu/SiO_2-Al_2O_3$ series with a copper amount ranging from 1 wt% to 12 wt%.
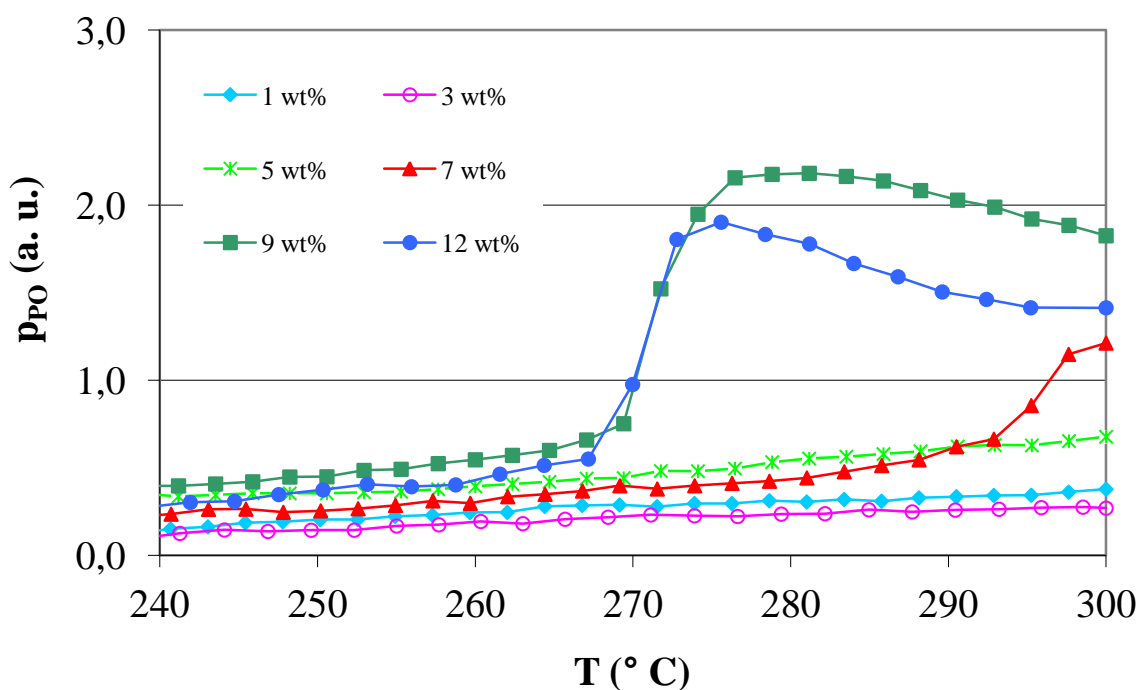
Figure 4.12. Propene epoxidation: reduced $Cu/SiO_2-Al_2O_3$ 13 CH catalysts, with 1-13 wt% of Cu.

The catalytic tests clearly show that only catalysts exposing metallic copper on the surface give an important partial pressure of PO. 1 and 3 wt% samples result in a negligible partial pressure of PO, while 5 wt% catalyst is again almost inactive. From 7 wt% of copper the PO partial pressure raises considerably, in coincidence with formation of an high fraction of easy reducible CuO phase with respect to total copper present on the sample.

The key role of metallic copper is definitely pointed out by comparing reduced and unreduced (dehydrated) 5 wt% silica and silica-alumina catalysts (Figure 4.13): unreduced catalysts, exposing Cu^{2+} and $Cu^{\delta+}$ (respectively CuO/SiO_2 332 and $CuO_x/SiO_2\text{-}Al_2O_3$ 13), show very low p_{PO}, while reduced Cu/SiO_2 332 exposing copper metal particles is the only one showing a high activity. In fact, as seen from characterization on SiO_2 a well reducible CuO phase is formed for any copper loading.
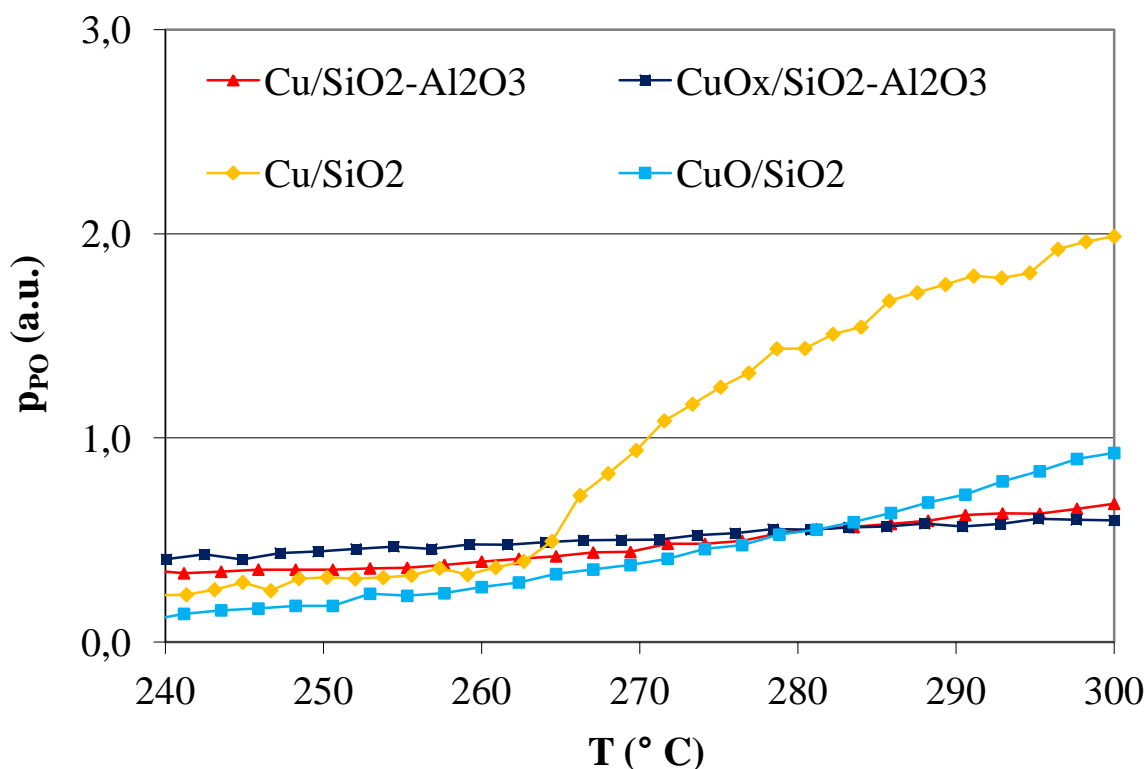
Figure 4.13. Propene epoxidation: dehydrated and reduced 5 wt% SiO_2 332 CH and $SiO_2\text{-}Al_2O_3$ CH catalysts.

On the other hand reaction profiles of reduced and dehydrated $Cu/SiO_2\text{-}Al_2O_3$ 13 catalyst are almost coincident because of the negligible influence of the reduction pretreatment on low loading silica-alumina catalysts. By contrast, the reductive pretreatment results to be effective with high loading materials (Figure 4.14).

From these results clearly appears the inefficiency of copper ions (Cu^{2+}, Cu^+ or $Cu^{\delta+}$) with respect to Cu (0), in the epoxidation of propene.
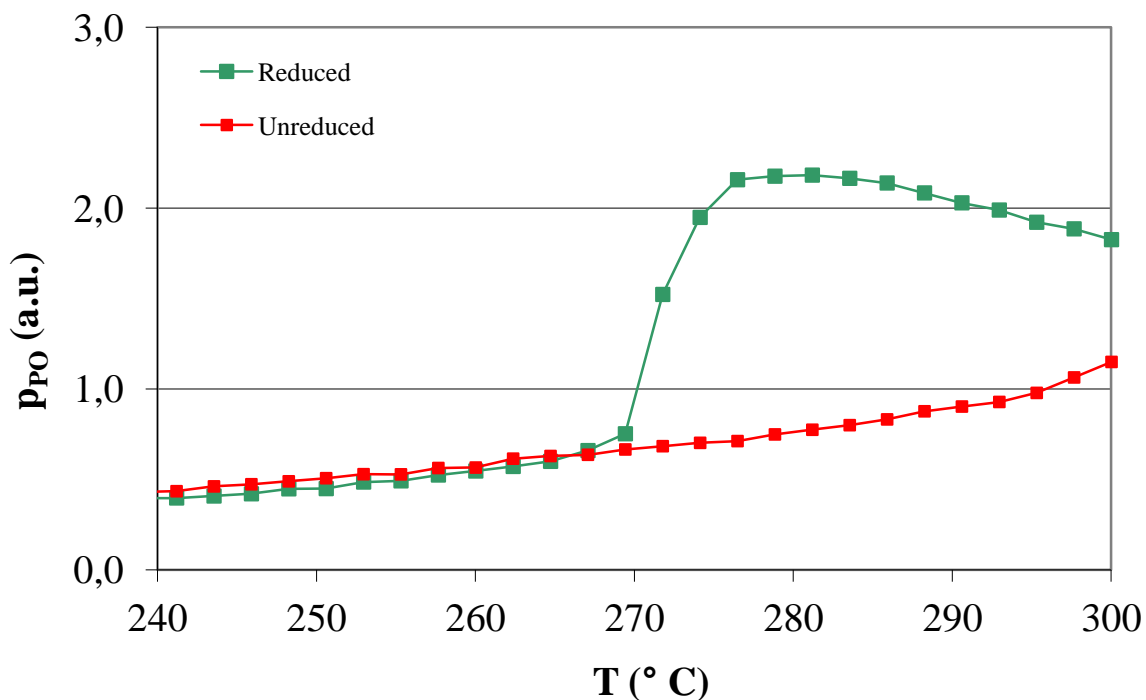
Figure 4.14. Propene epoxiation: 9 wt% reduced and unreduced $Cu/SiO_2-Al_2O_3$ 13 CH catalysts..

The optimum of temperature, from the PO productivity point o view, appears to be over 270 °C, for all the catalysts investigated.

Propene epoxidation: role of metal particles structure and size

The best catalyst for the epoxidation of propylene were found to be the silica supported ones: Al_2O_3, SiO_2-ZrO_2, SiO_2-TiO_2 and $SiO_2-Al_2O_3$ gave lower p_{PO}. In particular high copper loading (15 wt%) reduced Cu/SiO_2 catalysts show a high activity. In Chapter 2 we described how both reduced 8.5 wt% and 15 wt% SiO_2 Chrom CH materials show a high dispersion and very small metal particles (1.7 nm and 2.8 nm from EXAFS). In particular FT-IR spectra of adsorbed CO indicate that on the surface of 15 wt% sample well-formed copper nanoparticles exposing (111) facets are present, while 8.5 wt% one is composed mainly of zerovalent clusters and structured particles are only hint. The high activity of 15% Cu/SiO_2 Chrom is in agreement with the result reported by Lambert et al. (Figure 4.15): high dispersion of metallic copper nanoparticles which, differently to 8.5 wt% Cu/SiO_2, expose (111) planes [12, 15, 16]. It should be noticed, as deeply discussed on Chapter 2, that the ability in keeping a high dispersion even at very high copper loading is an intrinsic properties of the Chemisorption-Hydrolysis method.
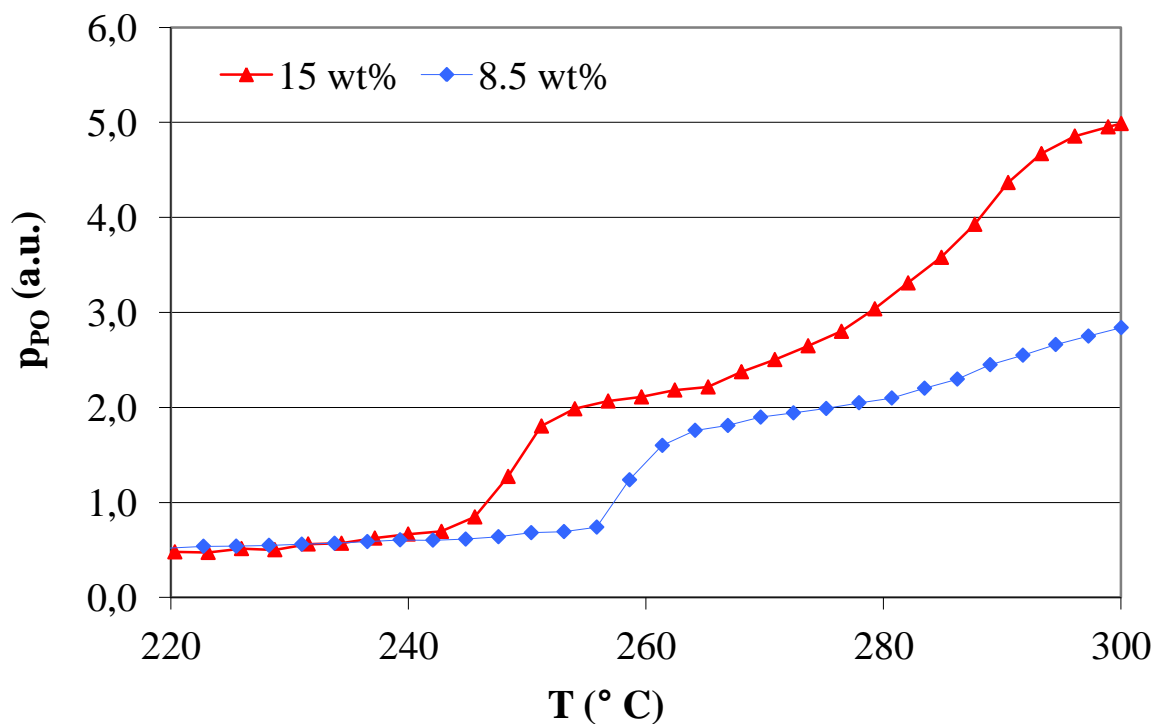
Figure 4.15. Propene epoxiation: 8.5 and 15 wt% reduced Cu/SiO Chrom CH catalysts.

Propene epoxidation: role of silica support

A series of 8.5 wt% Cu/SiO_2 CH catalysts, with different silica support (Table 4.5), having different surface area and porosity, was compared in the epoxidation of propene (Figure 4.16). The results obtained provided some indications about the importance of pore diameter: for similar surface area catalysts made by support having larger pores are the most active.

Support	SSA (m^2/g)	PV (ml/g)	DP_{av} (Å)
SiO_2 332	313	1,79	114
SiO_2 MP15300	297	1,29	156
SiO_2 SP550-10022	330	1,2	-
SiO_2 Chrom	480	0,75	60
$\underline{SiO_2 \ MP09300}$	478	1,04	86
SiO_2 360	564	0,99	35
SiO_2 MP04300	723	0,66	38
SiO_2 MI300	681	0,33	20
SiO_2 MP25300	201	1,34	251
SiO_2 MP20300	255	1,06	193

Table 4.5. Specific surface area, pore volume and size of the different supports.
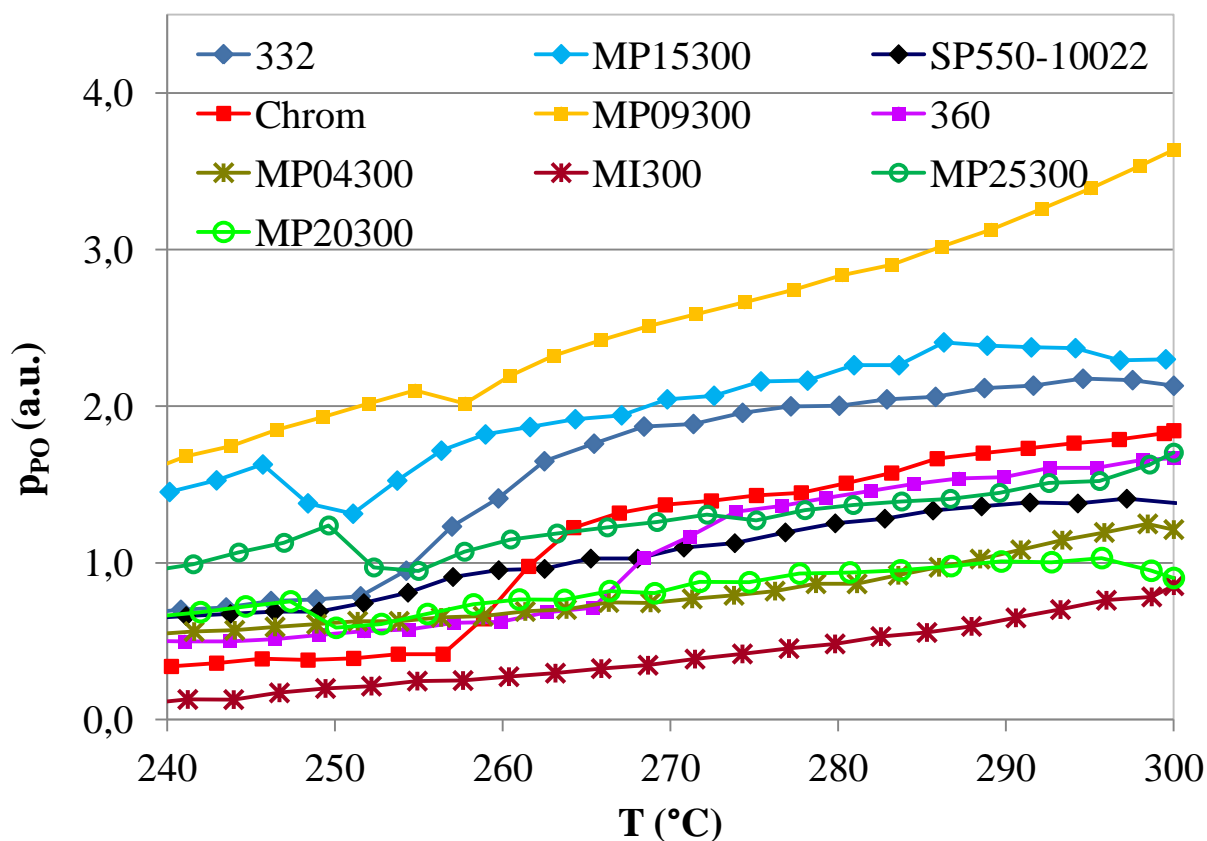
Figure 4.16. Propene epoxiation: 8.5 reduced Cu/SiO$_2$ catalysts.

For example between SiO$_2$ Chrom, 360 and MP09300 the latter is that with larger pores and corresponding copper catalyst shows the higher p$_{PO}$. In particular 15 wt% Cu/SiO$_2$ MP09300 was found to be the most active catalyst, in our opinion because its support provides the best compromise between a high surface area and large pore size that grants the formation of finely dispersed copper nanoparticles and ensures diffusion of reactant molecules.

Styrene adsorption

The interaction between copper surface and C=C double bond involved in the reaction was studied by an FT-IR investigation on reduced 15 wt% Cu/SiO$_2$ Chrom CH catalyst. However the adsorption enthalpy of propene is very low and under the analysis conditions alkene can easily desorb. Thus we used a suitable alkene, such as styrene, for this purpose. The use of styrene as model alkene and mimic of propene was already reported [14].

Figure 4.17 reports the spectra of pure styrene (a), styrene adsorbed on Cu/SiO$_2$ at RT (b), styrene on Cu/SiO$_2$ outgassed at RT (c) and at 200 °C (d).

Pure styrene spectrum shows distinctly aromatic and vinyl CH stretching over 3000 cm^{-1}: adsorption bands at 3080 and 3009 cm^{-1} were assigned to CH double bond stretching, while those at

3060 and 3027 cm^{-1} at aromatic CH stretching. From 2000 to 1700 cm^{-1} the weak bands are related to the combination of the aromatic ring vibrational modes, which are clearly detectable by the intense bands between 1600 and 1450 cm^{-1} (precisely at 1600, 1575, 1494 e 1449 cm^{-1}). The stretching of vinyl C=C double bond lies at 1630 cm^{-1}, whereas vinyl CH$_2$ deformation mode (bending) lies at 1412 cm^{-1}.
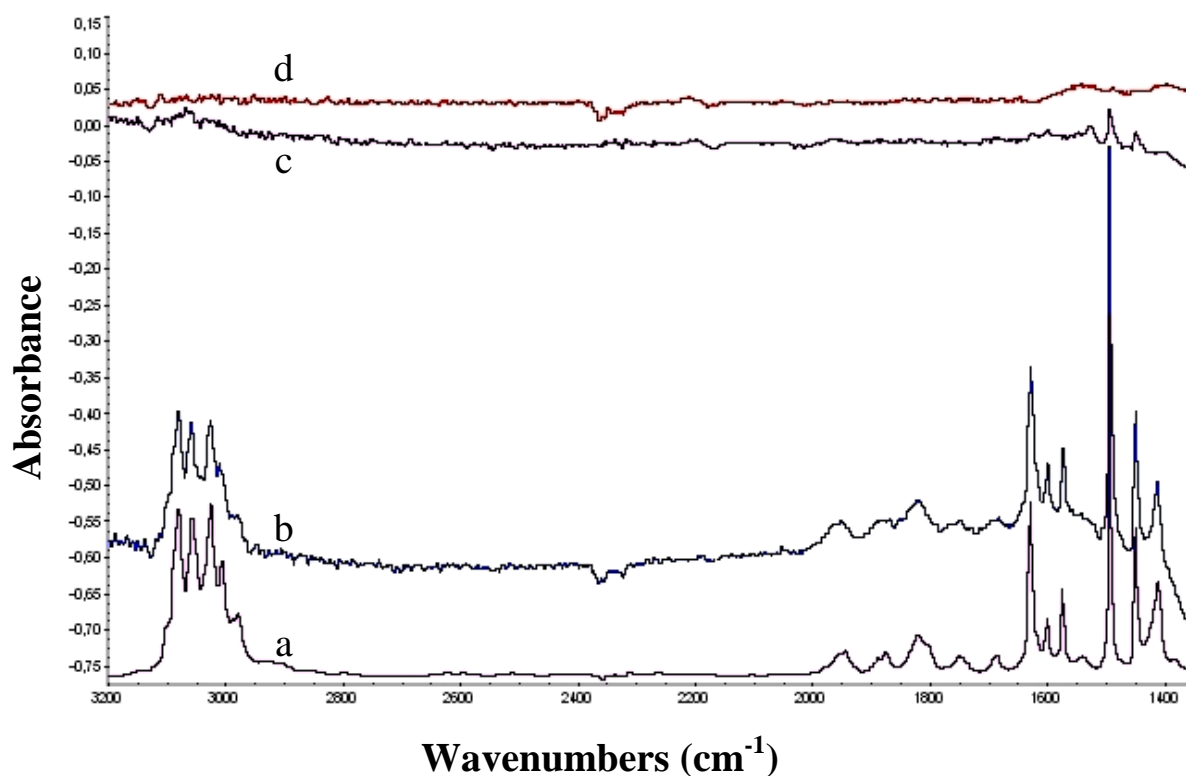

Figure 4.17. FT-IR spectra of: (a) pure liquid styrene; (b) styrene adsorbed on 15 wt% Cu/SiO$_2$ CH, RT; (c) after outgassing at RT; (d) after outgassing at 200 °C.

After the adsorption of styrene on Cu/SiO$_2$ at RT the resulting spectrum is almost coincident to that of pure styrene, indicating only a weak, molecular interaction between alkene and catalyst surface. The interaction does not modify substantially the structure of styrene.

Outgassing at RT led to a dramatic decrease in intensity of all the bands, pointing out the weak, molecular interaction between the molecule and the surface (Figure 4.17 (c) and Figure 4.18 (b)). The intense bands relative to the aromatic ring (1600, 1575, 1494 e 1449 cm^{-1}) are still detectable without significant shifts, even if now the adsorption are very weak.

On the other hand the band at 1630 cm^{-1} almost completely disappeared, while the CH$_2$ deformation mode shifted at 1399 cm^{-1} and a new band appeared at 1548 cm^{-1}. It seems reasonable to assign these changes, in particular the presence of a new band at 1542 cm^{-1} followed by the simultaneous

disappearance of band at 1630 cm^{-1}, to the formation of a π-complex between the vinyl double bond and the copper species. The surface copper involved in the interaction should be an electron withdrawing species (e.g. Cu (I)). In fact, an electron transfer occurs from the electron-rich double bond to the surface centres, leading to a decreased double bond character, thus to a lower vibrational frequency (shift from 1630 cm^{-1} to 1548 cm^{-1}). Similar complexes have been observed following styrene adsorption over Fe_2O_3, and for homogeneous organo-metal compounds [31, 32]. According to the EXAFS, FT-IT of adsorbed CO, FT-IT of adsorbed pyridine and TEM analysis, the copper species interacting with styrene can be a Cu metal phase showing an increased electron withdrawing character, rather than Cu (I). The characterization of reduced 15 wt% Cu/SiO_2 Chrom CH shows the formation of very small metal particles and pyridine desorption spectra indicate a marked Lewis acidity of this small metal crystals (see Chaper 2). A nanoscopic metallic phase has an electronic structure, and thus chemical properties, significantly different from those of mesoscopic or macroscopic copper [16].
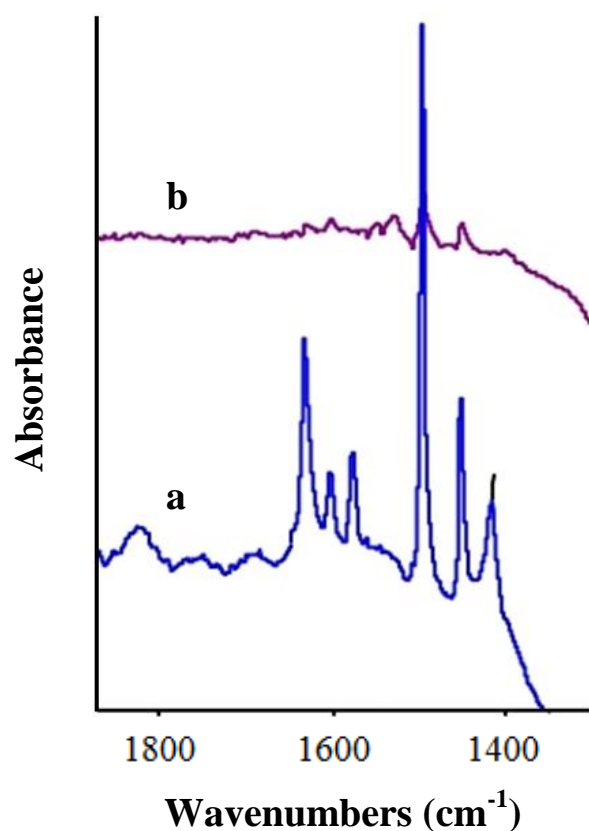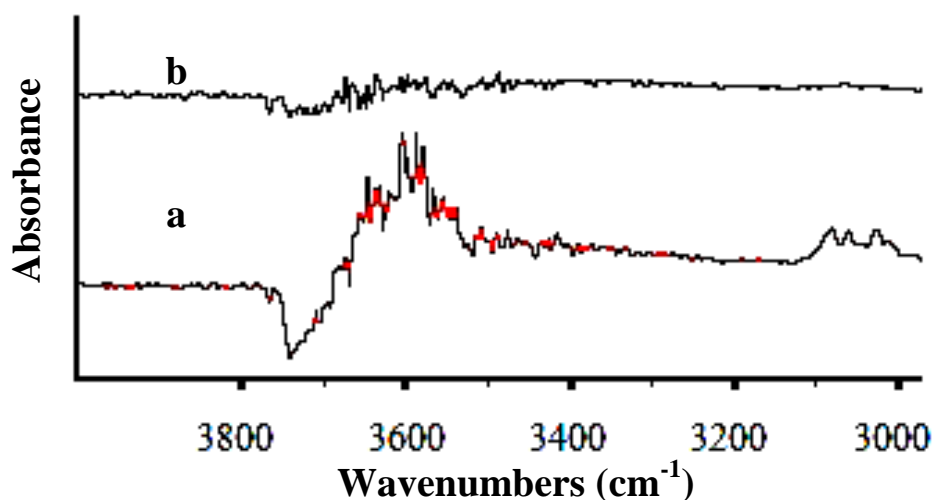

Figure 4.18. Low wavenumbers region magnification FT-IR spectra: (a) styrene on 15 wt% Cu/SiO_2 CH at RT; (b) after outgassing at RT.

On the other side, the aromatic ring seems to be only weakly involved in the interaction: likely styrene molecules lies perpendicular to the surface.

It is worth noting that the differences in the region of bonded or isolated silanol group (3450-3800 cm^{-1} [33], Figure 4.18): after alkene adsorption a negative band in the subtraction spectrum is present (interaction between silanol and styrene), but the adsorption is replaced by outgassig. This behaviour indicates that the strongest interaction occurs between styrene and copper species, not with silica support.

Figure 4.19. High wavenumbers region magnification FT-IR spectra: (a) styrene on 15 wt% Cu/SiO$_2$ CH at RT; (b) after outgassing at RT.
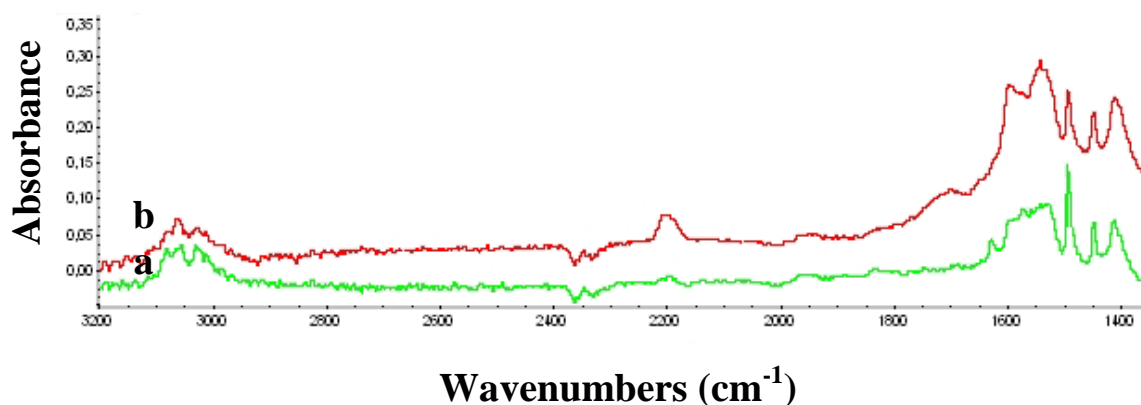
Figure 4.20. FT-IR spectra of styrene on 15 wt% Cu/SiO$_2$ CH: (a) after heating at 200 °C; (b) after heating at 300 °C.

All bands disappeared by heating the system under vacuum (Figure 4.17, spectrum (d)).

Heating at 200 °C and 300 °C in the presence of styrene vapors led to the detection of bands (around 1700, 1600, 1530, 1400 cm^{-1}, Figure 4.20) that indicate the formation of carbonyl species (aldehydes or ketones) and/or carboxylate species. These bands can be related to partial oxidation processes.

4.4 Conclusion

In this chapter we pointed out the superior activity of metal copper with respect to ionic copper species. The results clearly show that only catalysts exposing metallic copper after reduction give a p_{PO} higher than unreduced or partially reduced ones.

Silica based copper catalysts revealed the best activity: in fact, as shown by the deep characterization (see Chapter 2), only finely dispersed metallic copper is formed on SiO_2 after reduction. In particular high loading (15 wt%) Cu/SiO_2 Chrom CH shows an higher p_{PO} with respect to the 8.5 wt% sample because of the presence of well structured small metal particles, exposing (111) facets, on the surface, according to the literature [12, 15, 16].

FT-IR study of the interaction between catalyst surface and the alkene (styrene was taken as mimic of propene) indicates the formation of a π-complex between the vinyl double bond and the copper metal nanoparticles, having a Lewis acid character.

4.5 References

[1] Ullmann's, Encyclopedia of Industrial Chemistry, sixth ed. Wiley-VCH, 1998.

[2] A. Seubsai, M. Kahn, S., Senkan, ChemCatChem 3 (2011) 174.

[3] R. M. Lambert, F. J. Williams, R. L. Cropley, A. Palermo, J. Mol. Catal. A: Chem. 228 (2005) 27.

[4] Chemsystems PERP Program – Report Abstract – Propylene Oxide 07/08-6 – PERP Abstracts 2009 00101. 0008.4106.

[5] Kirk Othmer Report, (1999), http://www.dow.com/propyleneoxide/info/index.htm.

[6] Y. Wang, H. Chu, W. Zhu, Q. Zhang, Catal. Tod. 131 (2008) 496.

[7] J.O. Metzger, M. Eissen, C. R. Chimie 7 (2004) 569.

[8] D. Torres, N. Lopez, F. Illas, R. M. Lambert, Angew. Chem. Int. Ed. 46 (2007) 2055.

[9] T. Hayashi, K. Tanaka, M. Haruta, J. Catal.178 (1998) 566.

[10] B. Chowdhury, J. J. Bravo-Suárez, M. Daté, S. Tsubota, M. Haruta, Angew. Chem. Int. Ed. 45 (2006) 412.

[11] J. J. Cowell, A. K. Santra, R. Lindsay, R. M. Lambert, A. Baraldi, A. Goldoni, Surf. Sci. 437 (1999) 1.

[12] R. L. Cropley, F. J. Williams, A. J. Urquhart, O. P. H. Vaughan, M. S. Tikhov, R. M. Lambert, J. Am. Chem. Soc. 127 (2005) 6069.

[13] D. Torres, N. Lopez, F. Illas, R. M. Lambert, J. Am. Chem. Soc. 127 (2005) 10774.

[14] F. J. Williams, R. L. Cropley, O. P. H. Vaughan, A. J. Urquhart, M. S. Tikhov, C. Kolczewski, K. Hermann, R. M. Lambert, J. Am. Chem. Soc. 127 (2005) 17007.

[15] R. L. Cropley, F. J. Williams, O. P.H. Vaughan, A. J. Urquhart, M. S. Tikhov, R. M. Lambert, Surf. Sci. 578 (2005) L85.

[16] O. P. H. Vaughan, G. Kyriakou, N. Macleod, M. Tikhov, R. M. Lambert, J. Catal. 236 (2005) 401.

[17] A. K. Santra, J. J. Cowell, R. M. Lambert, Catal. Lett. 67 (2000) 87.

[18] Y. Liu, K. Murata, M. Inaba, N. Mimura, App. Catal. A Gen. 309 (2006) 91.

[19] A Palermo, A. Husain, M. S. Tikhov, R. M. Lambert, J. Catal. 207 (2002) 331.

[20] J. A. Rodriguez, J. Y Kim, J. C. Hanson, M. Pérez, A. I. Frenkel, Catal. Lett. 85 (2003) 247.

[21] J. B. Reitz, E. I. Solomon, J. Am. Chem. Soc. 120 (1998) 11467.

[22] H. Chu, L. Yang, Q. Zhang, Y. Wang, J. Catal. 241 (2006) 225.

[23] W. Zhu, Q. Zhang, Y. Wang, J. Phys. Chem. C 112 (2008) 7731.

[24] A. C. Kizilkayaa, S. Senkanb, I. Onala, J. Mol. Catal. A: Chem. 330 (2010) 107.

[25] C. L. Bracey, A. F. Carley, J. K. Edwards, P. R. Ellis, G. J. Hutchings, Catal. Sci. Technol. 1 (2011) 76.

[26] L. Yang, J. He, Q. Zhang, Y. Wang, J. Catal. 276 (2010) 76.

[27] W. Su, S. Wang, P. Ying, Z. Feng, C. Li, J. Catal. 268 (2009) 165.

[28] A. Gervasini, M. Manzoli, G. Martra, A. Ponti, N. Ravasio, L. Sordelli, F. Zaccheria, J. Phys. Chem. B 110 (2006) 7851.

[29] S. Bennici, A. Gervasini, N. Ravasio, F. Zaccheria, J. Phys. Chem. B 107 (2003) 5168.

[30] N. Scotti, D. Monticelli, F. Zaccheria, Inorg. Chim. Acta (2011) doi:10.1016/j.ica.2011.10.001

[31] G. Busca, T. Zerlia, V. Lorenzelli, A. Girelli, React. Kinet. Catal. Lett. 27 (1985) 429.

[32] K. Nakamoto, Infrared and Raman Spectra of inorganic and Coordination Compounds, Wiley Inc.Publication, 1986, USA

[33] Á. Szegedi, M. Popova, V. Mavrodinova, C. Minchev, App. Catal. A: Gen. 338 (2008) 44.

Chapter 5

Co and Co-Cu Catalysts Prepared by CH

5.1 Introduction

Cobalt catalysts

Cobalt catalysts, as well as copper materials, are considered as a suitable alternative to the high cost noble metal based catalysts [1-6]. Various effective cobalt catalysts have been developed for some important industrial processes, such as alkene epoxidation [7-9], methane or ethanol reforming [10, 11], ethane hydroformylation [12], Fischer-Tropsch synthesis [13-15], hydrogenation of aromatics [16] or aldehydes [17], NO_x removal [18].

It is well known that cobalt loading, dispersion, oxidative state, phase composition and reducibility could strongly affect the catalytic process. That is why the synthesis of efficient catalysts with desired properties is a problem strongly related to the control of the overall state of cobalt species. It was established that the ability of cobalt catalysts to undergo reduction is greatly affected by support, preparation conditions and metal loading. For example one of the most studied cobalt phase, the Co_3O_4 spinel, is well known to be reduced in two steps in the temperature range of 200-600 °C: first Co_2O_3 reduces to CoO and second, Co (II) phase reduces to metallic cobalt. In the literature it is reported that an increase of the particle support interaction with decreasing particle size results in species that can be reduced only at elevated temperature and this is true in particular for Co (II) species. As a matter of fact, divalent cobalt species show increasing resistance to reduction in the following order: Co^{2+} with little support interaction, Co^{2+} having slightly stronger interaction with the support, cobalt hydrosilicates, and cobalt silicate. Cobalt silicate is favored by high-pH preparation conditions and shows a TPR maximum at about 900 °C [19, 20]. The catalytic behavior of cobalt catalysts have been widely studied focusing the attention on the influence of metal particle size [21-27] and support pore diameter and structures, [5, 7, 14, 21, 28-35] but understanding of the correlation between these features and catalytic activity is far from being easy. Implications about catalysts preparation and consequent activity have been widely analyzed in this thesis.

Other than cobalt catalysts, bimetallic copper-cobalt based systems find application in different catalytic reactions, in particular redox reactions like CO and NO oxidation. They are also excellent catalyst precursors for higher alcohol synthesis from syngas [36]. Materials where two or more metals are in the same crystalline structure may provide, at relatively low temperature of calcination, well interdispersed mixed oxides characterized by fairly uniform small particle sizes, together with an high surface area [37]. Because of their interdispersed state, mixed oxides of transition metals are capable of mutual interactions (synergetic effect), leading to the formation of complex structure of spinel or perovskite type. The overall effect is a catalytic activity usually higher than the one of their individual components.

Aim of the work

The excellent results in terms of particle size and dispersion of copper showed by materials obtained by Chemisorption-Hydrolysis suggested us to apply this preparation methodology to a metal, such as cobalt.

In this chapter cobalt silica catalysts and bimetallic cobalt-copper silica catalysts were prepared by a modified CH procedure and characterized. A possible application as catalysts for the decomposition of methanol to CO and H_2 was also investigated.

This work is the result of a collaboration with professor Tanya Tsoncheva and Margarita Popova from Institute of Organic Chemistry with Centre of Phytochemistry, Bulgarian Academy of Sciences, Sofia, Bulgaria.

5.2 Experimental

Chemicals

All reagents were purchased from Aldrich and used without further purification.

Catalysts preparation

A commercial mesoporous material (Davisil C from Grace Davison), having a surface area of 529 m^2/g and a pore volume of 0.88 cm^3/g, was used a support for the catalysts. Co/SiO_2 and Co-Cu/SiO_2 catalysts (Table 5.1) were prepared as follows.

1. Co/SiO_2 CH catalysts

A modified Chemisorption-Hydrolysis procedure was used for the preparation of Co/SiO_2 CH samples. In order to stabilize Co(III) in basic solution we performed the following procedure. The right amount of $Co(NO_3)_2 \cdot 6H_2O$ were put into a water solution containing NH_4NO_3 (mol NH_4NO_3/mol Co =10/1) under stirring. The solution was cooled at 0 °C and slowly H_2O_2 (30%) was added, then, NH_4OH (28%) was very slowly added drop by drop. Finally the temperature was increased at 60 °C. After 2.5 hours the solution was cooled down at room temperature and the pH was adjusted to 9 or 10 with NH_4OH (28%) before adding the support (SiO_2). The silica suspension was diluted with water at 0°C after 0.5 or 24 hour and then filtered. The solid was washed with water, dried overnight at 100 °C and calcined in air at 500 °C for 4 h.

2. Co-Cu/SiO_2 CH catalysts

A modified Chemisorption-Hydrolysis procedure was used for the preparation of Co-Cu/SiO_2 CH samples. Co (III) basic solution was prepared as described above. For the preparation of copper (II) basic solution, we dissolved the right amount of $Cu(NO_3)_2 \cdot 3H_2O$ into water and adjusted the pH to 9 with NH_4OH (28%) at room temperature. The two equimolar solutions (Co(III) and Cu(II)) were mixed together and the pH was increased up to 9 or 10 with NH_4OH (28%). Next, silica support was added to the solution and left under stirring for 0.5 before the mixture was cooled at 0 °C and slowly diluted with water. Finally, the solid was separated by filtration, washed with water, dried overnight at 100 °C and calcined in air at 500 °C for 1 hour.

3. Co/SiO$_2$ IW

Cobalt oxide was supported by incipient wetness impregnation of the supports with aqueous solution of cobalt nitrate, followed by drying in ambient atmosphere overnight and its further decomposition in air at 500 °C.

Sample	Co content (wt%)	Cu content (wt%)	Cu/Co ratio	Method	Chemisorption
Co/SiO$_2$ IW	7.8	-	-	IW	-
Co/SiO$_2$ CH A	4.6	-	-	CH	pH=10, 0.5 h
Co/SiO$_2$ CH B	4.0	-	-	CH	pH=9, 0.5 h
Co/SiO$_2$ CH C	6.3	-	-	CH	pH=10, 24 h
Co-Cu/SiO$_2$ A	2.7	4.9	1.8	CH	pH=10, 0.5 h
Co-Cu/SiO$_2$ B	2.4	3.1	1.3	CH	pH=9, 0.5 h

Table 5.1. Cobalt and cobalt-copper silica caytalysts.

Co (III) complex precursor

The solid Co (III) complex was precipitated and isolated by a slow evaporation of the Co (III) basic solution obtained as describe above.

AA Spectroscopy

Cu loading was determined by Atomic Absorption Spectroscopy (Atomic Absorption Spectrometer 3100 – PerkinElmer; flame: acetylene/air) and an external calibration methodology, after microwave digestion of about 20 mg of oxidized sample in 3 ml of HNO$_3$.

Temperature Programmed Reduction (TPR)

TPR profiles were recorded with a modified version of the Micromeritics Pulse Chemisorb 2700 apparatus equipped with a thermal conductivity detector (TCD). The samples (25 mg) were diluted with an equal amount of quartz, calcined at 500 °C under O$_2$ (40 mL/min) for 1 h and then reduced at 8 °C/min with a 8% H$_2$/Ar mixture at 15 mL/min. The rate of hydrogen uptake was measured by an HP 3396A integrator.

FT-IR of adsorbed Pyridine

The FT-IR studies of pyridine adsorption and desorption were carried out with a BioRad FTS40 spectrophotometer equipped with mid-IR DTGS detector.

The experiments were performed on sample disk (15-20 mg) after a pre-treatment (dehydration: 500 °C, 40 min air + 40 min vacuum; reduction: 500 °C, 40 min air + 40 min vacuum + 40 min H_2) and pyridine adsorption at room temperature. Following desorption steps were carried out for 30 min at various temperature (from room temperature to 300 °C). All spectra were recorded at room temperature after pyridine desorption at each temperature and one spectrum was collected before pyridine adsorption.

XRD analysis

The powder X-ray diffraction spectra were recorded within the range from 1° to 80° 2θ with a step of 0.05° 2θ and counting time 1 s step^{-1} on Bruker D8 Advance diffractometer with Cu Kα radiation and SolX detector.

Elemental analysis (CHN)

CHN analysis of isolated Co (III) precursor were performed using a Perkin Elmer 2400 instrument.

Magnetic moment

The measurements of the magnetic susceptibility were performed at room temperature using a Magway MSB Mk1, Sherwood Scientific LTD magnetic balance.

Catalytic experiments

Methanol conversion was carried out in a flow reactor (0.055 g of catalyst, three times diluted with grounded glass), argon being used as a carrier gas (50 ml/min). The methanol partial pressure was 1.57 kPa. The catalysts were tested under conditions of a temperature-programmed regime within the range of 80–500 °C with heating rate of 1 °C/min. Before the reaction catalysts were pretreated at 500 °C under air for two hours and eventually other 2 h under H_2 at the same temperature. On-line gas chromatographic analyses were performed on HP apparatus equipped with flame ionization

and thermo-conductivity detectors, on a PLOT Q column, using an absolute calibration method and a carbon based material balance. The products selectivity was calculated as $X_i/X*100$, where X_i is the current yield of the product i and X is methanol conversion.

5.3 Results and discussion

Co (III) solution

Since the good results obtained through the employment of CH methodology to obtain highly dispersed copper oxide on SiO_2 catalyst using $[Cu(NH_3)_4]^{2+}$ as chemisorbing species, we focused our attention in the use of the same methodology for the preparation of Co/SiO_2 materials. In order to stabilize cobalt ions in aqueous solution at higher pH, we selected $[Co(NH_3)_6]^{3+}$ as a good candidate for the synthesis, thus preventing the precipitation of Co in alkaline conditions. In fact, Co (II) ions present low stability in basic solution, even in the presence of ammonia, while Co (III) is soluble at high pH. $[Co(NH_3)_6]Cl_3$ was already reported for the deposition of Co on silica and carbon through strong electrostatic adsorption [38, 39]. Alternatively, in this study in order to avoid the presence of chloride ions, the starting $Co(NO_3)_2 \cdot 6H_2O$ was oxidized to a Co (III) compound using a solution containing only H_2O_2 and NH_4OH. In particular, ammonia was added drop by drop: immediately the color of the solution became brown-green, but after 2.5 h of stirring the reaction mixture became dark red. Usually, in the literature, the oxidation of Co (II) to Co (III) was carried out in the presence of activated carbon [40], H_2O_2 and NH_4OH. In our synthetic procedure the use of the heterogeneous catalyst for the oxidation is avoided. If ammonia is added without the presence of H_2O_2 a Co (II) precipitate is obtained. On the contrary the oxidation was confirmed by the fact that no suspension is present in the basic solution and the measure of magnetic moment of isolated cobalt complex indicated the formation of a typical diamagnetic Co (III) compound. The Co complex formed should be $[Co(NH_3)_6](NO_3)_3$, $[Co(NH_3)_5H_2O](NO_3)_3$, $[Co(NH_3)_4(H_2O)_2](NO_3)_3$, or $[Co(NH_3)_5OH](NO_3)_2$. Elemental analysis (CHN) on the isolated complex and UV spectrum of the Co (III) solution (very broad band around 500 nm) suggest the formation of $[Co(NH_3)_4(H_2O)_2]^{3+}$, but more investigation are actually in progress.

In any case, from the collected data we can assert that a complexes of Co^{3+} (likely hexaammonia complex) was obtained oxidizing a water solution of $Co(NO_3)_2 \cdot 6H_2O$, without any catalysts.

Chemisorption-Hydrolysis of SiO_2 with Co (III) complex

Cobalt ions were anchored to the silica support using the same procedure reported for copper CH catalysts. A prolonged chemisorption time resulted in high cobalt loading of the sample Co/SiO_2 CH C. The measure of the magnetic moment (3.84 β_M) of the resulting Co/SiO_2 catalyst shows a value corresponding to three unpaired electrons, typical of $3d^7$ high spin Co (II) (3.87 β_M). TPR and

XPS analysis further reported confirmed this finding. In analogy with copper materials, a changing in the oxidation state of the starting metal ion was observed for catalysts supported on SiO_2-Al_2O_3.

TPR analysis

Temperature reduction profiles of CH Co and Co-Cu samples were reported in this section. According to the literature data [20, 22, 41], unsupported Co_3O_4 oxide fully reduces to metallic Co up to 500°C in two consecutive stages: $Co_3O_4{\rightarrow}CoO{\rightarrow}Co$. The reduction should be easier for the smaller particles. In the case of supported materials, the interpretation of TPR results is more complicated due to the existence of an interaction between the cobalt oxide species and the support [28]. The TPR-TG profile of the IW sample (not reported) showed three well distinguished peaks with maxima at about 270, 370 and 500 °C. The ratio between the intensities of the first TG effect and the sum of the second and the third ones is above 1:2. Thus, in agreement with the literature, we assigned the first peak mainly to the reduction of $Co_3O_4{\rightarrow}CoO$, and the second and the third ones to $CoO{\rightarrow}Co$ transition of particles with different dispersion and interaction with the silica support [22, 42, 43].
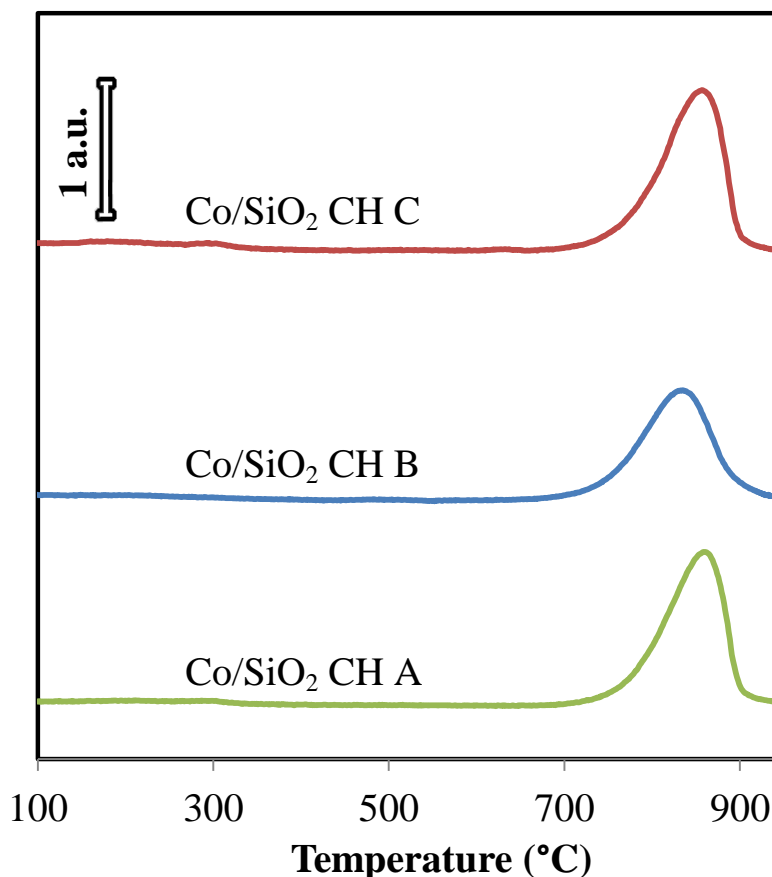
Figure 5.1. TPR profiles of Co/SiO$_2$ CH samples.

However the observed loss in weight in the whole temperature region corresponds to 70-80% reduction of Co_3O_4 to Co^0.

On the other hand Co/SiO_2 CH catalysts showed a main peak at very high temperature (around 830-860°C, Figure 5.1). According to the literature [22, 44-46] we assume that CH method facilitates the formation of cobalt species with low degree of crystallinity, which are in strong interaction with the silica support, such as finely dispersed Co (II) silicate or hydrosilicates species. This phenomenon was also observed by Sexton et al. [47] when Co nitrate was deposited on SBA-15 under basic conditions by deposition-precipitation with urea. The authors stressed that the solubility of amorphous silica in both water and salt containing aqueous solutions should not be neglected and they considered the possibility of a reaction between the cobalt- and dissolved silica species to Co_2SiO_4 [48 and refs therein]. It should be noted that the temperature at the peak maximum for Co/SiO_2 B is shifted of about 30 °C with respect to Co/SiO_2 A and B materials (830 versus 860 °C). This difference can be ascribed to the different pH during the chemisorption step: in fact the higher pH of the solution for samples A and C can favor the dissolution of silica and in consequence the formation of cobalt silicates more strongly interacting with the support.
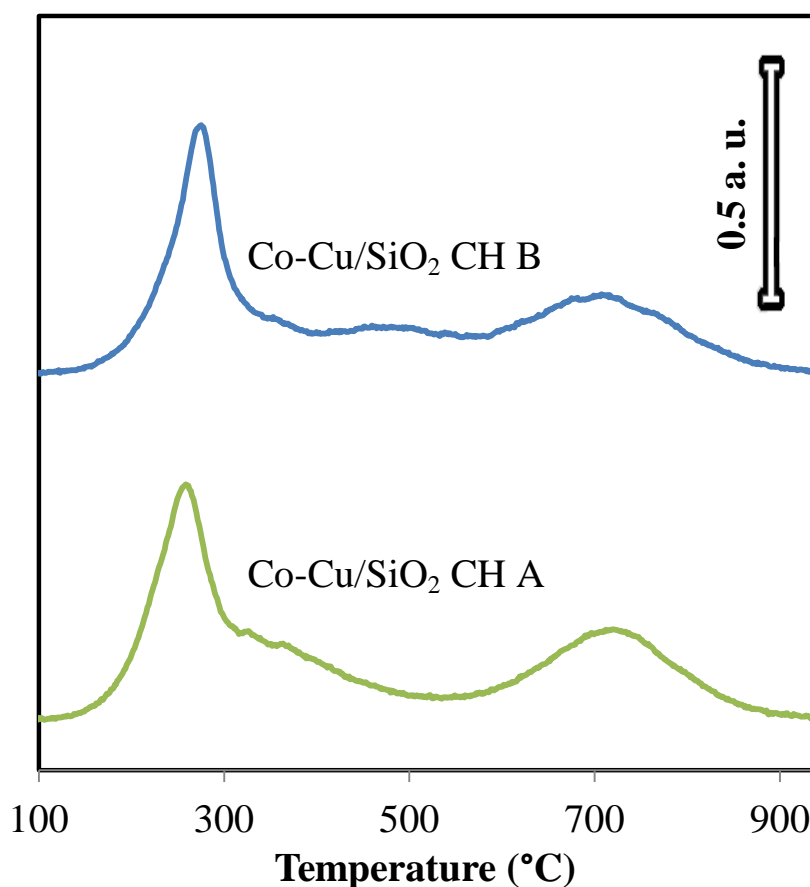
Figure 5.2. TPR profiles of $Co-Cu/SiO_2$ CH catalysts.

The degree of reduction for the three CH samples related to the high temperature peak is between 80 and 90%, while a very small peak (reduction of maximum 1-2 % of total Co loaded) around 250-400 °C may be identified and attributed to a definitely small amount of cobalt spinel present. The formation of a Co (II) species is in agreement with the measure of the magnetic moment for cobalt CH materials.

TPR profile of bimetallic Co-Cu/SiO$_2$ samples show a very complex situation in which almost three peaks are clearly detectable, suggesting the presence of different species (Figure 5.2). We assigned the relative sharp low reduction peak centered around 260 °C for Co-Cu/SiO$_2$ A and 275 °C for Co-Cu/SiO$_2$ B to the reduction of Cu-Co spinel, as reported in the literature [19, 37, 49]. However since the stoichiometric formula of copper-cobalt spinel is $Cu_xCo_{3-x}O_4$ (X<1) or $CuCoO_2$, the low reduction peak should be also the result of the reduction of CuO phase (the Cu/Co ratios for Cu/SiO$_2$ CH A and B are 1.8 and 1.3 respectively). The reduction phenomena occurring at higher temperature should be related to separate cobalt species. The broad reduction peak between 300 and 500 °C can be assigned to the two step reduction of spinel Co_3O_4 phase, while a reduction centered around 710 °C is diagnostic of a strong interaction between the metal and the support (hydrosilicate species) [19, 45, 46, 48]. In any case, the addition of copper favors the formation of more easily reducible cobalt species, thus indicating a strong interaction between cobalt and copper in the mixed oxide catalysts [37].

XPS analysis

Sample	Element	Position (eV)	Atomic concentration (%)	X/Si ratio
Co/SiO$_2$ CH A	Co 2p	781.7	1.89	0.07
	O 1s	532.4	70.19	2.71
	Si 2p	103.3	25.93	
Co/SiO$_2$ CH B	Co 2p	781.0	1.65	0.06
	O 1s	532.5	68.78	2.50
	Si 2p	103.3	27.52	
Co/SiO$_2$ CH C	Co 2p	781.7	3.78	0.15
	O 1s	532.5	67.60	2.62
	Si 2p	103.5	25.80	

Table 5.2. Co 2p, O 1s and Si 2p Binding energy and atomic concentration for Co/SiO$_2$ CH samples.

In order to get more information about the surface structure of the CH-obtained materials, XPS measurements were also carried out. Figure 5.3 shows XPS spectra of the CH-samples, obtained under different conditions in the Co 2p region. The binding energies of Co $2p_{3/2}$, Si 2p and O 1s peaks and the atomic concentration of different components are listed in Table 5.2. The Co $2p_{3/2}$ peaks are observed at 781.7; 781.0 and 781.7 eV for the Co/SiO$_2$ A, Co/SiO$_2$ B and Co/SiO$_2$ C materials, respectively, with the appearance of satellite peak at ca. 5.5 eV higher energy side from the Co $2p_{3/2}$ peak. According to the literature data [50], these BEs do not correspond to the BE, typical of polycrystalline Co$_3$O$_4$ and CoO phase, which is 778.5 eV with a satellite peak at 6 and 9 eV higher BE, respectively. The higher BE for these materials in comparison with the reference polycrystalline oxides could be assigned to the presence of silicate Co$_2$SiO$_4$ phase in strong interaction with the silica support, as shown by TPR profiles [51]. Moreover both Co/SiO$_2$ CH A and Co/SiO$_2$ C catalysts, obtained at higher pH, show the same higher BE with respect to the samples prepared at lower pH (Co/SiO$_2$ CH B).
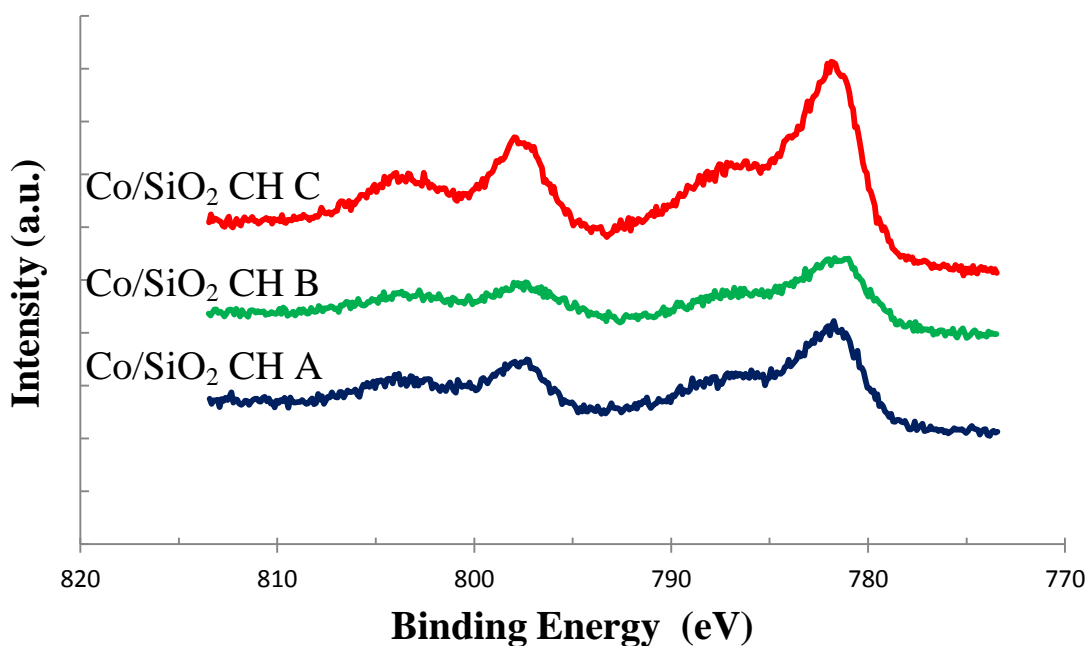
Figure 5.3. XPS spectra in Co2p region of Co/SiO$_2$ CH modified materials.

XRD analysis

Figure 5.4 reports the XRD spectra of cobalt materials prepared both by CH and IW.
The XRD patterns of the Co/SiO$_2$ IW material represent well defined reflections at 2θ of 31.30, 36.90, 45.00, 59.4 0 and 65.20, are typical of spinel Co$_3$O$_4$ phase [52]. The average particle size, estimated with the Debye-Scherrer formula from the full width at half maximum (FWHM) of the

(400) diffraction (2θ=45.00), was of 9.7 nm. At the same time, the XRD patterns of the samples obtained by the CH procedure do not exhibit reflections of any cobalt containing phase and indicate for the presence of finely dispersed cobalt oxide nanoparticles or non-crystallized cobalt phase, strong interacting with the silica support. This behavior reflects the one observed for copper based catalysts, in which materials prepared by CH show very weak broad reflection only increasing the counting time of the analysis (see Chapter 2).
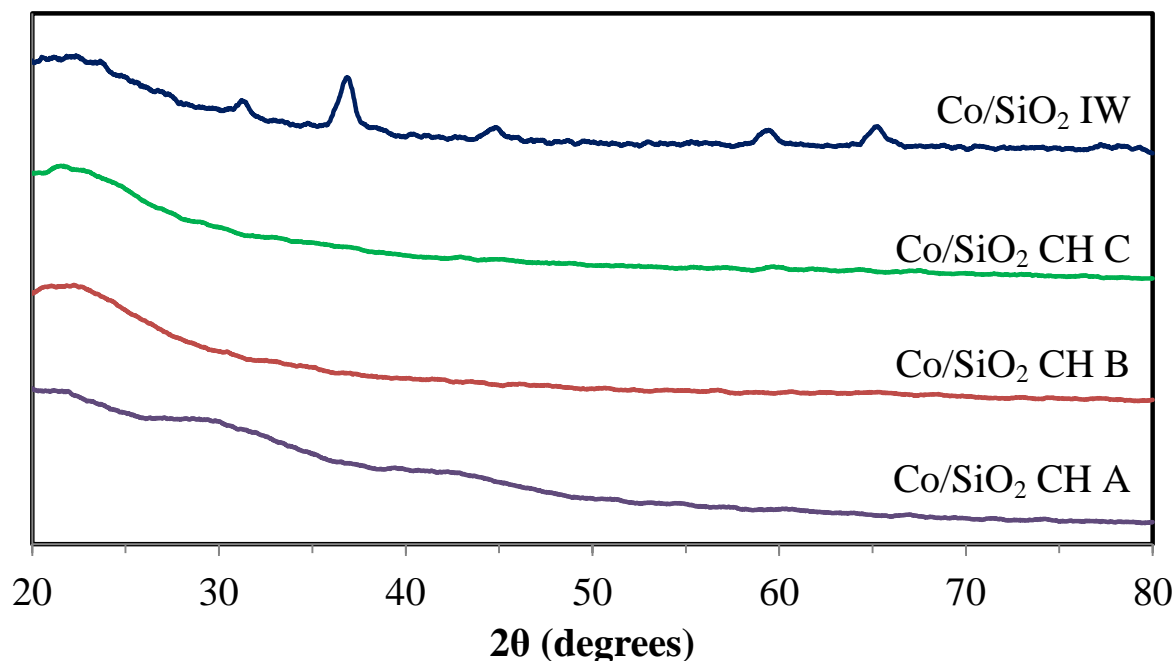
Figure 5.4. XRD spectra of Co/SiO$_2$ catalysts.

FT-IR of adsorbed pyridine

As reported in Chapter 2, the typical IR absorption bands for adsorbed pyridine lies in the range 1400-1700 cm^{-1}: Lewis acid sites give rise to the bands around 1450 cm^{-1} and 1610 cm^{-1} that can be assigned to pyridine bounded to Lewis acid sites, while Brønsted acid sites bring to a band at 1550 cm^{-1} followed by other peaks near 1620 cm^{-1} and 1640 cm^{-1}. Finally the nature of a band around 1490 cm^{-1} is not clearly assigned. Physisorption results in the presence of a band in the range 1440-1450 cm^{-1} together with another one at 1580-1600 cm^{-1}[53-57].

The spectra pointed out several differences that depend on the preparation methodology. The presence of the metal clearly introduced Lewis acidity related to the bands at 1611 cm^{-1} and 1451 cm^{-1} for CH samples (Co/SiO$_2$ CH B Figure 5.5, Co/SiO$_2$ CH A and C not reported). Differently to the bands related to physisorbed pyridine these bands were still present beyond 150 °C. A strong

difference in acidity was revealed for the IW sample (Figure 5.6) where the same bands were not clearly detectable even at RT. The pretreatment (dehydration or reduction) did not seem to deeply influence the ability to absorb pyridine by the samples, even if IW sample would seem to show very weak bands corresponding to a Lewis acid sites. For CH samples this feature can be related to the extremely difficult reduction to metallic. phase. Spectra of pure SiO_2 Davisil C exhibit only the absorption related to physisorbed pyridine, likewise to those reported in Chapter 2 for SiO_2 Chrom.
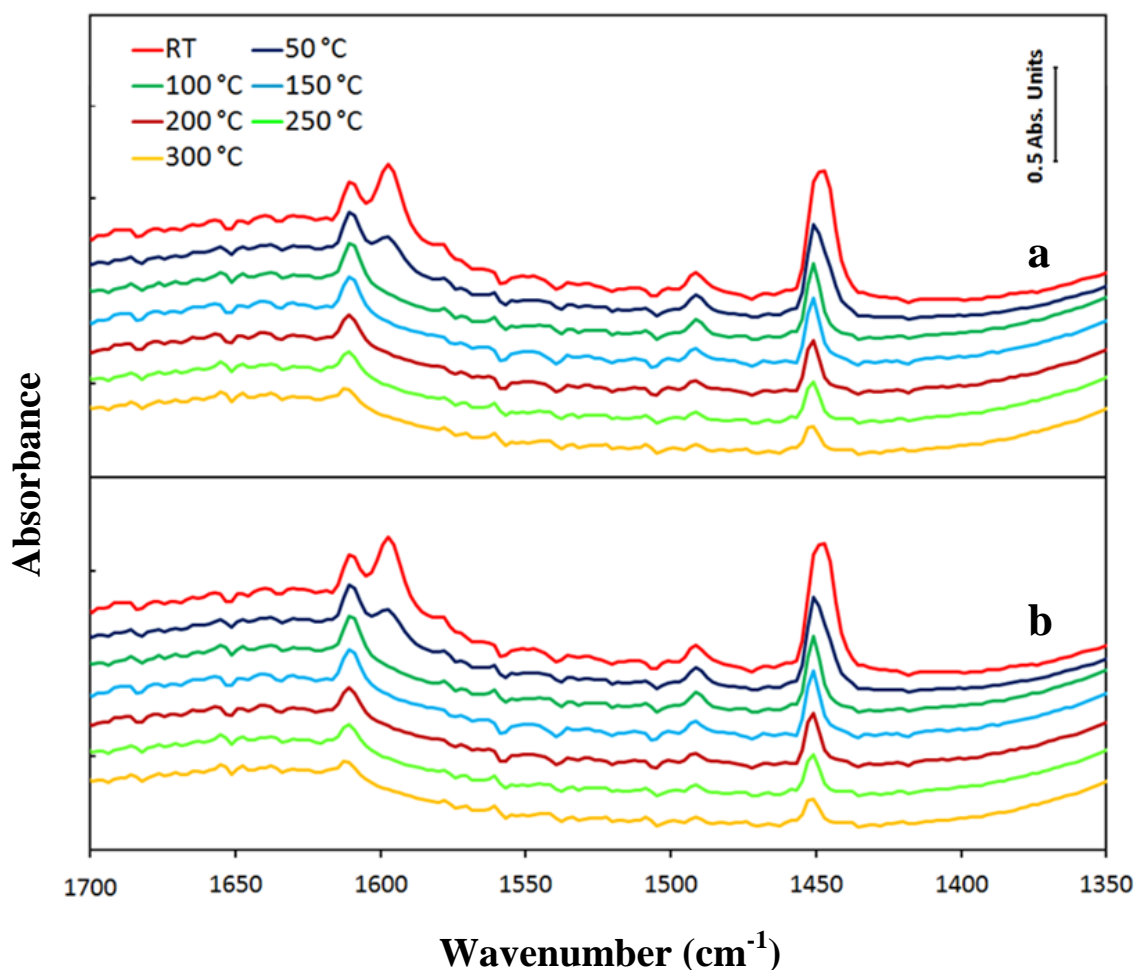
Figure 5.5. Pyridine desorption spectra on Co/SiO_2 CH B: (a) dehydrated samples; (b) reduced samples.

The spectra of pyridine on bimetallic Co-Cu/SiO_2 catalysts showed very strong absorption in the range characteristic of Lewis acidity (e.g. spectra of Co-Cu/SiO_2 A, Figure 5.8). The peak at 1490 cm^{-1} is clearly evident even at high desorption temperature (300 °C), indicating a high resistance to evacuation. Moreover as the desorption temperature increased this band broadens. Unfortunately the unspecific interaction between catalysts surface and pyridine that generates this band makes the results hardly understandable, however we can suppose that stronger Lewis acid sites are generated on Co-Cu/SiO_2 samples than either alone Cu or Co silica materials.
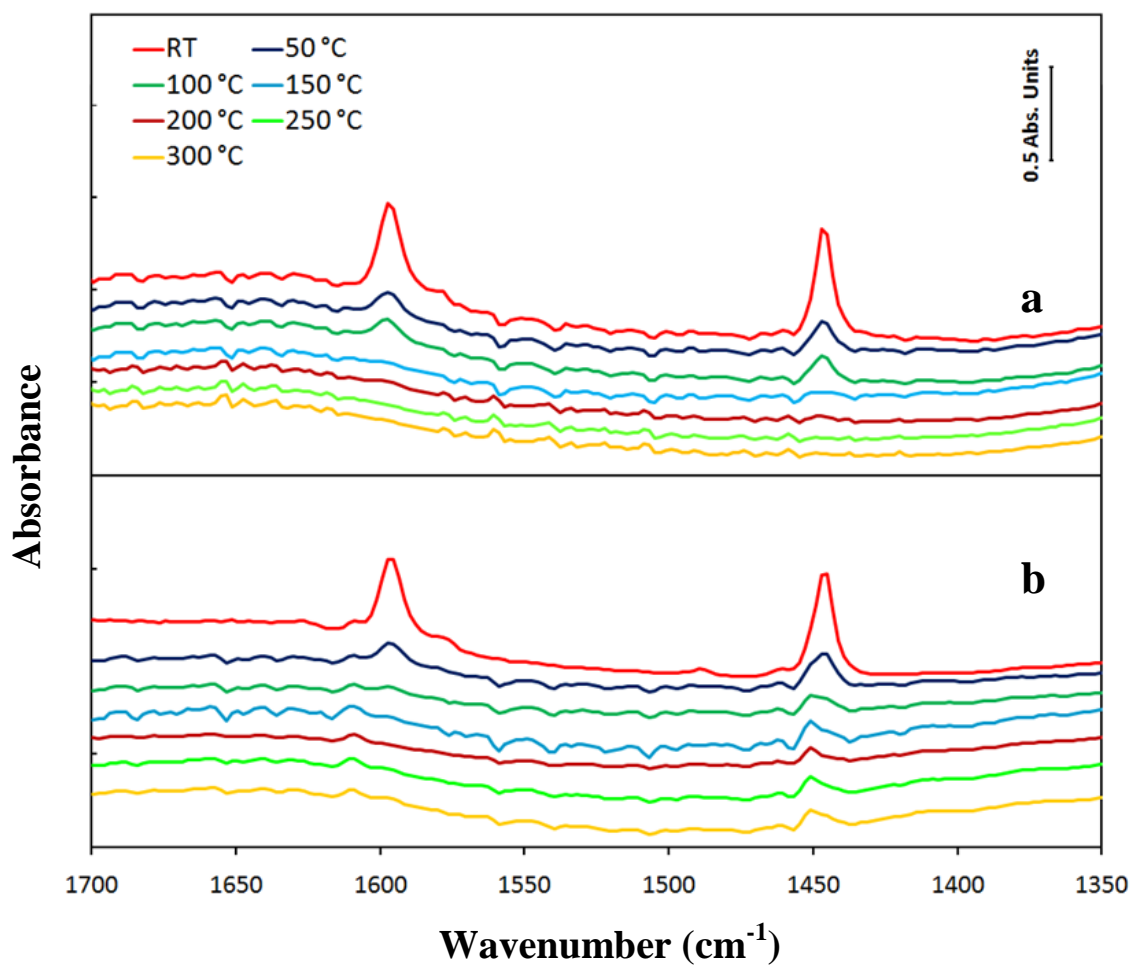
Figure 5.6. Pyridine desorption spectra on Co/SiO_2 IW: (a) dehydrated samples; (b) reduced samples.
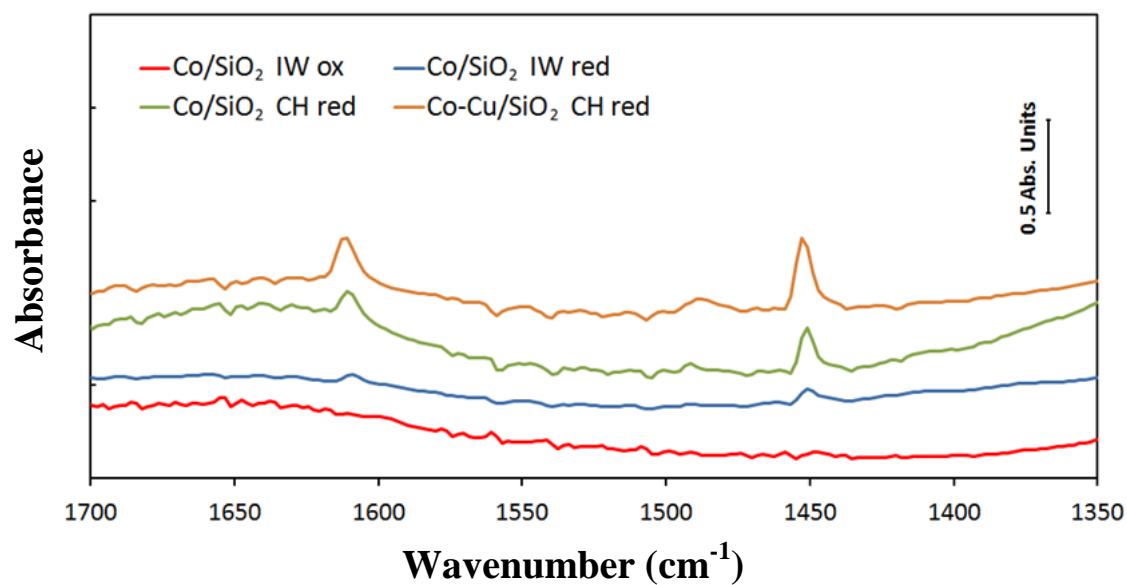
Figure 5.7. Pyridine desorption spectra recorded at 200 °C: comparison between Co/SiO_2 IW dehydrated samples and reduced, reduced Co/SiO_2 CH B and reduced $Co-Cu/SiO_2$ CH A.
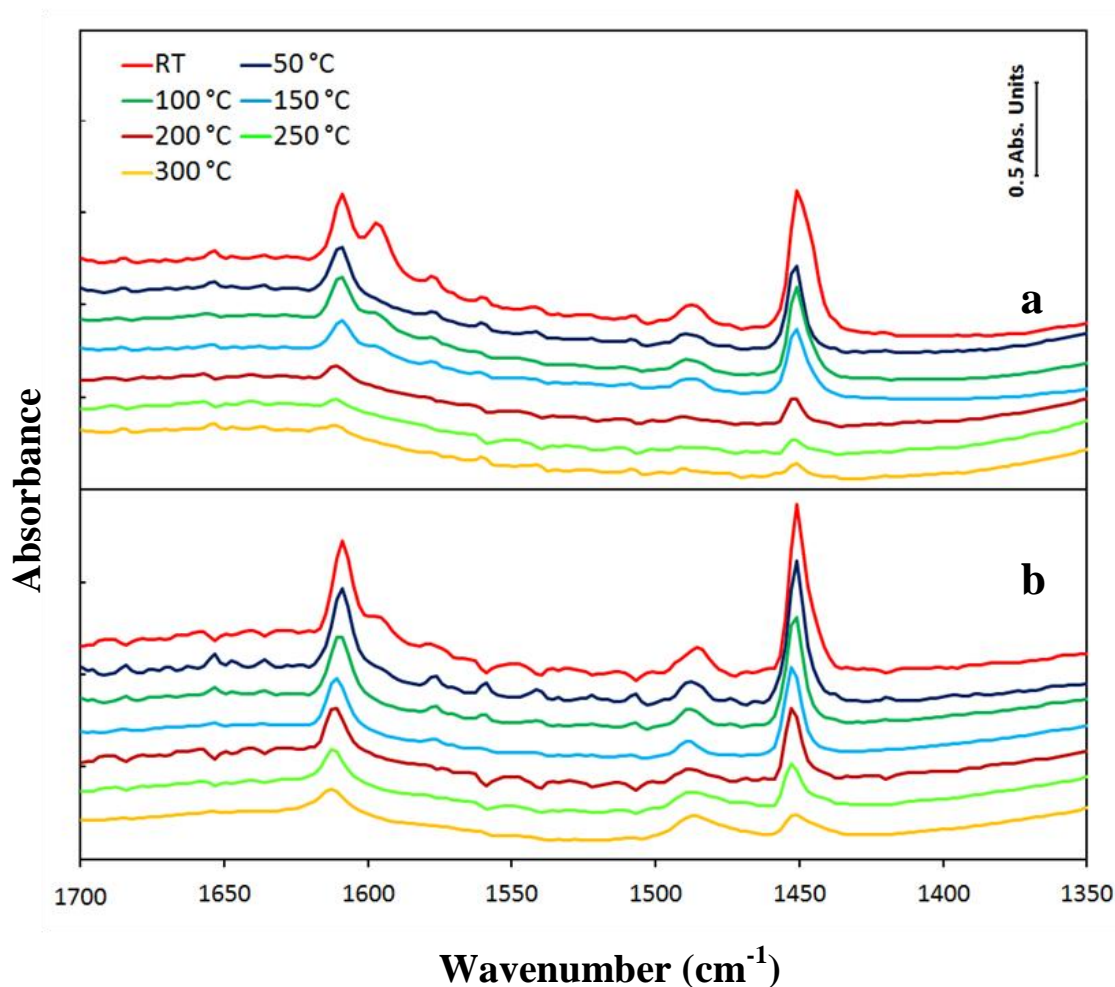
**Figure 5.8.** Pyridine desorption spectra on Co-Cu/SiO$_2$ CH A: (a) dehydrated samples; (b) reduced samples.

Figure 5.7 reports the comparison between the desorption spectra of Co/SiO$_2$ CH B, Co/SiO$_2$ CH C and Co-Cu/SiO$_2$ CH A taken at 200 °C.

Catalytic properties

Results of the catalytic tests for the reaction of methanol decomposition to CO and H$_2$ in the presence of CH and IW catalysts, were reported in Figure 5.9, Figure 5.10, Table 5.3.

The samples pretreated only in the oxidized atmosphere do not significantly differ in their catalytic activity despite the method of preparation used. They predominantly decomposed methanol to CO and hydrogen above 280 °C and about 85-95% conversion was achieved at 450 °C. Only in the case of Co/SiO$_2$ CH A a significantly lower catalytic activity was registered in the whole temperature range. CO$_2$, CH$_4$ and dimethyl ether (DME) were usually detected as by-products, but the samples differ significantly in the products distribution (Table 5.3). CH$_4$ dominated among the by-products

of Co/SiO$_2$ IW, while only 5% CH$_4$ and around 20% CO$_2$ were registered for all CH materials. Note that a small amount of DME was detected only in the case of the latter materials, which reveal the existence of acidic catalytic sites and well correlates with the data reported for the FT-IR of adsorbed pyridine. The best selectivity to CO was provided by IW sample at 380 °C (91%).
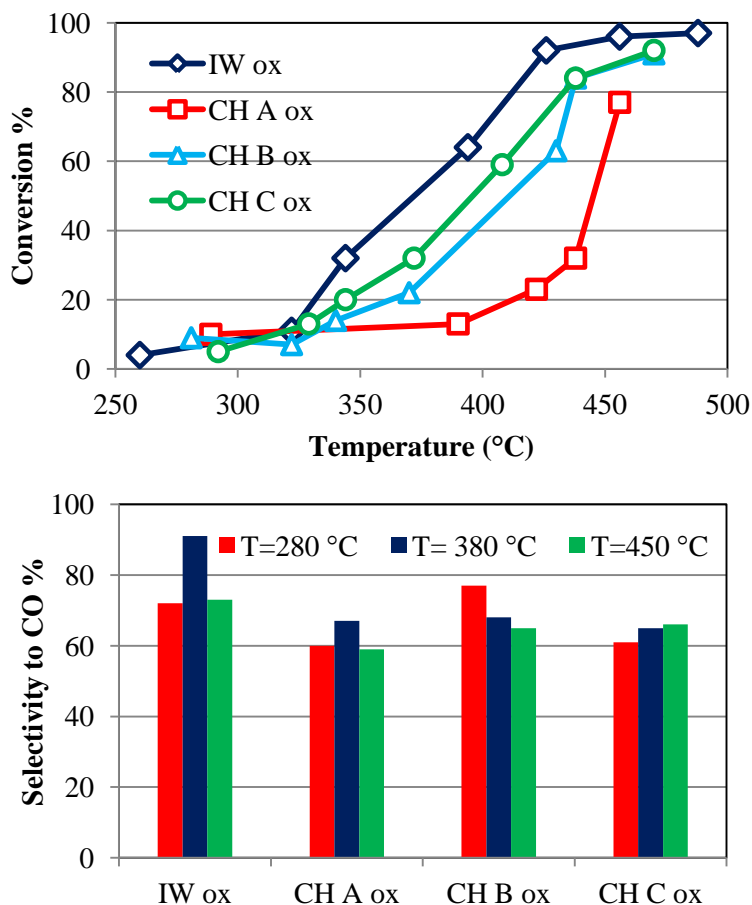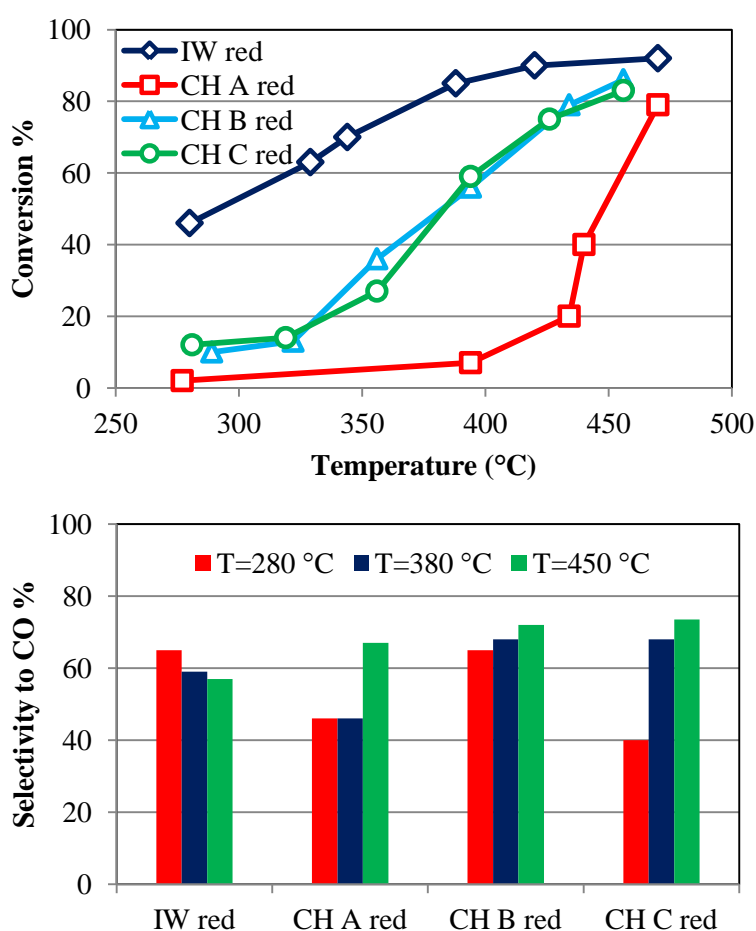

Figure 5.9. Conversion and CO selectivity for Co/SiO$_2$ IW and CH (A, B and C) catalysts after pretreatment in oxidized atmosphere.

The pretreatment of the CH samples in hydrogen did not significantly influence their catalytic activity, because of the high resistance of the loaded cobalt phase to reduction transformations, in agreement with the characterization data. The small changes can be correlated with the low fraction of reducible cobalt. A decrease in DME and CO$_2$ yields as well as an increase in methane formation was the only observed effect in this case. On the other hand, the reduction pretreatment increased the catalytic activity of the Co/SiO$_2$ IW in a high extent, but at the expense of CO selectivity.

In order to precise the catalytic data, we calculated the specific catalytic activity (SCA) as converted methanol (%) per 1 wt% Co at selected temperature. The SCA values significantly differ for the CH obtained materials, indicating variations in the state of the active cobalt species in them. In

particular, the results show an high activity of the catalytic sites for the sample Co/SiO$_2$ CH B, which was obtained under the lower pH. The increased catalytic performance of Co/SiO$_2$ CH B catalyst can be explained with TPR and XPS analysis, that show the presence on this sample of cobalt silicate species less interacting with the support. At the opposite, taking into account the extremely lower values of SCA calculated for Co/SiO$_2$ CH A, we assume the negative effect of the stronger alkaline solution and shortened chemisorption step during the CH procedure, leading to predominant formation of a less active cobalt silicate species. The prolonging of the chemisorption procedure under the same conditions, that is the case of Co/SiO$_2$ CH C sample, increases the specific catalytic activity. More investigations are required to elucidate this point.

Figure 5.10. Conversion and CO selectivity for Co/SiO$_2$ IW and CH (A, B and C) catalysts after reductive pretreatment.

The preliminary result for oxidized Co-Cu/SiO$_2$ CH catalysts (figures not reported) showed an higher methanol conversion with respect to monometallic copper and cobalt catalysts containing the same total amount of metal (about 8 wt% of Cu or Co). In particular the bimetallic catalyst with an

higher Cu/Co ratio (about 1.7, Co-Cu/SiO$_2$ CH A) exhibit a very high CO selectivity, higher than 80% already from 380 °C. Further investigations are currently in progress.

Sample	T$_{50\%}$[b] °C	SCA[c]	Conversion[a] mol%	Product yields[a] mol%			
				CH$_4$,	CO$_2$	DME	CO
Co/SiO$_2$ IW ox	369	9.4	96	14	9	0	73
Co/SiO$_2$ CH A ox	446	3.7	77	5	19	4	45
Co/SiO$_2$ CH B ox	411	11.0	84	3	18	4	55
Co/SiO$_2$ CH C ox	394	8.9	85	3	18	4	56
Co/SiO$_2$ IW red	289	11.2	90	13	26	0	51
Co/SiO$_2$ CH A red	446	2.3	79	9	15	1	53
Co/SiO$_2$ CH B red	320	15.3	86	9	13	1	62
Co/SiO$_2$ CH C red	320	9.8	83	8	12	1	61

[a] Conversion and yields of various products at 450 °C.
[b] Temperature of 50% conversion
[c] Specific catalytic activity (SCA) at 400 °C calculated as methanol conversion per 1 wt% Co.

Table 5.3. Catalytic data for Co/SiO$_2$ CH and IW catalysts.

5.4 Conclusions

The Chemisorption-Hydrolysis method successfully employed for the preparation of well dispersed copper catalysts was applied in a new preparation of cobalt catalysts. Cobalt (III) amino complex (likely a $[Co(NH_3)_4(H_2O)_2]^{3+}$) was prepared by oxidation of Co (II) nitrate salt in the presence of H_2O_2 and NH_4OH, without the use of active carbon. As evidenced by magnetic moment measurements the oxidation effectively took place, but after the chemisorption and hydrolysis steps a Co (II) species was generated on support surface. TPR and XPS analysis show the formation of a hardly reducible silicate phase on these samples. The fact is ascribed to the high pH used in the chemisorption step, that can favor the dissolution of silica generating a strong interaction with the support. Differently, the formation of silicate species on copper silica catalysts prepared under same condition (pH=9, t=0.5 h) was not observed.

On the other hand classical Incipient Wetness technique generates spinel Co_3O_4 phase easier reducible between 300 and 500 °C, on Co/SiO_2 catalyst.

The addition of a $[Cu(NH_3)_4]^{2+}$ solution to the Co (III) solution and the following addition of silica support allows one to prepare a bimetallic $Co-Cu/SiO_2$ CH catalyst. The modification with copper generates easier reducible cobalt species, likely by the formation of the spinel phase between the two metals. Nevertheless the TPR profile indicates also the formation of a certain amount of cobalt hydrosilicate, even if with a lower reduction temperature with respect to the one generated on Co/SiO_2 CH.

Catalytic experiments indicate an high specific catalytic activity for Co/SiO_2 B sample ascribable to a low pH during its preparation. However the best CO selectivity was provided by IW sample at 380 °C (91%). About bimetallic catalysts preliminary results indicate that $Co-Cu/SiO_2$ A shows higher CH_3OH conversion and higher CO selectivity if compared to single Co and Cu metal catalysts with the same total amount of metal.

More investigation and other (more) suitable applications for these materials are still in progress. In particular they can be a good candidates for the epoxidation reaction both in liquid (styrene and stilbene) and gas phase (propylene) we are currently studying.

5.5 References

[1] H. Y. Wang, E. Ruckenstein, Journal of Catalysis 199 (2001) 309.

[2] T. V. Choudhary, S. Banerjee, V. R. Choudhary, Appl. Catal. A: Gen. 234 (2002) 1.

[3] M. Labaki, S. Siffert, J.-F. Lamonier, E. A. Zhilinskaya, A. Aboukais, Appl. Catal. B: Environ. 43 (2003) 261.

[4] F. Grillo, M. M. Natile, A. Glisenti, Appl. Catal. B: Environ. 48 (2004) 267.

[5] T. Tsoncheva, L. Ivanova, J. Rosenholm, M. Linden, Appl. Catal. B: Environ. 89 (2009) 365.

[6] T. Garcia, S. Agouram, J. F. Sánchez-Royod, R. Murillo, A. M. Mastral, A. Aranda, I. Vázquez, A. Dejoz, B. Solsona, Appl. Catal. A: Gen. 386 (2010) 16.

[8] J. Jiang, R. Li, H. Wang, Y. Zheng, H. Chen, J. Ma, Catal. Lett. 120 (2008) 221.

[9] X.-Y. Quek, Q. Tang, S. Hu, Y. Yang, Appl. Catal. A: Gen. 361 (2009) 130.

[7] H. Cui, Y. Zhanga, Z. Qiu, L. Zhao, Y. Zhu, Appl. Catal. B: Environ. 101 (2010) 45.

[10] E. Ruckenstein, H. Y. Wang, Appl. Catal. A: Gen. 204 (2000) 257.

[11] A. Karim, Y. Su, J. Sun, C. Yang, J. Strohm, D. King, Y. Wang, Appl. Catal. B: Environ. 96 (2010) 441.

[12] T. A. Kainulainen, M. K. Niemela, A. O. I. Krause, Catal. Lett. 53 (1998) 97.

[13] K. Okabe, X. Li, M. Wei, H. Arakawa, Catal. Tod. 89 (2004) 431.

[14] A. Y. Khodalkov, R. Bechara, A. Griboval-Constant, Appl. Catal. A: Gen. 254 (2003) 273.

[15] J. Panpranot, S. Kaewkun, P. Praserthdam, J. G. Goodwin, Catal. Lett. 91 (2003) 95.

[16] S. W. Ho, J. M. Cruz, M. Houalla, D. M. Hercules, J. Catal. 135 (1992) 173.

[17] C. Ando, H. Kurokawa, H. Miura, Appl. Catal. A: Gen. 185 (1999) 181.

[18] B. Wichterlova, Top. Catal. 28 (2004) 131.

[19] M. L. Smith, A. Campos, J. J. Spivey, Catal. Tod. (2011) doi:10.1016/k.cattod.2011.07.026

[20] D. Potoczna-Petru, L. Kępiński, Catal. Lett. 73 (2001) 41.

[21] A. Y. Khodakov, A. Griboval-Constant, R. Bechara, V. L. Zholobenko, J. Catal. 206 (2002) 230.

[22] A. Martínez, C. López, F. Márquez, I. Díaz, J. Catal. 220 (2003) 486.

[23] I. T. Ghampson, C. Newmand, L. Kongd, E. Pierd, K. D. Hurley, R. A. Pollock, B. R. Walsh, B. Goundie, J. Wright, M. C. Wheeler, R. W. Meulenberg, W. J. DeSisto, B. G. Frederick, R. N. Austind, Appl. Catal. A: General 388 (2010) 57.

[24] A. Y. Khodakov, W. Chu, P. Fongarland, Chem. Rev. 107 (2007) 1692.

[25] E. Lira, C. M. Lopez, F. Oropeza, M. Bartolini, J. Alvarez, M. Goldwaser, F. L. Linares, J.-F. Lamonier, M. J. P. Zurita, J. Mol. Catal. A: Chem. 281 (2008) 146.

[26] O. Borg, P. D. C. Dietzel, A. I. Spjelkavik, E. Z. Tveten, J. C. Walmsley, S. Diplas, S. Eri, A. Holmen, E. Ryttera, J. Catal. 259 (2008) 161.

[27] G. L. Bezemer, J. H. Bitter, H. Kuipers, H. Oosterbeek, J.E. Holewijn, X. D. Xu, F. Kapteijn, A. J. van Dillen, K. P. de Jong, J. Am. Chem. Soc. 128 (2006) 3956.

[28] A. Y. Khodakov, A. Griboval-Constant, R. Bechara, F. Villain, J. Phys. Chem. B 105 (2001) 9805.

[29] T. Vrålstad, W. R. Glomm, M. Rønning, H. Dathe, A. Jentys, J. A. Lercher, G. Øye, M. Stocker, J. Sjoblom, J. Phys. Chem. B 110 (2006) 5386.

[30] H. Li, S.Wang, F. Ling, J. Li, J. Mol. Catal. A: Chem. 244 (2006) 33.

[31] A. Y. Khodakov, Catal. Tod. 144 (2009) 251.

[32] J. Hong, P. A. Chernavskii, A. Y. Khodakov, W. Chu, Catal. Tod. 140 (2009) 135.

[33] H. L. Li, J. L. Li, H. K. Ni, D. C. Song, Catal. Lett. 110 (2006) 71.

[34] W. Chu, P.A. Chernavskii, L. Gengembre, G. Pankina, P. Fongarland, A. Y. Khodakov, J. Catal. 252 (2007) 215.

[35] O. Gonzalez, H. Perez, P. Navarro, L. C. Almeida, J. G. Pacheco, M. Montes, Catal.Tod. 148 (2009) 140.

[36] D. V. Cesar, C. A. Peréz, M. Schmal, V. M. M. Salim, App. Surf. Sci. 157 (2000) 159.

[37] G. Fierro, M. Lo Jacono, M. Inversi, R. Dragone, P. Porta, Top. Catal. 10 (2000) 39.

[38] L. D. Souza, L. Jiao, J. R. Regalbuto, J. T. Miller, A. J. Kropf, J. Catal. 248 (2007) 165.

[39] L. Jiao, R. Regalbuto, J. Catal. 260 (2008) 329.

[40] J. Bjerrum, J. P. McReynolds, Inorg. Synth. 2 (1946) 216.

[41] M. Voss, D. Borgmann, G. Wedler, J. Catal. 212 (2002) 10.

[42] D. Yin, W. Li, W. Yang, H. Xiang, Y. Sun, B. Zhong, S. Peng, Micropor. Mesopor. Mater. 47 (2001) 15.

[43] S. Esposito, M. Turco, G. Ramis, G. Bagnasco, P. Perniced, C. Pagliuca, M. Bevilacqua, A. Aronned, J. Solid State Chem. 12 (2007) 3341.

[44] A. Y. Khodakov, V. L. Zholobenko, R. Bechara, D. Durand, Micropor. Mesopor. Mater. 79 (2005) 29.

[45] A. Kogelbauer, J. C. Weber, J. G. Goodwin Jr., Catal. Lett. 34 (1995) 259.

[46] S.-J. Jong, S. Cheng, Appl. Catal. A Gen. 126 (1995) 51.

[47] B. Sexton, A. Hughes, T. Turney, J. Catal. 97 (1986) 390.

[48] F. Boubekr, A. Davidson, S. Casale, P. Massiani, Micropor. Mesopor. Mater. 41 (2011) 157.

[49] D. Li, X. Liu, Q. Zhang,Y. Wang, H. Wan, Catal Lett 127 (2009) 377.

[50] T. Mochizuki, T. Hara, N. Koizumi, M. Yamada, App. Catal. A: Gen. 317 (2007) 97.

[51] K. S. Chung, F. E. Massoth, J. Catal. 64 (1980) 320.

[52] G. Laugel, J. Arichi, H. Guerba, M. Molière, A. Kiennemann, F. Garin, B. Louis, Catal. Lett. 125 (2008) 14.

[53] C. R. Reddy, G. Nagendrappa, B. S. J. Prakash, Catal. Comm. 8 (2007) 241.

[54] A. Gervasini, S. Bennici, A. Auroux, C. Guimon, App. Catal. A: Gen. 331 (2007) 129.

[55] D. R. Brown, C. N. Rhodes, Catal. Lett. 45 (1997) 35.

[56] G. Busca, G. Martra. A. Zecchina, Catal. Tod. 56 (2000) 361.

[57] E. P. Parry, J. Catal. 2 (1963) 371.

Chapter 6

Shape control in gold nanoparticles

6.1 Introduction

Shape Control in Catalysts

Metal nanoparticles (NPs) are of interest because of their application as catalysts, photocatalysts, sensors and their use in medicine and electronic, optical, magnetic devices [1-3]. The control of morphology (size, shape and surface structures) is a very important method in order to tune catalytic, electronic and optical properties of metal nanoparticles [2, 4]. As reported also in Chapter 1 and Chapter 3, atoms in a metallic crystal lying on different facets and/or having different coordination possess different electronic structures and thus are expected to have different catalytic properties. Not only in kinks, steps and terrace, but also atoms in different crystal planes, such as (100), (111) and (110), are differently packed and have different coordination number. In a fcc lattice, for example, (110) facets is less closely packed than (100): this surface is rough and highly anisotropic and offers a wide variety of adsorption sites. On the other hand, on a fcc crystal, (111) plan is the most densely packed. The situation is reversed on a bcc lattice, where (111) is the most open surface. Generally more open is the surface, more reactive it is [5].

(111) **(100)** **(110)**
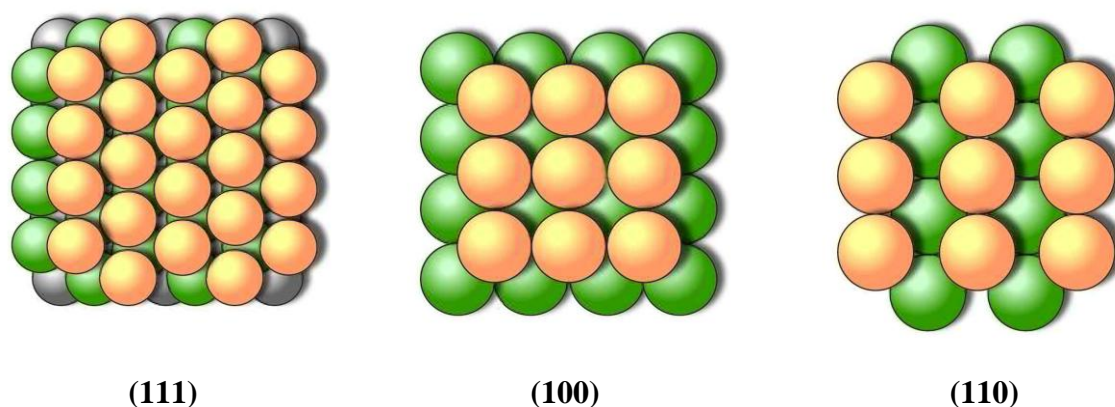
Figure 6.1. Crystal planes on fcc lattice
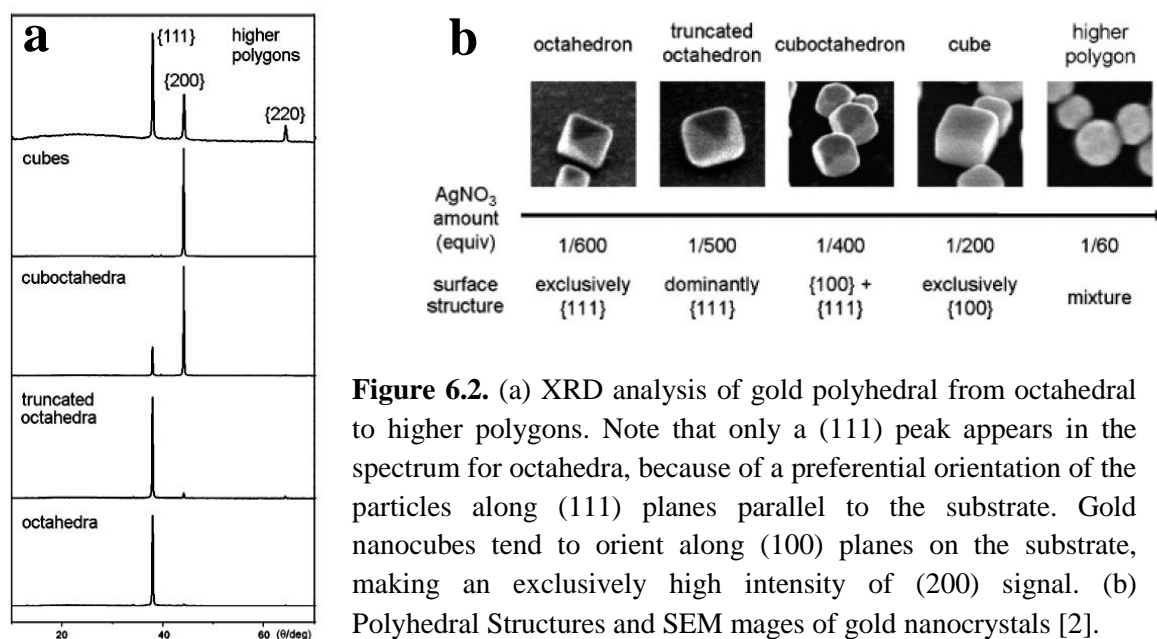
Figure 6.2. (a) XRD analysis of gold polyhedral from octahedral to higher polygons. Note that only a (111) peak appears in the spectrum for octahedra, because of a preferential orientation of the particles along (111) planes parallel to the substrate. Gold nanocubes tend to orient along (100) planes on the substrate, making an exclusively high intensity of (200) signal. (b) Polyhedral Structures and SEM mages of gold nanocrystals [2].

Therefore the potential use of metallic nanoparticles of the same metal but with different shapes in catalysing different kind of reactions has been suggested [4]. As a first approximation, shape determines which crystal facets comprise the surface of a nanocrystal. For example, Seo et al. reported the preparation of polyhedral gold nanocrystals (NCs) of different shape: octahedra, truncated octahedra, cuboctahedra, cubes and higher polygons. An octahedron exposes only (111) facets on its surface, a cube exposes only (100) plans, whereas truncated octahedra, cub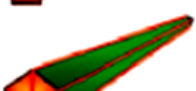octahedra expose both (111) and (100) [2, 6]. The characterization of these materials using different techniques, in particular SEM, TEM, XRD (Figure 6.2), shows that the shape control was achieved with excellent results. Thus the shape controlled synthesis provides the opportunity to tune, as desired, the distribution of different crystal facets of a catalyst. Moreover, shape determines the number of atoms located at the edges or corners. Thus both the reactivity and selectivity of a catalyst can be tailored by controlling the shape of a nanocrystal. Single crystal studies, for example, showed that Cu (111) facets are most active then Cu (110) in the epoxidation of styrene and that Pt (111) surface is from three to seven times more active than Pt (100) for aromatization reactions [6-8]. A direct comparison between single crystal studies and nanoparticles behavior was provided by Somorjai and co-workers in the benzene hydrogenation reaction. This reaction has been shown to produce only cyclohexane on Pt (100) and both cyclohexene and cyclohexane on Pt (111), thus cubic and cuboctahedral Pt nanoparticles are suitable for a shape-dependent selectivity study. In fact, cubic particles consist of only Pt (100) planes (NCs size around 12 nm), whereas cuboctahedral particles expose both Pt (100) and Pt (111) (NCs size around 13.5 nm). Therefore the

(111) surface in cuboctahedral nanoparticles would promote the production of both cyclohexene and cyclohexane, unlike to what happens on cubic nanoparticles where only cyclohexane should be formed. The results confirmed the hypothesis: when cubic nanocrystals were used as catalysts, only cyclohexane was produced, while both the hydrogenation products were observed for cuboctahedrons. Thus, this interesting work illustrated how nanocrystals with well-defined shapes can be used to improve the selectivity of a catalyst. Regardless of shape, a threefold increase in turnover rate was measured as compared to bulk single crystals [9].

During the past decade, a variety of metal nanoparticles with well defined shapes in a fcc lattice have been synthesized, but most of synthetic strategies yield nanostructures with convex shapes enclosed by low index planes, such as tetrahedron, octahedron, decahedron, and icosahedron, enclosed by (111) facets, cube by (100), cuboctahedron by (111) and (100), and rhombic dodecahedron by (111). However, the shape controlled synthesis of metal nanocrystals bounded by high-index facets is a potential route to obtain materials with enhanced catalytic performance, since high-index crystal planes generally show much higher activity than that of the most common stable low-index planes, due to high surface energy and roughness [10, 11]. An example of nanoparticles exposing high index facets is represented by platinum tetrahexahedron (THH) NCs. These structures, synthesized in high quality by Tian and coworkers, exhibit much enhanced catalytic activity per unit surface area for the electro-oxidation of small organic molecules (formic acid and ethanol), than platinum spheres of similar dimension and commercial 3.2 nm Pt/C catalysts. The effect can be related to high density of stepped atoms (roughness) on the surfaces of THH.
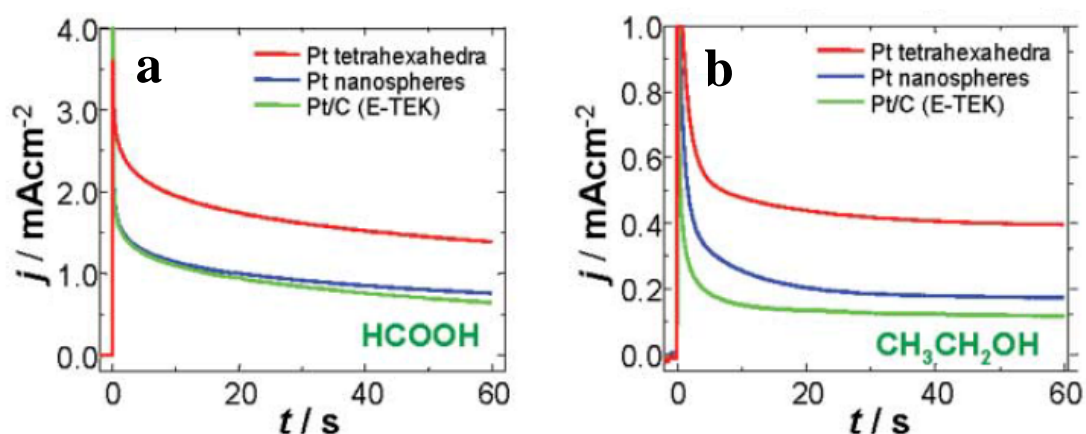
Figure 6.3. Comparison of catalytic activity per unit Pt surface area on THH Pt NCs, Pt nanospheres, and 3.2-nm Pt/C catalyst. (a) Transient current density curves of formic acid oxidation at 0.25 V. (b) Transient current density curves of ethanol oxidation at 0.30 V [10].

Structures	Shapes	Schematic drawings	Metals
single-crystal	perfect/truncated cube[a]		Pd, Ag, Au, Pt, Cu, Rh, Bi, Fe
	perfect/truncated octahedron[a]		Pd, Ag, Au, Pt
	perfect/truncated tetrahedron[a]		Ag, Au, Pt, Rh
	rectangular bar		Pd, Ag, Pt
	octagonal rod		Pd, Au, Fe, Co, Ni
	rectangular or octagonal wire		Pb, In, Sn, Sb, Fe, Co
singly twinned	right bipyramid		Pd, Ag
	beam		Ag
multiply twin-ned	decahedron[a]		Pd, Ag, Au
	icosahedron[a]		Pd, Au
	five-fold twinned pentagonal rod		Pd, Ag, Au, Cu
	five-fold twinned pentagonal wire		Ag, Au, Cu
	triangular/hexagonal plate		Pd, Ag, Au, Cu, Pb, Bi, Co, Ni
	disc		Sn, Co

[a] Platonic solid.

Table 6.1. A summary of different shapes that have been achieved for various metal nanocrystals [6].

On the other hand catalytic activity per unit weight of Pt is lower for THH nanocrystals then for 3.2 nm Pt/C [10]. This phenomena is clearly due to the very different particle size of two platinum systems (around 100 nm for THH versus 3.2 nm for carbon supported catalyst), because of lower surface/volume ratio of high index facets based material, as deeply explained in Chapter 1. After all,

shaped controlled materials usually have an average size of an order of magnitude of 100 nm, quite big for catalytic application (specially for gold based systems), so future research must be focused in particular on the preparation of smaller particles.

Because of the high activity of nanocrystal the well-defined shape can be lost during catalysis. Low stability and the presence of a capping agent (used for NCs preparation) on the surface of the particles can have a negative effect on the catalytic performance.

Further improvements regard, other than the size of crystals, the synthesis procedure, the stability of the nanocrystals, the discovery of new (high index plans) shapes, new metals and the dispersion of the particles on a support. Although a real catalytic application of shape controlled nanoparticles is still far, this field is growing rapidly and the possible advantages arising from this research can reward for the efforts. It becomes clear that maximization of surface, edge, and corner sites should be the criteria for designing superior nanocatalysts [6]. A futurable ideal heterogeneous catalyst should be composed by exactly the same nanometric size metal nanoparticles, uniformly dispersed in the support. Actually these materials can be useful in mechanistic and theoretical catalysis studies, as previously reported here.

Gold Nanoparticles

Gold nanoparticles are widely used because of their high thermal and chemical stability associated to an intense surface plasmon resonance and also to an easy synthetic procedure [12, 13].

A large variety of different gold nanocrystals have been synthesized by different preparation methods: octahedra, cuboctahedra, cubes, spheres, but also decahedra, icosahedra, tetrahexahedra (THH), nanorods, wires, plates, branched structures and others [2, 6, 14-32]. Gold nanocrystals are assuming a great attention in different fields (biochemistry, biomedicine, electronics and catalysis) but, except for spherical particles, the complicate synthetic procedure (low-scale production and poor reproducibility) prevents a large use of these materials [2, 33].

In a simplified approach, a typical synthesis of well defined nanoparticles can be divided into three distinct stages:

1. Nucleation
2. Evolution of nuclei into seeds (seeds are defined as something larger than nuclei)
3. Growth of seeds into nanocrystals.

Metal precursor is decomposed or reduced to generate zero-valent atoms. Once the concentration of atoms reaches a point of supersaturation, the atoms start to aggregate into small clusters (nuclei). Finally nuclei grow to give seeds and then nanocrystals [6].
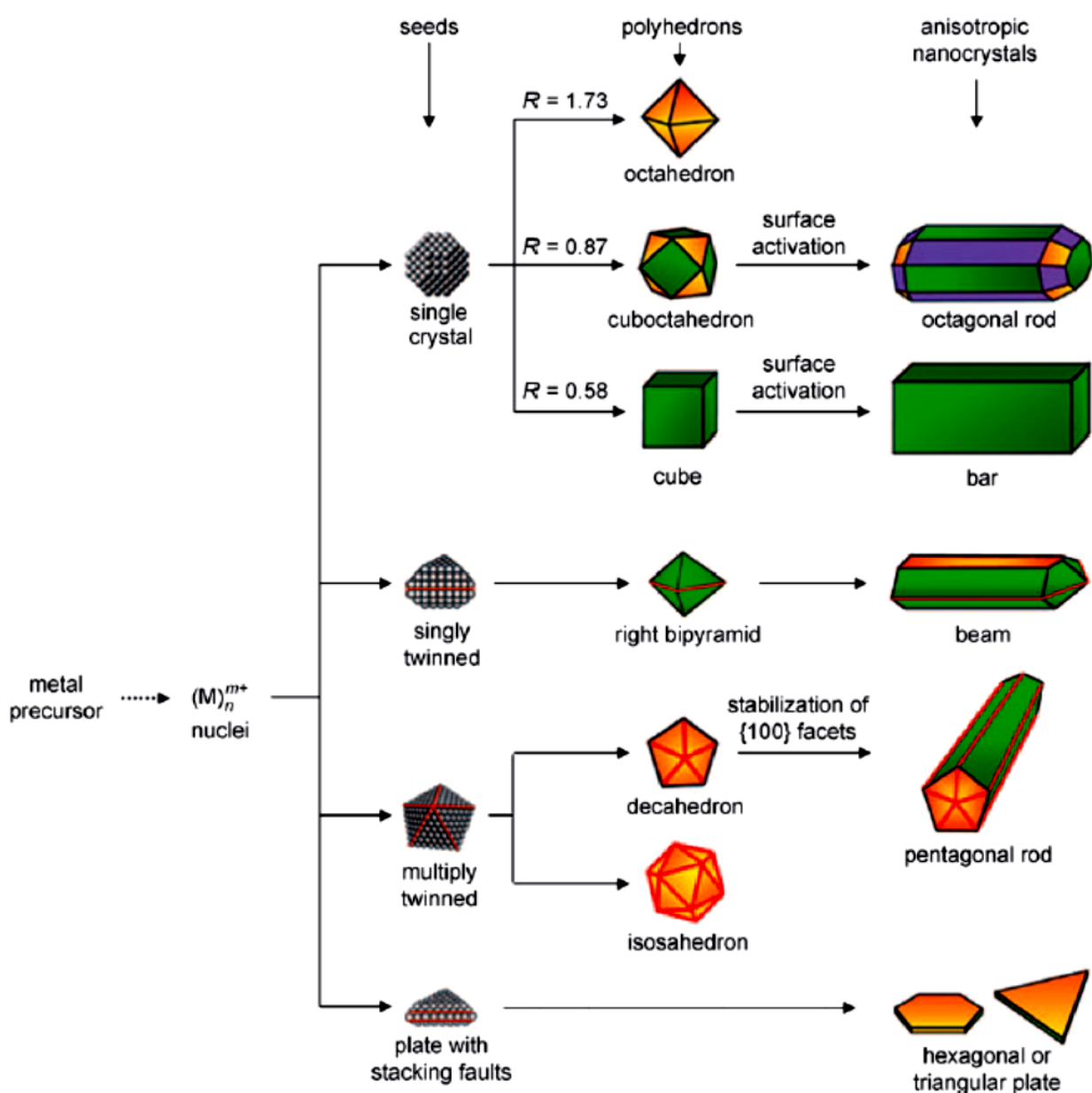
Figure 6.4. Reaction pathways that lead to fcc metal nanocrystals having different shapes. First, a precursor is reduced or decomposed to form the nuclei (small clusters). Once the nuclei have grown past a certain size, they become seeds with a single-crystal, singly twinned, or multiply twinned structure. Green, orange and purple colors represent respectively (100), (111) and (110) planes [6].

A general and tunable synthetic procedure for the preparation of shape controlled metal nanoparticles is the modified polyol process, proposed by Xia. This methodology employs metal chlorides and nitrates in a polyol solvent (like ethylene glycol, EG, or 1,5-pentanediol, PD), in the presence of poly(vinyl pyrrolidone) (PVP). This procedure can fit with the synthesis of different metal or metal oxide, or semiconductor colloids in different shape under appropriate modifications. In particular numerous noble metal (silver, gold, platinum and palladium) nanostructures have been

prepared. In this context, the use of PD as the solvent and as reducing agent is very effective for the shape evolution of gold structures at high temperature. In the modified polyol process the rate of reduction is modulated both by temperature and solvent, with the latter which should have enough reduction power for the reduction of the metal ions. On the other hand, PVP acts as a surface regulating agent, affecting the size and, to a lesser extent, the shape of the particles. A finer shape control can be achieved by introducing foreign ions (e.g. Ag^+) during the nanocrystal growth process [2, 6, 34-36].

BSA as regulating agent

The synthesis of octahedral, cuboctahedra, cubes, spheres and nanorod [2, 29, 31] in the presence of PVP and 1,5-pentanediol as solvent was already reported. However, the stabilization of gold nanoparticles by an appropriate surfactant is important, not only for the synthetic implication and the long-term stability, but also for the application. From this point of view the use of a biological molecule, like a protein, instead PVP can lead to new important application in biomedicine and biotechnology, other than to different shapes and structures.
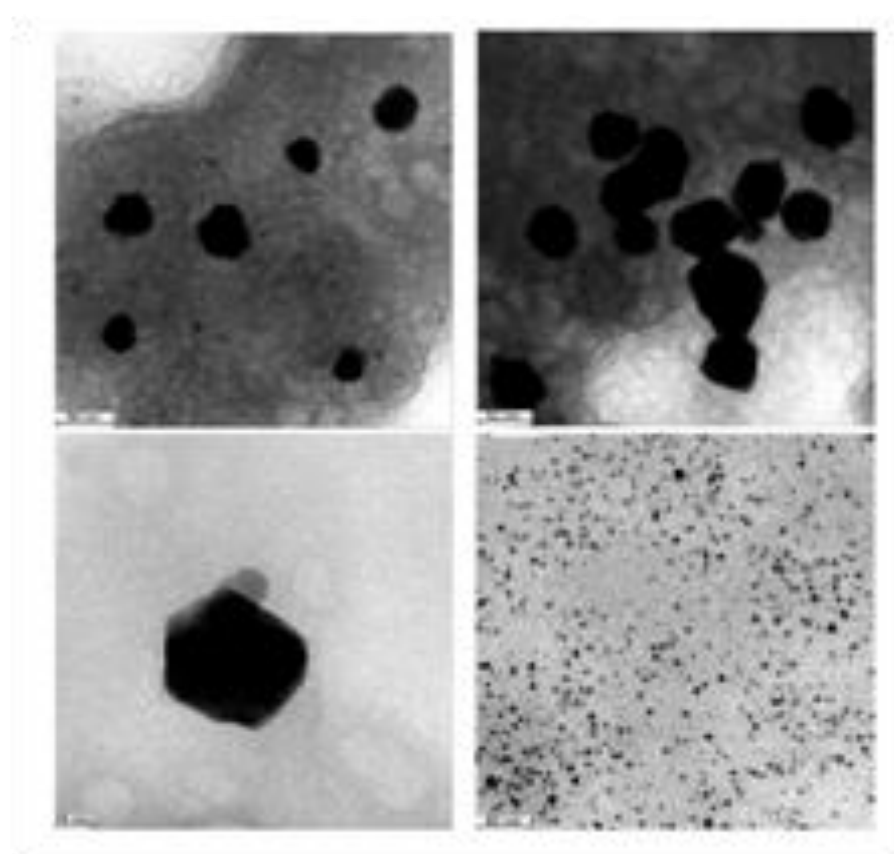
Figure 6.5. An example of gold NCs BSA stabilized reported in literature, TEM images [33].

Serum albumin is the most abundant protein in mammals plasma and is essential for the regulation of the colloidal osmotic pressure and maintenance of pH levels in blood. In particular bovine serum albumin (BSA), the protein made from bovine blood, is one of the most thoroughly characterized, inexpensive and used proteins. BSA has been used in the synthesis of metal nanoparticles (Au, Pt, Ag and alloy) and gold microplates. All these points suggest a possible biomimetic role for BSA as "soft template" in materials chemistry, however a real and effective control of the shape of nanoparticles has not yet been reported [33, 37-42].

Aim of work

In this chapter we reported the synthesis of gold nanocrystals of different shape (octahedral, cube and tetrahxaedron) by a modified polyol processs, mediated by BSA protein or PVP.

The present work was conducted in collaboration with Professor Hyunjoon Song at the Nanoparticles Research Group, KAIST institute (South Korea).

Song and coworkers already synthesized gold nanoparticles using poly(vinyl pyrrolidone) as regulating agent and they already clarified the important role of $AgNO_3$ in shape control [2]. By means of these knowledge we could prepare shape controlled gold nanocrystals employing BSA instead of PVP. Gold PVP mediated particles were also synthesized and compared with those prepared with the protein. The NCs were characterized mainly by TEM, SEM, XRD and UV. Moreover FT-IR analysis was carried out in order to investigate the degree of denaturation of the protein bounded on gold surface. However further investigation are still required to elucidate this point.

6.2 Experimental

Chemicals

Tetrachloroaurate trihydrate ($HAuCl_4 \cdot 3H_2O$, 99.9+%), silver nitrate ($AgNO_3$, 99+%), poly(vinyl pyrrolidone (PVP), bovine serum albumin (BSA), and 1,5-pentanediol (PD, 96%) were purchased from Aldrich and used without further purification.

Synthesis of Polyhedral Gold Nanocrystals with PVP

For 0.15 M PVP solution PVP was added to PD and the resulting mixture was mixed with the aid of a sonicator until complete dissolution of PVP to obtain a solution.

0.15 mL of $AgNO_3$ solution in PD and 0.20 ml of PVP solution were added, at the same time, to 5.0 mL of boiling PD (242 °C). Next 3.0 mL of $HAuCl_4$ (0.050 M) PD solution and 2.8 mL of BSA solution were alternatively added every 30 s over 7.0 min. The resulting mixture was refluxed for 1 h. The final solution was cooled, and the particles were separated from large aggregates by centrifugation at 10,000 rpm for 15 min. The product was purified by repetitive dispersion/precipitation cycle with ethanol to remove excess PVP and wastes, and finally dispersed in ethanol (30 mL) with the aid of sonication.

Different concentrations of $AgNO_3$ solution in PD were used for the syntheses of octahedra (1.25 mM, Ag/Au molar ratio=1/800), cuboctahedra (2.2 mM, Ag/Au=1/450), cubes (5.0 mM, Ag/Au molar ratio=1/200), nearly spherical particles (16.7 mM, Ag/Au=1/60) and higher polygons (33.3 mM, Ag/Au=1/30).

Synthesis of Polyhedral Gold Nanocrystals with BSA

For shape optimization 5 ml of PD (instead than 7) were used in octahedra synthesis.The BSA solution was prepared by adding H_2O to BSA, by mixing the resulting solution and finally by adding PD (BSA=0.0294 g/l, H_2O=8.88% v/v).

0.15 mL of $AgNO_3$ solution in PD and 0.20 ml of BSA PD/H_2O solution were added, at the same time, to 7.0 mL of boiling PD (242 °C). Next 3.0 mL of $HAuCl_4$ (0.050 M) PD solution and 2.8 mL of BSA solution were alternatively added every 30 s over 7.0 min. The resulting mixture was refluxed for 1 h. The final solution was cooled, and the particles were separated from large aggregates by centrifugation at 10,000 rpm for 15 min. The product was purified by repetitive

dispersion/precipitation cycle with ethanol to remove excess BSA and wastes, and finally dispersed in ethanol (30 mL) with the aid of sonication.

Different concentrations of $AgNO_3$ solution in PD were used for the synthesis of octahedra (1.25 mM, Ag/Au molar ratio=1/800), cubes (8.3 mM, Ag/Au=1/120), tetrahexahedron, (20.0 mM, Ag/Au molar ratio=1/50) and higher polygons (33.3 mM, Ag/Au=1/30).

A sample without BSA (or any surfactant) was also prepared and for comparison samples with PVP and the same concentration of $AgNO_3$ used for BSA Au NCs were synthesized.

For shape optimization 5 ml of PD (instead than 7) were used in octahedra synthesis.

Characterization of gold nanocrystals.

Transmission electron microscopy (TEM) and high-resolution TEM (HRTEM) images were obtained on a Tecnai F20 FE-TEM operated at 200 kV at KAIST. SEM images were obtained using a Philips XL30S FEG operated at 10 and 3 kV at KAIST. The samples were prepared by placing a few drops of the colloidal solutions either on copper grids coated with lacey carbon film (Ted Pella, Inc.) for TEM, or on small pieces (5 mm 5 mm) of silicon wafer (P-100) for SEM. The UV/vis absorption data were collected on a Jasco V530 UV/vis spectrophotometer using colloidal ethanol suspension. The FT-IR spectrum was recorded on a Bruker EQUINOX 55 spectrometer, after samples deposition on silicon wafer**.**

6.3 Results and discussion

Synthesis of Polyhedral Gold Nanocrystals

Gold nanocrystals were synthesized by a modified polyol process which uses a diol (in this case 1,5-pentanediol) both as solvent and as reductant, in the presence of an surface regulating polymer (i.e. BSA or PVP). In the reaction procedure, PD solutions of tetracholoroaurate and BSA/PVP were added to the reaction mixture slowly. Different amounts of $AgNO_3$ solution were introduced to boiling PD prior to adding the reactants (Eq. 1). The overall reaction was carried out under reflux at the temperature of boiling PD (242 °C).

$$HAuCl_4 + BSA \ (or \ PVP) \ + AgNO_3 \ \xrightarrow{\text{Diol, }\Delta} \ Gold \ Polyhedrons \quad (1)$$
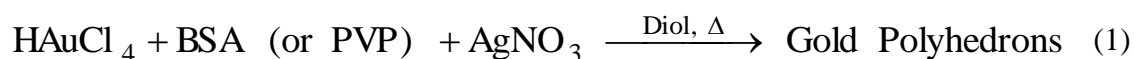
Song and coworkers proposed a mechanism of gold nanoparticles formation and growth for this reaction in the presence of PVP; we can hypothesize that also the BSA mediated synthesis of Au NCs using different amount of $AgNO_3$ follows the same pathways. Without any additives, the surface structure of gold commonly prefers to grow along (111) faces. On the other hand, the addition of $AgNO_3$ alters a relative stability between different facets. In fact, Ag species generated from $AgNO_3$ enhance the selective growth of (111) and/or suppress the growth of (100) [2, 29, 43, 44]. Thus, by increasing the amount of silver in the reaction media the shape conversion between octahedrons and cubes occurs (please note that octahedra are bounded only by (111) facets while cubes expose only (100) planes). In between $AgNO_3$ concentration results in the formation of truncated octahedra and cuboctahedra. Only a small amount of silver is required for the shape conversion (Ag/Au molar ratio is in the range of 1/1000 to 1/30), indicating that Ag effectively works on the surface during the reaction progress [2, 44].

During the reaction, the yellowish solution turned red immediately after the addition of gold precursors and the final colloidal solution was reddish brown. Repetitive precipitation/dispersion can purify gold nanocrystals from the mixture of unreacted metal precursors and excess of PVP/BSA. The re-dispersed colloidal solutions of Au NCs obtained using PVP were stable for several weeks. On the other hand the particles obtained with BSA as regulating agent tend to aggregate during the purification process, while unwashed colloidal solution appears stable for more weeks. The aid of sonication allows one to re-disperse these small aggregates, anyway they are still visible in SEM image. We also tried to purify Au nanoparticles with different solvent, such as acetone, water, water solution of BSA, acetonitrile and other, but the problem still remains and

further improvements are required from this point of view. The problem was already found by Housni and coworkers [33].

Figure 6.6. BSA NCs at the end of the reaction

### *Characterization - SEM, TEM XRD, UV/vis and FT- IR*

Gold nanocrystals prepared with PVP were characterized only via SEM analysis. More information about these systems are already available in the literature [2, 29].

The new materials made using BSA as regulating agent conditions were analyzed via SEM, TEM, XRD, UV/vis and FT-IR.

The results obtained for the preparation of Au NCs mediated by PVP confirm what was previously reported [2, 29]. For a Ag/Au ratio of 1/800 (Ag solution=1.25 mM) octahedra were obtained, while when Ag/Au was 1/200 (Ag solution=5mM) the shape of NCs was cubic. In between AgNO$_3$ concentration resulted in cuboctahedra formation (Ag/Au=1/450, Ag solution=2.2 mM). Finally, a 16.7 mM solution of silvers (Ag/Au=1/60) led to nearly spherical particles were obtained (higher polygons).

In presence of BSA instead of PVP the situation changes (Figure 6.7). Low Ag/Au ratio (1/800, Ag solution=1.25 mM) resulted again in the formation of octahedra, but cubes were obtained with lower Ag concentration (Ag/Au=1/120, Ag solution 8.3 mM) with respect to that used for Au PVP cubes. For comparison, if a 8.3 mM silver solution and PVP was used, over grown cubes were

135

obtained. It is also possible to prepare truncated octahedra (Ag/Au=1/600) and cuboctahedra by using in between AgNO$_3$ solution.
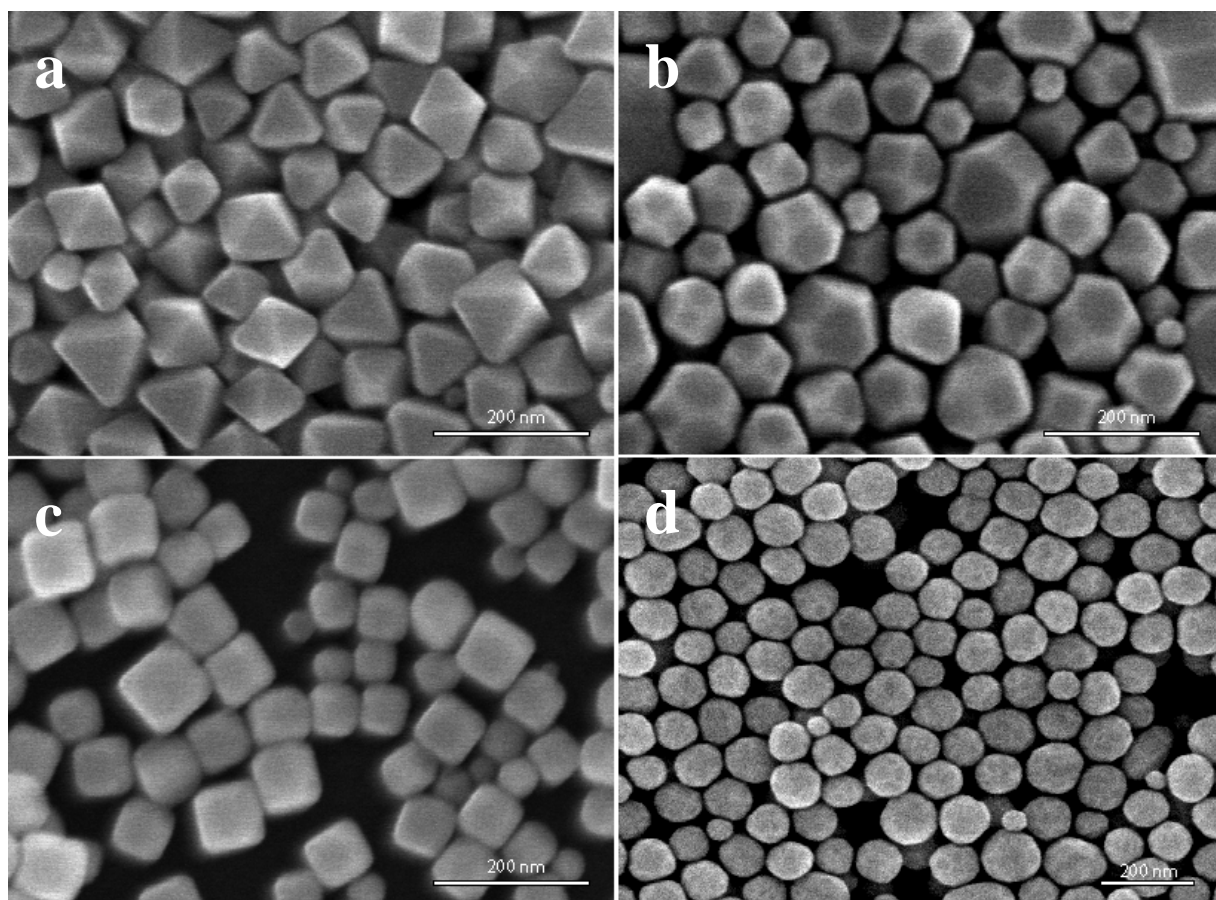
Figure 6.7. PVP Au NCs, SEM images. (a) Octahedron (size: 108±13 nm). (b) Cuboctahedra (size: 112±8 nm). (c) Cubes (size:77±7 nm). (d) Nearly spherical particles (size:103±13 nm).

Figure 6.8 (a) shows representative images of gold octahedral. A regular hexagon is given by a two-dimensional particle projection, when the crystal is aligned along their C$_3$ axes normal to the surface. The C$_4$ symmetric structures are also shown in Figure 6.8 (a') and they are indicative of ideal O$_h$ nanocrystal symmetry. The average edge length is 73±9 nm.

Figure 6.8 (b) shows cubic nanoparticles. From TEM image we can see a two-dimensional square shape where the average edge length is 138±12 nm.

However, the surprising result was given for an Ag/Au ratio of 1/50 (Ag solution=20 mM): this silver concentration allowed to prepare unusual gold tetrahexahedral (THH) nanoparticles. A tetrahexahedron can be imagined as cube wherein each faces is capped with a pyramid. Note that the same Ag/Au ratio and the presence of PVP, rather than bovine serum albumin, led to the formation of nearly spherical NCs. The formation of tetrahexahedra gold nanoparticles is an unexpected and a surprising result because this shape is rarely reported in the literature. THH

structures were reported by Tian et al. and Ming at al. for Pt and Au based nanoparticles [10, 32]. Apparently, from a shape control point of view, the great advantages of the use of BSA protein for synthesis lies on the formation of THH gold NCs, shape not obtained by employing PVP. THH is a shape bounded by high-index planes: these facets generally show much higher activity with respect to the low-index planes, due to high surface energy and roughness. Therefore the synthesis of this kind of nanocrystals is a potential route to obtain materials with enhanced catalytic performances.
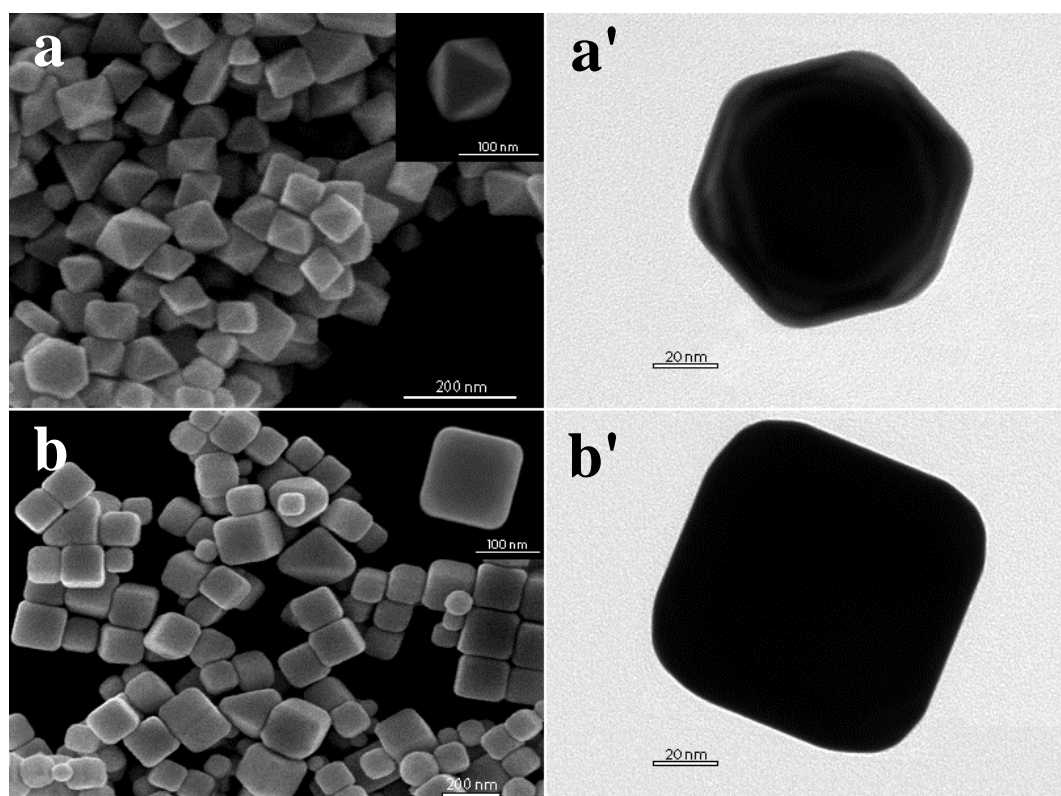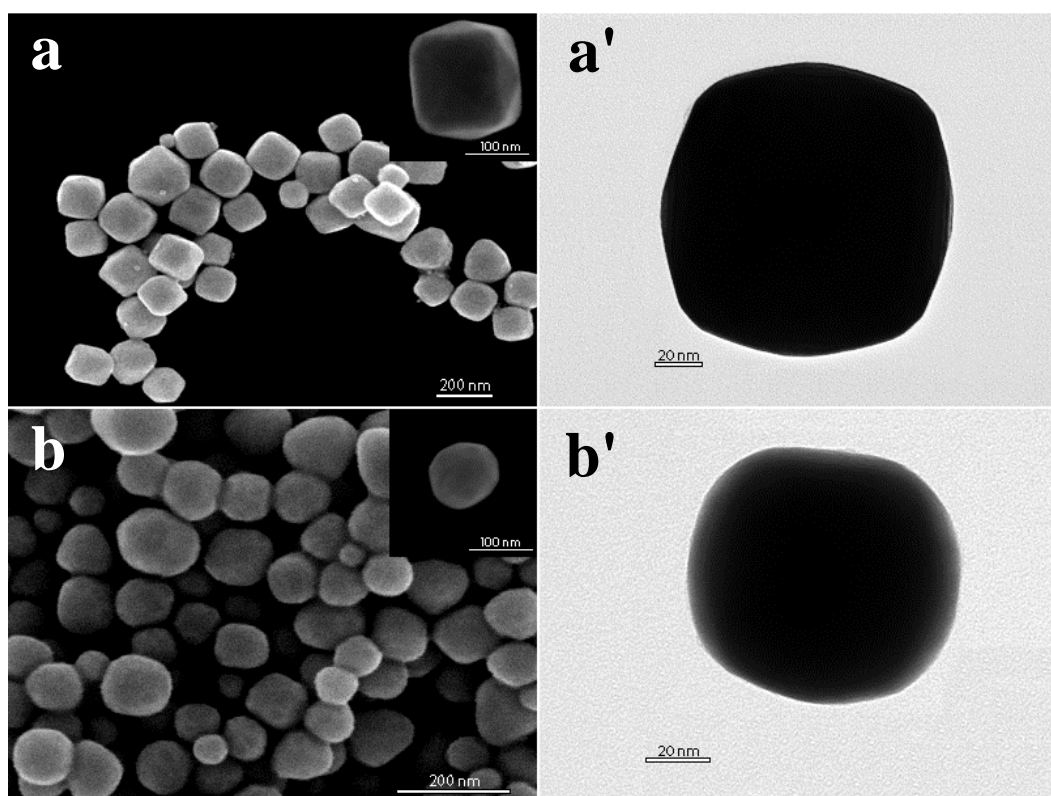

Figure 6.8. SEM and TEM images of BSA Au NCs. (a) SEM images of octahedra. (a') TEM image of octahedra. (b) SEM images of cubes. (b') TEM image of cubes.

Figure 6.10 (a) shows this kind of particles. In particular TEM image shows the octahedreal two-dimensional projection of the tetrahexahedral nanoparticles. The average edge length of the ideal cubic structures of each tetrahexahedron is 133 ± 11 nm.

When more than 20 mM AgNO$_3$ solution is used the shape control of nanoscrystals disappears and for Ag/Au=1/30 we could not control the crystallinty of the materials and only rounded smooth nanoparticles were obtained, both when the surfactant was PVP and BSA (Figure 6.10, b).

The reaction in absence of both PVP and BSA led to the formation of large agglomerate of gold (Figure 6.9, b) and pointed out the pivotal role of surfactant, in particular the less known role of BSA, on the nanoparticles formation.

Figure 6.10. SEM and TEM images of BSA Au NCs. (a) SEM images of tetrahexahedra. (a') TEM image of tetrahexahedra. (b) SEM images of higher polygons. (b') TEM image of higher polygons.
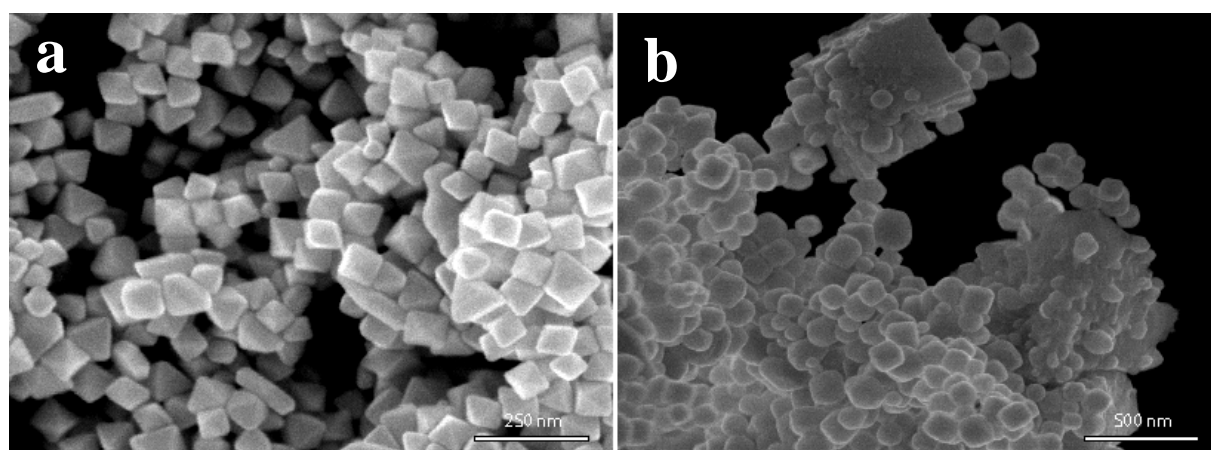

Figure 6.11. (a) SEM image indicative of the aggregation of BSA samples. (b) SEM images of samples obtained without surfactant.

TEM and SEM characterization clearly demonstrate that bovine serum albumine can be properly used as surface regulating agent, instead of classic surfactant as PVP, and that the shape control was achieved also in the presence of the protein. On the other hand the images show that the quality of Au BSA NCs do not reach the same level of Au PVP NCs, because of the aggregation of the materials made with the protein.

XRD data of gold single crystal in a bulk form shows the typical diffraction patterns of face-centered cubic lattice, where (111), (200) and (220) crystal facets, with the relative intensities of 1:0.5:0.3 respectively, are observed [2]. All gold BSA nanocrystals show diffraction intensity ratios quite similar to the bulk materials (Figure 6.13). XRD spectrum of octahedral nanocrystals shows a (little) prevalence of (111) peak, due to the preferential orientation of the particles along (111) planes parallel to the substrate. However, this effect is not so pronounced as expected, in fact (200) and (220) peaks are clearly visible. The phenomena is assigned to the propensity of the nanoparticles to aggregate together, instead of alienating along (111) plane. On the other hand, gold nanocubes tend to orient along (100) planes, making an high (but not exclusively as expected) intensity of (200) signal, that becomes the most intense peak. The same consideration made for octahedra are valid also in this case. Finally tetrahexahedral structure and higher polygons show spectra very close to the one of bulk gold. These XRD patterns cannot confirm the high shape uniformity of the nanocrystals. However, if from XRD data it is reasonable to assert that the quality and the purity of BSA NCs is lower than PVP NCs, TEM and SEM images show a good shape uniformity and the aggregation phenomena (Figure 6.12 a) certainly affects the grade of x-ray diffraction spectra.

Gold nanocrystals normally show very intense color due to surface plasmon resonance scattering, which is highly dependent upon particle size and shape [2, 45-49]. The UV/vis absorption spectrum of the octahedra in ethanol shows a relatively sharp peak at 582 nm, whereas cubes and tetrahexahedra have similar UV spectrum with a broader peak around 570 nm. Finally, the broad peak of higher polygons is shifted at 548 nm. These data (Figure 6.14) are in good agreement with UV/vis spectra of gold octahedral, cubic and almost spherical nanocrystals made in the presence of PVP reported by Seo et al. [29]. UV/vis analysis of THH structured were not found in literature.

Bovine serum albumin can hardly survive on the surface of gold nanoparticles during the reaction, due to the high temperature (around 240 °C). The results reported until now showed that BSA plays the same role of PVP [44, 50]: it acts as surface regulating molecule, by bonding the nanoparticles and promoting the selective deposition of gold atoms to certain facets as well as the stabilization of the entire surface after nanoparticles formation.
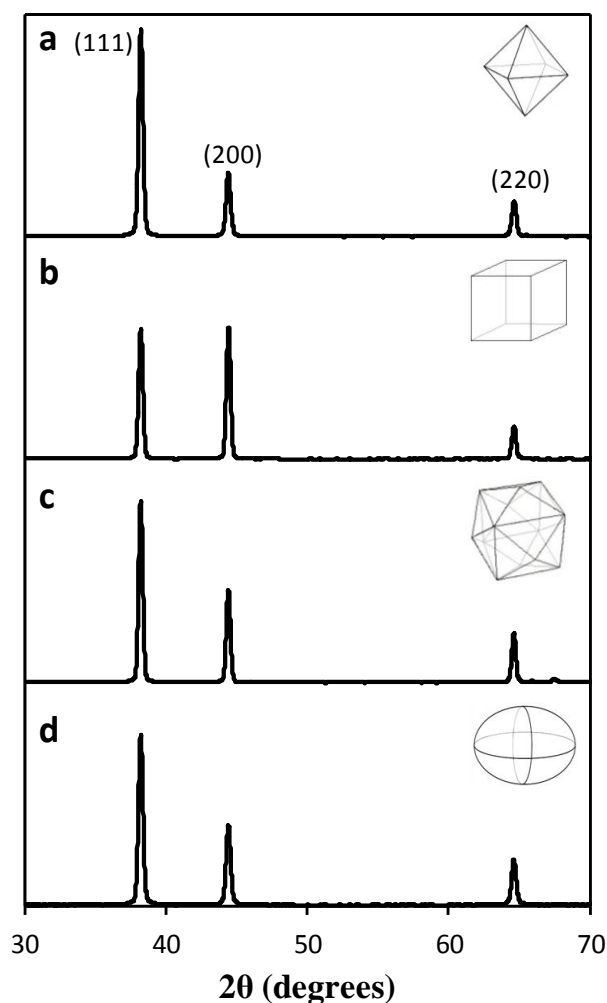
Figure 6.13. XRD spectra of BSA Au NCs: (a) octahedra, (b) cubes, (c) tetrahexahedra, (d) higher polygons

The degree of stabilization reached by BSA is lower than that of PVP, as shown by a certain extent of aggregation of gold crystals. This is probably due to the denaturation of the protein (visible also as a thin brown layer present on the flask wall at the end of the reaction). However it is possible that a small part of BSA bonding the surface of Au particles survives without (a fully) degradation. We tried to evaluate the degree of degradation by a FT-IR analysis of Au BSA nanocrystal samples and of pure BSA. Figure 6.15 (a) reports the acquired spectra. BSA structure is very complicated, but on the base of literature [51-53] we can try to assign the spectrum bands. The spectrum of pure BSA shows very clearly two main peaks at 1655 cm^{-1} and 1539 cm^{-1} assigned respectively to Amide I and Amide II signals. The Amide I mode is primary a C=O stretching band. However it may have some contributions from C-N stretching and C-C-N deformation. The Amide II mode is due to an out-of-phase combination of largely N-H in plane bending and C-N stretching and smaller contributions from C=O in-plane bending and N-C stretching. A small broad peak is assignable to

Amide III mode that is an in phase combination of N-H in-plane bending and C-N stretching, while less intensive is contribution from C-C stretching and C=O bending. At last the bands at 1396 cm^{-1} is related to COO^{-} stretching. The spectrum region relative to N-H stretching (3000-3400 cm^{-1}) appears quite confused.
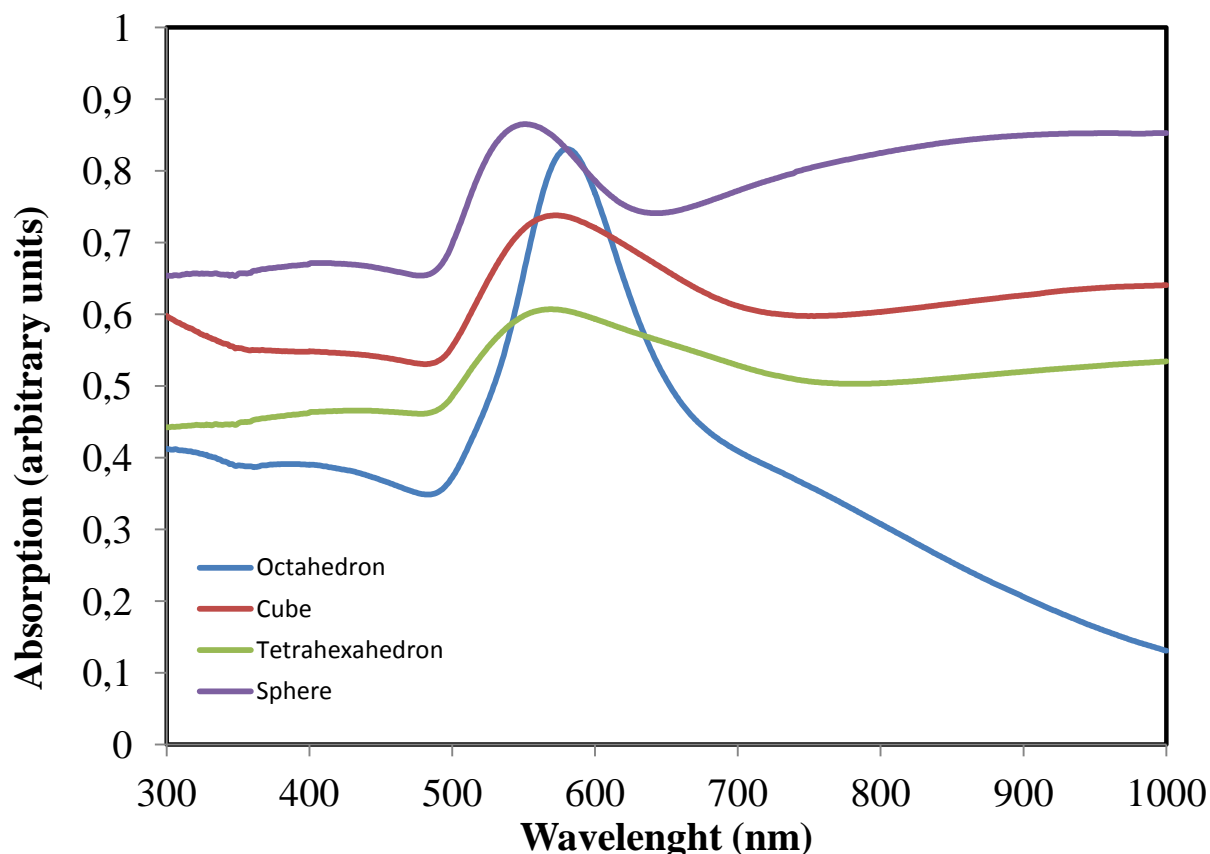
Figure 6.14. UV/vis spectra of BSA Au nanoparticles

Figure 6.15 (b) shows the spectrum of BSA gold nanoparticles. The main structural bands of albumin (i.e. the peptide chain, characterized from Amide I, II and III signals) do not change and are still clearly detectable. Nevertheless the band at 1396 cm^{-1} disappears almost completely and a new band at 1718 cm^{-1} appears, while the region between 1180-1250 cm^{-1} changes substantially. Moreover an increase in absorption in the range of 3700 cm^{-1} (OH stretching) is observed. The results should be consistent with the transformation of -COO^{-} groups of the lateral amino acids of albumin into esters or acids (COOH, according to the enhancement in the region of 3700 cm^{-1}). Anyway, more investigation are still required.
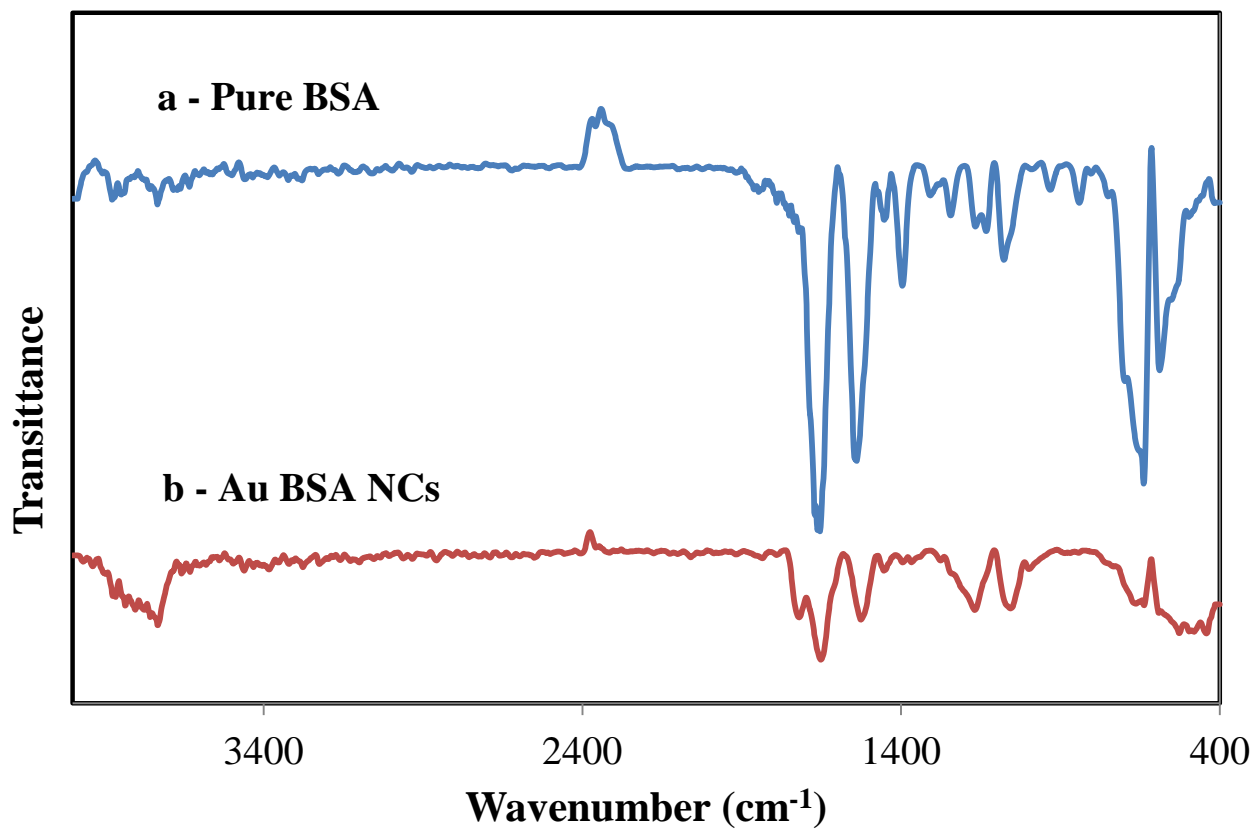
Figure 6.15. FT-IR spectra of pure BSA and BSA Au nanocrystals

6.4 Conclusions

In this work, the shape controlled synthesis of gold nanocrystals was achieved using BSA as regulating agent, instead of classical polymer (like PVP). The results show how BSA allows one to prepare high quality nanoparticles with different shape, depending on the amount of $AgNO_3$ used: octahedrea, cubes, tetrahexaedra and higher polygons were obtained (Figure 6.16). In particular the innovative use of BSA allows one to synthesize tetrahexahedra, that is an unusual shape for a metal nanocrystals. THH particles potentially possess enhanced catalytic performances due to NCs bounding by high-index planes that generally show much higher activity than that of low-index ones. The work presented here is the first example in which the shape control was attain by means of BSA, while few examples report the use of this protein for the synthesis of gold nanocrystal, without shape selectivity. However PVP is a better surfactant than BSA: in fact Au BSA NCs tend to form aggregates as shown by SEM images and XRD spectra.

We tried to evaluate also the degree of denaturation of the protein bonding gold nanocrystals at the end of the reaction, but the work is still in progress.

The futurable use of these materials (both made with PVP and BSA) in catalysis has to go through a reduction of the size of particles (as already reported in this chapter and in Chapter 1 Au is very sensitive from this point of view). The use of different metals (such as copper, or cobalt) and the dispersion of the particles on a support (SiO_2, Al_2O_3,…) are taken into account.
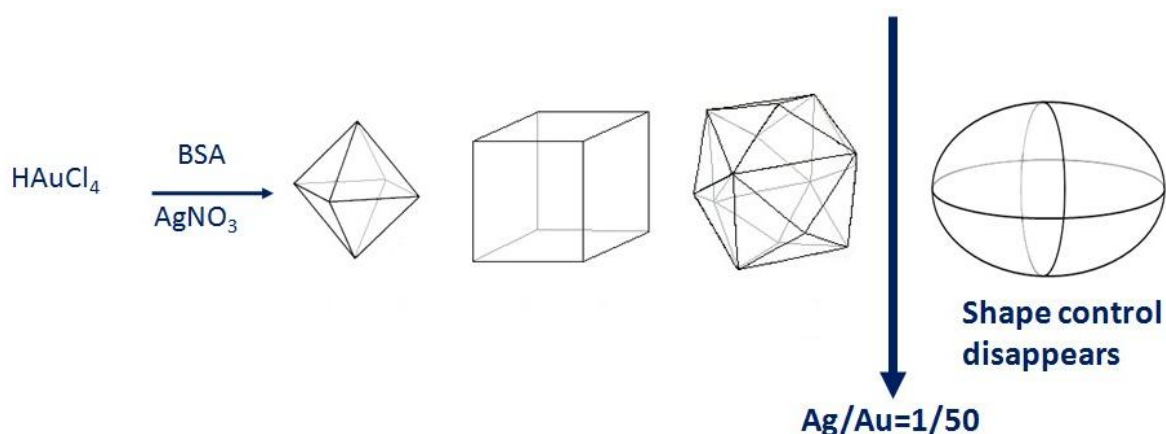
Figure 6.16. Au BSA nanoparticles: from octahedra to higher polygons.

6.5 References

[1] T. S. Ahmadi, Z. L. Wang, T. C. Green, A. Henglein, M. A. El-Sayed, Science 272 (1996) 1924.

[2] D. Seo, J. C. Park, H. Song, J. Am. Chem. Soc. 128 (2006) 14863.

[3] O. Salata, J. Nanobiotechnology 2 (2004).

[4] El-Sayed, M. A. Acc. Chem. Res. 34 (2001) 257.

[5] I. Chorkendoff, J.W. Niemantsverdriet, Concepts of Modern Catalysis and Kinetics, Wiley-VCH Verlag GmbH & Co. KGaA, Weinheim, 2003.

[6] Y. Xia, Y. Xiong, B. Lim, S. E. Skrabalak, Angew. Chem. Int. Ed. 48 (2009) 60.

[7] A. K. Santra, J. J. Cowell, R. M. Lambert, Catal. Lett. 67 (2000) 87.

[8] G. A. Somorjai, D.W. Blakely, Nature 258 (1975) 580.

[9] K. M. Bratlie, H. Lee, K. Komvopoulos, P. Yang, G. A. Somorjai, Nano Lett. 7 (2007) 3097.

[10] N. Tian, Z.-Y. Zhou, S.-G. Sun, Y. Ding, Z. L. Wang, Science 316 (2007) 732.

[11] J. Zhang, M. R. Langille, M. L. Personick, K. Zhang, S. Li, C. A. Mirkin, J. Am. Chem. Soc. 132 (2010) 14012.

[12] M.-C. Daniel, D. Astruc, Chem. Rev. 104 (2004) 293.

[13] A. C. Templeton, W. P. Wuelfing, R. W. Murray, Acc. Chem. Res. 33 (2000) 27.

[14] S. Link, M. A. El-Sayed, J. Phys. Chem. B 103 (1999) 8410.

[15] Y.-Y Yu, S.-S. Chang, C.-L. Lee, C. R. C. Wang, J. Phys. Chem. B 101 (1997) 6661.

[16] C. J. Murphy, T. K. Sau, A. M. Gole, C. J. Orendorff, J. Gao, L. Gou, S. E. Hunyadi, T. Li, J. Phys. Chem. B 109 (2005) 13857.

[17] C. J. Murphy, T. K. Sau, A. Gole, C. J. Orendorff, Mater. Res. Soc. Bull. 30 (2005) 349.

[18] C. J. Murphy, N. R. Jana, Adv. Mater. 14 (2002) 80.

[19] F. Kim, J. H. Song, P. Yang, J. Am. Chem. Soc. 124 (2002) 14316.

[20] C. S. Ah, Y. j. Yun, H. J. Park, W.-J. Kim, D. H. Ha, Y. S. Yun, Chem. Mater. 17 (2005) 5558.

[21] L. Wang, X. Chen, J. Zhan, Y. Chai, C. Yang, L. Xu, W. Zhuang, B. Jing, J. Phys. Chem. B 109 (2005) 3189.

[22] J. E. Millston, S. Park, K. L. Shuford, L. Qin, G. C. Schatz, C. A. Mirkin, J. Am. Chem. Soc. 127 (2005) 5312.

[23] S. Chen, Z. L. Wang, J. Ballato, S. H. Foulger, D. L. Carroll, J. Am. Chem. Soc. 125 (2003) 16186.

[24] C .H. Kuo, M. H. Huang, Langmuir 21 (2005) 2012.

[25] E. Hao, R. C. Bailey, G. C. Schatz, J. T. Hupp, S. Li, Nano Lett. 4 (2004) 327.

[26] Y. Chen, X. Gu, C.-G. Nie, Z.-Y. Jiang, Z.-X. Xie, C.-J. Lin, Chem. Commun. (2005) 4181.

[27] L. Pei, K. Mori, M. Adach, Langmuir 20 (2004) 7837.

[28] C.-H. Kuo, T.-F. Chiang, L.-J. Chen, M. H. Huang, Langmuir 20 (2004) 7820.

[29] D. Seo, C. I. Yoo, J. C. Park, S. M. Park, S. Ryu, H. Song, Angew. Chem. Int. Ed. 47 (2008) 763.

[30] M. Liu, P. Guyot-Sionnest, J. Phys. Chem. B 109 (2005) 22192.

[31] D. Seo, J. H. Park, J. Jung, S. M. Park, S. Ryu, J. Kwak, H. Song, J. Phys. Chem. C 2009, 113, 3449.

[32] T. Ming, W. Feng, Q. Tang, F. Wang, L. Sun, J. Wang, C. Yan, J. Am. Chem. Soc. 131 (2009) 16350.

[33] A. Housni, M. Ahmed, S. Liu, R. Narain, J. Phys. Chem. C 112 (2008) 12282.

[34] B. Wiley, Y. Sun, B. Mayers, Y. Xia, Chem. Eur. J. 11 (2005) 454.

[35] B. Wiley, Y. Sun, J. Chen, H. Cang, Z.-Y. Li, X. Li, Y. Xia, Mater. Res. Soc. Bull. 30 (2005) 356.

[36] F. Kim, S. Connor, H. Song, T. Kuykendall, P. Yang, Angew. Chem. Int. Ed. 43 (2004) 3673.

[37] L. Au, B. Lim, P. Colletti, Y.-S. Jun, Y. Xia, Chem. Asian J. 5 (2010) 123.

[38] A. V. Singh, R. Patil, M. B. Kasture, W. N. Gade, B. L. V. Prasd, Colloids Surf. A 69 (2009) 239.

[39] P. Huang, Z. Li, H. Hu, D. Cui, J. Nanomater. (2010) Article ID 641545.

[40] P. Murawala, S. M. Phadnis, R. R. Bhonde, B. L. V. Prasad, Colloid. Surf. B: Bioint. 73 (2009) 224.

[41] A. V. Singh, B. M. Bandgar, M. Kasture, B. L. V. Prasad, M. Sastry, J. Mater. Chem. 15 (2005) 5115.

[42] J. Zhang, B. Han, J. Chen, Z. Li, Z. Liu, W. Wu, Biotechnol. Bioeng. 83 (2005) 274.

[43] M. C. Giménez, M. G. Del Pópolo, E. P. M. Leiva, S. G.García, D. R. Salinas, C. E. Mayer, W. J. Lorenz, J. Electrochem. Soc. 149 (2002) E109.

[44] D. Seo, H. Song., Bio-Inspired Materials Synthesis (2010), pp. 75-97 ISBN: 978-81-308-0401-9 Editor: Yanfeng Gao

[45] E. Hutter, J. H. Fendler, Adv. Mater. 16 (2004) 1685.

[46] K. L. Kelly, E. Coronado, L. L. Zhao, G. C. Schatz, J. Phys. Chem. B 107 (2003) 668.

[47] J. J. Mock, M. Barbic, D. R. Smith, D. A. Schultz, S. Schultz, J. Chem. Phys. 116 (2002) 6755.

[48] N. R. Jana, L. Gearheart, C. Murphy, J. Chem. Mater. 13 (2001) 2313.

[49] K. R. Brown, D. G. Walter, M. Natan, J. Chem. Mater. 12 (2000) 306.

[50] F. Bonet, K. Tekaia-Elhsissen, K. V. Sarathy, Bull. Mater. Sci. 23 2000 165.

[51] J. Grdadolnik, Bull. Chem. Technol. Macedonia, 21 (2002) 23.

[52] J. Gradolnik, Y. Maréchal, Biopolymers (Biospectroscopy), 62 (2001) 40.

[53] G. Iucci, G. Polzonetti, G. Infante, L. Rossi, Surf. Interface Anal. 36 (2004) 724.

Appendix A

List of Publications

The following list summarizes the publications involved on my Phd work.

[1] F. Zaccheria, S. Brini, R. Psaro, N. Scotti, N. Ravasio, ChemSusChem 2 (2009) 535.

[2] T. Tsoncheva, V. Dal Santo, A. Gallo, N. Scotti, M. Dimitrova, D. Kovacheva, App. Catal. A: Gen. 406 (2011) 13.

[3] M. Popova, M. Dimitrov, V. Dal Santo, N. Ravasio, N. Scotti, Catal. Comm. 17 (2012) 150.

[4] N. Scotti, D. Monticelli, F. Zaccheria, Inorg. Chim. Acta (2011) doi:10.1016/j.ica.2011.10.001.

[5] T. Tsoncheva, A. Gallo, N. Scotti, M. Dimitrov, R. Delaigle, E. M. Gaigneaux, D. Kovacheva, V. Dal Santo, N. Ravasio, Submitted to App. Catal. A: Gen.

[6] Cu/SiO_2 Catalysts Prepared by Chemisorption-Hydrolysis: Structure Sensitivity on Hydrogenation and Etherification reaction, Manuscript in Preparation.

[7] Catalytic Activity of $Co-Cu/SiO_2$ Catalysts Prepared by Chemisorption-Hydrolysis on Methanol Decomposition, Manuscript in Preparation.

[8] Unraveling on the acidic properties of CuO/SiO_2 catalysts, Manuscript in Preparation.

Appendix B

The main abbreviations used in this thesis are summarized here.

BSA = bovine serum albumin

CH = Chemisorption-Hydrolysis

IW = Incipient Wetness

N_B (n_B) = number (moles) of bulk atoms

N_{HS} (n_{HS}) = number (moles) of high-coordination atoms

N_{LS} (n_{LS}) = number (moles) of low-coordination atoms

N_S (n_S) = number (moles) of surface atoms

N_T (n_T) = total number (moles) of atoms

NPs = nanoparticles

NCs = nanocrystals

pPO = partial pressure of propylene oxide

PD = 1,5-pentanediol

PO = propylene oxide

PVP = poly(vinyl pyrrolidone)

THH = tetrahexahedra

TOF = turnover frequency